

**UCSF**

**UC San Francisco Electronic Theses and Dissertations**

**Title**

Biochemical and structural insights into the activation mechanism of the Arp2/3 complex

**Permalink**

<https://escholarship.org/uc/item/7qb30558>

**Author**

Kelly, Alexander E

**Publication Date**

2005

Peer reviewed|Thesis/dissertation

Copyright © 2005

by

Alexander E. Kelly

## Acknowledgements

I would like to thank...

My parents, Richard and Beverly, who have been through so much with me. I apologize for not being home for the past seven years . . . but it's been worth it. I'm so excited to finally get back to New York.

My brother and sister, James and Elizabeth, for reminding what not to do, and for preventing me from being a complete nerd.

Volker Dötsch who put his faith in my ability and potential by taking me in as one of his first students. I am indebted to him for teaching me how to be a careful, thorough scientist and for teaching me the ins and outs of practical and theoretical NMR and structural biology. He showed me that structural biologists should strive to tackle all parts of biology and not limit themselves. Lastly, I have to thank him for sending me to the 2001 NMR Keystone conference, it changed my life.

Dyche Mullins, my mentor and boss man for the past four years, for teaching me that the key to science is not getting depressed about the 95% failure rate. He taught me to loosen up and do the easiest experiment that gets at the question at hand and that you can be quantitative and daring at the same time. His enthusiasm has allowed me to grow not only as a scientist but also as a person. I feel very prepared for the future and feel that he is the main reason. I thank him for supporting me through tough times and I look forward to seeking his advice for a long time.

Ron Vale and David Agard for their advice and encouragement over the years. I hope to achieve at least some of their success and wisdom.

Dale Mierke for taking me out of the pre-med track and getting me interested in basic research. He is the reason I went to graduate school and has continued to support me to this day. I also thank him for introducing me to cigars, corn with lime and scotch.

Julie Ransom for her friendship and keeping me out of trouble. She is irreplaceable.

The Dötsch lab for being hardcore and supporting me the whole time. I miss the eighteen-hour days and dishwashing. I would especially like to thank Zach Serber for keeping me thinking about the big picture. We would wrestle and fight just like a pair of brothers but in the end we both share the same goals and ideals.

The Mullins lab, the source of all man-love. I don't have enough room to express my thanks and gratitude. I will miss all of you dearly. I'm afraid of the future, as I know that I will never find such a great group of people again.

Ojichan, Takao Sato, for sharing his joy and teaching me to look at things with a sense of humor.

Drs. Stephen Paul, Nancy Tarbell, and Stephen Sallan at DFCI for saving my life. You set the standard for excellence and caring. My experiences at DFCI were the source for my scientific interests.

To Kyoko Kelly, my wife, for believing in me and being my best friend and ghostwriter. She is by far the best thing that happened to me in graduate school.



# **Biochemical and Structural Insights into the Activation Mechanism of the Arp2/3 Complex**

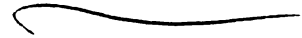
Alexander E. Kelly

## **Abstract**

The dynamic assembly of actin filaments is responsible for generating the forces needed for directed motility within eukaryotic cells – required for many processes including organelle movement, cell locomotion, and pathogenic invasion. This work has focused on understanding the molecular mechanisms involved in the regulation and activation of the Arp2/3 complex. The Arp2/3 complex consists of seven subunits, including two actin-like proteins known as Arp2 and Arp3, and works together with the WASP/Scar-family proteins to create motile actin filament networks. Much is known about the inventory of proteins involved in these events, but much less is known about the mechanism of activation of the intrinsically inactive Arp2/3 complex at the molecular and atomic level.

Multiple advances in the field of NMR spectroscopy have made it possible to obtain detailed information about multi-protein complexes in a short amount of time. This data, when combined with biochemical and kinetic information, gives rise to a detailed picture of the steps involved in biological mechanisms. Using a combination of NMR, chemical crosslinking, binding and activation assays, we have formulated a model to explain how monomeric actin, the C-terminal domain of Scar1 and Arp2/3 act in concert to nucleate new actin filaments. We determine for the first time, the secondary structure of the WH2 domain from a WASP/Scar protein bound to an actin monomer and show that it is equivalent to that of the ciboulot actin-binding motif. In addition, we find

that the C domain binds to both monomeric actin and the p40 subunit of the Arp2/3 complex, and using a battery of point mutants, we observe a direct correlation between affinity for monomeric actin and the ability to stimulate the Arp2/3 complex. From these studies, we propose a model for Arp2/3 activation in which the C domain induces a conformational change on the Arp2/3 complex and then steers an actin monomer onto the Arp2/3 complex to form an Arp2/Arp3/Actin hetero-trimer. Together, the data in this thesis help to advance both the field of Arp2/3 complex mediated actin polymerization and macromolecular structure determination.



---

R. Dyche Mullins, Ph.D.

Advisor and Committee Chairman

## Contributions

Part of this thesis is a reproduction of material previously published. The text of Chapter 3 is reproduced with permission from the *Journal of the American Chemical Society* 124, 12013-12019 (2002), Copyright 2002 American Chemical Society.

Hong D. Ou assisted in preparing NMR samples and acquiring NMR spectra. Rich Withers assisted in acquiring the sensitivity measurements.

The text of Chapter 2 was submitted to the *Journal of Biological Chemistry* on July 8<sup>th</sup>, 2005 and is currently under review. Heather Kranitz made several DNA constructs and helped purify some proteins for this project.

With these exceptions, the rest of the work was performed by Alexander E. Kelly under the direction and supervision of Volker Dötsch and R. Dyché Mullins.

## TABLE OF CONTENTS

<b>Preface</b>	Copyright	ii
	Acknowledgements	iii, iv
	Abstract	v, vi
	Contributions	vii
	Table of Contents	viii
	List of Tables	ix
	List of Tables	x
<b>Chapter 1</b>	Introduction	1
<b>Chapter 2</b>	Actin Binding to the C Domain of WASP/Scar Proteins Plays a Critical Role in the Activation of the Arp2/3 Complex	32
<b>Chapter 3</b>	Low-conductivity buffers for high-sensitivity NMR measurements	79
<b>Chapter 4</b>	Future Directions	109
<b>Appendix A</b>	Targeted espins reveal a novel, WH2 domain-dependent mechanism for making actin bundles in cells	114
<b>Appendix B</b>	Biochemical Studies of Human Scar1	120
<b>Appendix C</b>	Permissions	124

## LIST OF TABLES

### Chapter 2

**Table I:** Affinities and activities for all Scar1 VCA mutations.....65

### Chapter 3

**Table 1:**  $R_s/R_c$  values, expected sensitivity factor L and DC conductivity of.....104  
several different salts, all at 200 mM concentration

**Table 2:**  $R_s/R_c$  values, expected sensitivity factor L, and DC conductivity for several..105  
buffers, adjusted to specific pH values with different acids or bases

# LIST OF FIGURES

## **Chapter 1**

Figure 1.....	27
Figure 2.....	28
Figure 3.....	29
Figure 4.....	30
Figure 5.....	31

## **Chapter 2**

Figure 1.....	66
Figure 2.....	67, 68
Figure 3.....	69
Figure 4.....	70
Figure 5.....	71
Figure 6.....	72
Figure 7.....	73
Figure S1.....	76
Figure S2.....	77
Figure S3.....	78

## **Chapter 3**

Figure 1.....	106
Figure 2.....	107
Figure 3.....	108

## **Appendix A**

Figure 1.....	119
---------------	-----

## **Appendix B**

Figure 1.....	123
---------------	-----

## **Chapter 1**

### **Introduction**

## Actin

### *Actin structure and kinetics*

All eukaryotic cells use networks of actin filaments to perform essential functions – to move; to change shape; to divide; and to transport intracellular cargo. Actin is a 375 residue globular protein that binds and hydrolyzes ATP and adopts a hexokinase-like fold that self-polymerizes into helical filaments (1). The sequence is highly conserved amongst all eukaryotes, with sequence identities averaging about 90-95%. The recent discovery of the prokaryotic actin homologs, ParM and MreB, suggest that these self-polymerizing systems evolved very early in history (2). The actin monomer consists of two structurally homologous lobes, possibly the result of gene duplication. Actin binds ATP or ADP and a divalent cation, either  $\text{Ca}^{2+}$  or  $\text{Mg}^{2+}$ , with nanomolar affinity deep in a cleft formed between the two lobes (3) (Fig. 1). The structural features of the actin monomer can be further divided into four subdomains. The barbed end of the molecule is located on subdomains 1 and 3 whereas the pointed end is found at subdomains 2 and 4. The cleft between subdomains 2 and 4 make up the nucleotide binding site; the hinge between subdomains 1 and 3 is highly dynamic and the spacing between the two is thought to be one of the main differences between the monomer and filament conformation. The actin filament consists of two parallel protofilaments that wrap around each other, forming a right-handed helix, with a twist repeating every 37 nm (Fig. 2). Multiple contacts are made between monomers in both a longitudinal and latitudinal direction, also referred to as the ‘long-pitch’ or ‘short-pitch’ connectivities, respectively. There are extensive interactions made between a loop in subdomain 2 of one monomer



and subdomains 1 and 3 in the next monomer in the long-pitch helix as well as contacts to the adjoining protofilament.

Actin filaments grow in a polarized fashion via the addition of ATP-actin monomers to the filament barbed end. Subunit addition at the barbed end is diffusion limited and the rate of elongation is directly proportional to the concentration of monomers in the solution with a rate constant for the barbed end of  $11.6 \mu\text{M}^{-1} \text{s}^{-1}$  (4,5). As a filament ages, ATP is rapidly hydrolyzed and phosphate is released. The structural consequence of conversion of ATP to ADP has been realized recently with the crystal structure of monomeric ADP-actin (3). The loss of the  $\gamma$ -phosphate causes a major conformational change in the loop in subdomain 2 that makes extensive long-pitch monomer-monomer contacts, thereby making the filament unstable. Filamentous ADP-actin is then disassembled by the removal of subunits from the polymer's slow growing or pointed end, and the ADP moiety is exchanged for ATP to ready actin monomers for another round of polymerization by a protein called profilin.

As the rate-limiting step in the formation of an actin filament from purified actin-ATP monomers is the generation of dimeric and trimeric actin nuclei, actin filament nucleation is the key point of control in forming new filaments. Actin has very low spontaneous nucleation with a  $K_d$  for the monomer-dimer transition approaching 4-5 M. Once a trimer is formed, polymerization is explosive and depends only on the concentration of free monomers in solution. Recent molecular modeling has proposed that the most favorable pathway to nucleation is the formation of a dimer in the long-pitch orientation followed by addition of a third monomer in the short-pitch position (5). In the presence of  $\text{Mg}^{2+}$  and KCl, the critical concentration (the  $K_d$  for a monomer

binding to one end of a filament) is lower at the barbed end (0.1  $\mu\text{M}$ ) than at the pointed end (0.6  $\mu\text{M}$ ), resulting in polarized growth of the filament.

#### *Regulation of polymerization*

A number of proteins bind to the barbed and/or pointed end to make actin polymerization a highly regulated process in the cell (6). Two proteins, thymosin  $\beta 4$  and profilin, serve to maintain a pool of unpolymerized monomeric actin. Profilin binds ATP-actin monomers preventing spontaneous nucleation and allowing for polymerization from the barbed end of existing filaments. Thymosin  $\beta 4$  blocks nucleation as well as growth from either end, and also helps to maintain a large pool of monomeric actin ready for use by the cell. The fact that profilin binds more tightly to actin than thymosin  $\beta 4$  allows for a population of monomers that can be used to elongate barbed ends.

Two other proteins that regulate the actin polymer are capping protein (CP) and cofilin (7). CP binds and caps the barbed ends of existing filaments, literally stunting their growth. This has many effects not only on the balance of monomer and filament but also on the physical properties of the filament. Cofilin serves to depolymerize aged filaments into monomers by recognizing ADP-actin within the filament and severing the connection to other monomers. All of these proteins serve to regulate the most important factor in the kinetics of actin polymerization, the concentration of free barbed ends.

#### *Small molecule inhibitors of polymerization*

Actin polymerization and depolymerization is inhibited by many drugs, the most notable being phalloidin and latrunculin. Phalloidin, a toxin isolated from the mushroom *Amanita phalloides*, prevents the disassembly of F-actin by stabilizing monomer-monomer contacts and keeping actin in the ATP bound state (8). Latrunculin is isolated

from marine red sea sponges and prevents polymerization by binding in the nucleotide binding cleft, adjacent to the bound ATP and thereby stabilizing the ATP form of the protein (9). Latrunculin does not actively disassemble filaments; its mode of action is on the pool of monomeric actin and captures monomers that are coming on and off an existing filament. Latrunculin does not affect the binding of actin-binding proteins that bind the barbed end and therefore has been used recently to solve structures of these proteins bound to actin, which was otherwise impossible due to the critical concentration of actin.

### *Purification*

Actin needs to be purified from a native source to fold correctly and exhibit normal kinetics. The CCT family of chaperones serves to help fold both actin and microtubules in many eukaryotes (10). Actin can be obtained in an *in vitro* translation/transcription system but with only nanogram yields. To obtain biochemical quantities of actin, one must purify the actin from a source such as *Acanthamoeba castellanii* or rabbit muscle. We prefer *Acanthamoeba* actin since the percent sequence identity to human cytoplasmic actin is higher than that of muscle actin (95% vs. 90%).

### ***De Novo Nucleation***

Spontaneous nucleation is too slow to account for the rapid assembly of filaments seen *in vivo*. It wasn't until recently, however, that the proteins that speed up this process were discovered. Currently, there are three known nucleators of actin filaments: the formins, spir and the Arp2/3 complex (11). They all share a common mechanism of action by overcoming the largest energetic barrier to nucleation: formation of the initial actin dimer. The first two generate parallel actin filaments by directly assembling actin

monomers together. The formins work through the action of two adjacent domains, FH1 and FH2. The FH1 domain is a stretch of poly-proline residues of varying lengths that recruits profilin, which in turn binds ATP-actin monomers. These monomers are then loaded onto the FH2 domain, which forms a dimer with two actin-binding sites. The amazing structural features of the FH2 dimer force the two monomers into a 'pseudo short-pitch' dimer orientation that allows for nucleation from the barbed end (12). The formins undergo cycles of allowing monomer addition and detachment that results in the formation of a 'processive cap' resulting in rapid insertional polymerization. The mechanism of action of spir is not as well understood. Spir contains four WH2 domains (see below) that are linked by short, well-conserved peptides (13). The combined action of actin monomer recruitment by the four WH2 domains as well as the actin binding linker 3 motif help to assemble a long-pitch dimer which then assembles into one strand of the filament helix. The consequences of the additional activities of this protein, such as pointed-end capping, are unknown.

Unlike other known nucleators, the Arp2/3 complex does not recruit actin monomers to form a dimer. Instead, the complex is thought to work by using two actin related proteins, Arp2 and Arp3, to form an actin-like dimer that serves as a platform for nucleation (4). The additional activity of filament side binding results in the generation of highly crosslinked, branched filaments that provide the orthogonal forces necessary for most motile processes. Another major difference between it and other nucleators is that the Arp2/3 complex is itself inactive unless turned on by a group of highly regulated proteins known as nucleation promoting factors (NPFs). These factors, either directly or through other proteins, bind the Arp2/3 complex and recruit monomeric and/or

filamentous actin upon localization to lipid rich environments. The highly branched dendritic arrays are formed with 70 degree-angles between the 'mother' and 'daughter' filaments that are optimal for force production. Whether inside the cell pushing out or powering a rocketing *Listeria* or vesicle, this geometry is essential to motility. How these activities are produced and regulated are fundamental questions I have tried to address in this thesis.

### **The Arp2/3 Complex**

The Arp2/3 complex is highly conserved through all eukaryotes. Its activities are responsible for a number of physiological processes including morphogenetic movements during embryonic development (14,15), movement of axons and dendrites during development and remodeling of the nervous system (16), chemotactic movement of immune cells, and migration of fibroblasts during wound healing. The complex was originally identified by searching for proteins that bound a profilin-poly-L-proline column (17). Its importance was verified by its identification as the actin nucleating machinery on the bacterium *Listeria monocytogenes* (18), as a component required to assemble actin filament patches in budding yeast (19), as a factor required for the small GTPase Cdc42 to activate actin filament assembly in cytoplasmic extracts of frog eggs (20) and as the major nucleator of actin filaments in *Acanthamoeba Castellani* (21).

The Arp2/3 complex consists of seven tightly associated subunits, including actin-related proteins 2 and 3 (called Arp2 and Arp3), p40, p21, p20, p35 and p16. As mentioned above, this complex nucleates new filaments from the side of existing filaments upon activation by a class of proteins known as the NPFs. In the following

sections, I discuss the current understanding of the architecture of the Arp2/3 complex and the mechanism and regulation of activation of the complex.

### *Arp2/3 structure*

A combination of crosslinking, analytical ultracentrifugation, biochemical reconstitution, electron microscopy and X-ray crystallography has revealed the overall architecture of the Arp2/3 complex alone and bound to the side of a mother filament (21-25). This information has become the basis for our understanding of the core mechanics of nucleation by the Arp2/3 complex.

The Arp2/3 complex is thought to nucleate new filaments by providing an actin-like dimer created by the proper orientation of the Arp2 and Arp3 subunits from which a new filament can form with the pointed end of a daughter monomer binding the barbed end of either Arp2 or Arp3. Mullins *et al.* originally identified the overall architecture of the complex using a combination of crosslinking and analytical ultracentrifugation (21). This placed the Arp2 and Arp3 subunits next to each other, which was expected from the model. In addition, the arrangement of the other subunits was made clear, illustrating that p35 and p20 subunits can crosslink to the sides of actin filaments. EM and analytical ultracentrifugation revealed that the complex was a horseshoe shaped molecule that sits at the junction of the side of a mother filament and a growing daughter filament. The affinity of the Arp2/3 complex for the pointed end and the side of a filament are quite strong. From this work, it was originally proposed that a dimer of actin would load onto the complex; however, as shown later, it appears to be a monomer.

The structure of the Arp2/3 complex was solved in 2001 by X-ray crystallography to a resolution of 2.0 Å (23). The overall architecture of the complex matches exactly to

that determined by chemical crosslinking (21). A small portion of the electron density was very weak which allowed only a backbone trace of subdomains 1 and 2 of the Arp2 subunit. The absence of strong density for this region could potentially mean that this region is sampling multiple conformational states. In addition, ATP was missing from the nucleotide binding pockets on Arp2 and Arp3. This is not too surprising, however, given the 100 fold lower affinity of the Arps for nucleotide when compared to actin.

The horseshoe shape of the complex was again confirmed by the crystal structure (Fig. 3). The two Arps are adjacent to each other, and each has an actin-like fold. There are a number of loops and insertions in each Arp making multiple contacts with neighboring subunits. The structural core of the complex is a long anti-parallel coiled-coil formed by the p35 and p20 subunits. At opposite ends of the helices are globular folds contributed by each subunit. These two subunits do not share significant sequence homology yet have nearly identical folds. The globular domain of p20 makes a number of contacts with Arp2, p40 and p16 whereas the analogous domain in p35 contacts only Arp3. The high thermal and chemical stability of the complex can be attributed to the fact that more than 8000 Å<sup>2</sup> of surface area is buried for both p35 and p20. The most intriguing subunit in the complex is p40, which adopts a β-propeller fold with seven blades. This fold has been found in many proteins and is used to bind a vast number of protein targets. Interestingly, a short helix between blades 6 and 7 makes a crystal contact with the Arp3 subunit of an adjacent molecule. This contact is formed by a helix extending from the p40 subunit which binds to the barbed end of the Arp3 subunit, much in the same way a WH2 domain, gelsolin, or profilin does. In fact, it has recently been shown that this helix can bind to monomeric actin (Bruce L Goode, ASCB). The p16

subunit has a novel all alpha-helical fold that makes a number of inter-subunit contacts with the majority of its interaction with the p40 subunit. Both p40 and p16 subunits are phosphorylated in mammalian cells. Lastly, the p21 subunit also adopts a novel all alpha-helical fold, using its contact to the Arp3 subunit as its only attachment to the complex.

Recent crystal structures of the Arp2/3 complex bound to ATP or ADP show only modest changes in the overall structure of the complex (26). The most pronounced changes are the closing of the clefts between subdomains 2 and 4 of the Arp3 subunit. Surprisingly, subdomains 1 and 2 were again missing from the electron density suggesting that the flexibility of those regions seen in the original structure is not due to the absence of nucleotide. The fact that the structures of the ATP and ADP bound forms are so similar indicate that hydrolysis of ATP is not the driving force behind the major conformational change needed to bring the Arps together in a short-pitch-like dimer (Fig. 4). It is possible, however, that this event stabilizes this conformation caused by binding of an NPF and the mother filament.

Our understanding of the architecture of the Arp2/3 complex was furthered by reconstitution studies by the Welch laboratory (22). Using a baculovirus expression system, the stability and activity of the complex was examined by deletion of combinations of subunits. They found that the p35/p20 heterodimer was stable on its own and retained its ability to bind to actin filaments. Removal of the p21 subunit, a subunit that was originally identified by yeast two-hybrid to interact with the acidic domain of NPFs (27), decreases but does not kill the nucleation activity of the Arp2/3 complex. Lastly, the p40 and p16 subunits form a stable sub-complex. Upon removal of



this sub-complex, the rest of the complex is still stable, but completely loses its nucleation ability.

The structure of the *Acanthamoeba Castellani* Arp2/3 complex at the branch point of the mother and daughter actin filament by two-dimensional reconstructions of cryo-electron micrographs is considerably different from that given by the crystal structure (24). If both Arp2 and Arp3 form the first two monomers in the daughter filament, then one of the subunits would have to drastically change its orientation from the crystal structure. If, however, only one of the subunits is part of the branch (as I argue in the last section) then more realistic structural changes are needed.

### **Nucleation Promoting Factors**

There are two main classes of NPFs, those that bind monomeric actin and those that recruit filamentous actin (28). The former are much more potent activators *in vitro*, although each of these proteins recruits a number of other scaffolds that may normalize their activity *in vivo*. They share a common mechanism in that they have a region that binds to the Arp23 complex, consisting of the C and A domains, and this binding event is thought to induce a conformational change in the complex. The recruitment of actin monomers to the Arp23 complex appears to be a much more efficient mechanism of activation and is the focus of this thesis.

#### *WASp and WAVE/Scar proteins*

The WASp/Scar family of proteins is the best understood of the monomer-recruiting Arp2/3 complex activators (Fig. 5A). The WASp/Scar family of proteins

includes WASp, N-WASp and three isoforms of Scar/WAVE as well as the *S. cerevisiae* protein Bee1 and the *Listeria monocytogenes* protein ActA. WASp/Scar proteins are largely unfolded, with modular signaling domains differentiating each protein from one another. The WASp and N-WASp proteins are regulated by the upstream GTPase Cdc42, the Scar/WAVE and bee1p proteins by the GTPase Rac and the *Listeria monocytogenes* protein ActA is constitutively active. Each protein shares a common C-terminal peptide that is necessary and sufficient for activation of the Arp2/3 complex. This peptide is defined by a verprolin homology or WH2 domain that binds actin monomers, and central (C) and acidic (A) regions that bind to the Arp2/3 complex, which together stimulate the actin-nucleating activity of the Arp2/3 complex (4). Each protein is spatially and temporally regulated by different upstream signals, owing to their distinct signaling domains. Both WASp and N-WASp each contain an EVH1 domain which binds the protein WIP that localizes it to the membrane; a basic region that binds to phospholipids with a preference for PIP<sub>2</sub>; a GTPase binding domain (GBD) that together with the basic region serves to repress activation; and a long stretch of poly-prolines which have been shown to recruit a number of SH3 domain containing proteins, some which relieve autoinhibition or help to incorporate WASp/N-WASp into larger scaffolds. N-WASp is slightly different from WASp in that it has a calmodulin binding site of unknown function and two WH2 domains instead of one. The WAVE/Scar proteins have a similar domain architecture but responds to a different set of upstream signals. Each isoform consists of an N-terminal Scar Homology domain (SHD); a phospholipid-binding basic region; a 100 residue stretch of conserved residues (see appendix A); a stretch of poly-prolines and lastly the VCA region.

The mechanism of WASp and N-WASp inhibition is well known, where once WASp/N-WASp is targeted to the membrane, both Cdc42 and the lipid PIP<sub>2</sub> act to relieve the autoinhibitory contacts between the GBD and the C domain of the VCA region of the same molecule (29). The GBD-C domain interaction prevents nucleation possibly by preventing binding of both actin and the Arp23 complex. Cdc42 binds to a distinct conformation of the GBD and therefore shifts the equilibrium to the “off” state. PIP<sub>2</sub> binding to the basic region adjacent to the GBD is thought to not only bias the conformational equilibrium of the GBD but also to relieve an inhibitory contact between the basic region and the Arp2 subunit on the Arp2/3 complex. However, recently *toca-1* has recently been discovered to bypass the need for PIP<sub>2</sub> by serving to enhance the activity of Cdc42 directly.

The regulation of WAVE/Scar activity is more complex (29). The WAVE/Scar proteins do not contain a GBD and are intrinsically active molecules. WAVE/Scar proteins appear to exist as part of a pentameric complex that prevents its own degradation by the proteasome. This complex includes PIR121 (p53 inducible messenger RNA), Nap1 (Nck-associated protein), Abi (Abl interactor), and HSPC300. It is thought that this pentameric complex is inactive and that upon binding either Rac or Nck (which also binds to the poly-proline region) at the membrane results in the loss of the complex and full activation of WAVE/Scar. The role of PIR121 is likely to mediate the interaction of the complex with Rac as it is homologous to a known Rac effector, p140Sra-1. Abi appears to make the main connection between WAVE/Scar and the rest of the complex. Interestingly, the coiled-coil domain from Abi contacts not the C domain of WAVE/Scar but rather the SHD. This domain is also predicted to be a coiled-coil and may make a

hetero-dimer with Abi. Therefore, how this complex inhibits WAVE/Scar is still not understood and it appears that another set of protein-protein interactions is necessary for inhibition.

### *The WH2 domain*

The WH2 domain is found in a large class of proteins (42 total) (SMART database), all with distinct outputs. The exact role in which this domain plays in determining these activities is not understood. Previous studies have identified the WH2 domain as a short peptide of about 25 residues that binds the barbed-end of monomeric actin with micromolar affinity (30). The domain prevents spontaneous actin polymerization, favors ATP over ADP-actin and allows for barbed-end elongation. Marchand et al showed that the Scar WH2 domain is unfolded by itself and presumably becomes structured upon binding monomeric actin. This disorder to order transition is advantageous in that it allows for high specificity with micromolar affinity seen in most cytoskeletal interactions. Recent studies have suggested that the thymosin  $\beta$ 4 and ciboulot actin-binding domains are structurally and functionally related to the WH2 domain of WASP/Scar proteins even though the sequences are fairly divergent (Fig. 5B) (31). The crystal structure of the ciboulot WH2 domain complex with actin is defined by an N-terminal helix of 16 residues C-terminally capped by 5 helix breaking residues, immediately followed by a four-residue LKKT motif in an extended conformation (with L being leucine, K a lysine and T a threonine). The helix is defined by a  $\phi\phi x x \phi$  motif found in many other helical peptides such as the nuclear hormone co-activator GRIP1 and transcriptional co-activator CBP/p300 (32). The helix-breaking residues are usually glycines (found in all WH2 domains from WASP/Scar proteins), prolines and aspartate.

This helix binds to a cleft in the barbed end that is the binding site for many proteins such as thymosin  $\beta$ 4 and profilin, both of which compete with the WH2 domain from WASp/Scar proteins. It was proposed that in the case of ciboulot/thymosin the WH2 domain consisted of the secondary structure elements described above as well as the actin-binding peptides C-terminal to the L++ $\phi$  motif.

One possible role of the WH2 domain is that of an adapter module serving to increase the local concentration of monomeric actin, suggesting that it is the C-terminal extension of WH2 domains that dictates the activity of each protein. This is seen in thymosin- $\beta$ 4, which contains an N-terminal WH2 domain followed by a helical C-terminal region that binds the pointed-end, resulting in the sequestration of monomers (33). This point is most evident in the case of the spir protein, which we have shown to nucleate polymerization in the absence of Arp2/3 and formins (13). Spir contains four WH2 domains, linked by three highly conserved tethers. The WH2 domain is dispensable to the basic mechanism of spir, the minimal nucleation region is the third peptide tether. It was proposed that this peptide stabilizes actin dimers and that the WH2 domain helps increase the efficiency of the reaction by providing an increase in the concentration of monomers.

A number of proteins contain multiple WH2 domains. In these cases, it is entirely possible that higher-order effects of multiple WH2 domains will result in activities more complex than just increasing the local concentration of actin. Replacement of portions of the linker regions of spir retained minor activity, possibly by the ability of four actin binding WH2 domains to make a nucleus-like structure. However, it is still unexplained how the spir protein caps the pointed end of filaments and this activity might confuse this

interpretation. On the other hand, the N-WASP protein does not require both of its WH2 domains for wild-type activity (25). Interestingly, the Ciboulot protein has three LKKT repeats but only one contains an N-terminal alpha helix and binds actin with measurable affinity (31). Another higher-order activity of the WH2 domain could be the ability to bind to the barbed-end of a filament. This has been postulated in the case of the yeast Arp2/3 activator, Pan1p (34). Although structurally feasible, we feel that the F-actin binding sequence of Pan1p is not a WH2 domain and actually part of a larger coiled-coil region that binds filaments since the isolated WH2-like region was unable to bind either G- or F-actin. Further experiments are needed to confirm the possibility that the WH2 domain can bind filaments.

In addition to increasing the local concentration of monomers, we believe another role of the WH2 domain is to compete with profilin for binding actin. In the case of the Scar WH2 domain, this competition is only possible when attached to the C domain. Alone, the affinity for monomers is 3  $\mu$ M but together the affinity is 200 nM, strong enough for direct competition with profilin. The proline-rich domains found in all WASP proteins, which bind profilin-actin complexes, could amplify this effect. These complexes might be fed into the VCA domains in which the VC peptide would compete for free monomer, which would then be delivered to the Arp2/3 complex. Therefore, the WH2 domain could simply be a modular domain that when positioned near other binding elements, provides a high concentration of ATP-actin monomers while occupying minimal actin surface area. It remains to be seen if the WH2 domains have their own intrinsic nucleation ability.

*The C domain*

The C domain is an amphipathic peptide highly conserved among all NPFs and is a potential hotspot for regulation that translates upstream signals to activation of the Arp2/3 complex. Deletions and mutations in the C domain cause major defects in the nucleation promoting ability of Arp2/3, while phosphorylation serves to augment Arp2/3 activity *in vitro* and *in vivo* (35). Furthermore, C domain binding to the GTPase binding domain (GBD) promotes autoinhibition of WASP and N-WASP, while *trans* inhibition may occur through the C domain in Scar proteins upon binding to the Nap125-Abi complex (36-38). The C domain adopts a helical conformation upon binding the GBD, with all conserved hydrophobic residues making important contacts (39). In context of the full-length VCA peptide, these same residues were shown by nuclear magnetic resonance (NMR) analysis to make multiple contacts with Arp2/3 (40). Additionally, there is no correlation between affinity for the Arp2/3 complex and nucleation promoting activity of C domain mutants. This further supports the model that there is an activation step subsequent to binding of the VCA peptide to the complex. A recent study suggested a role for C domain binding to the Arp2/3 complex, illustrating that the CA domain of WASP induced a conformational change on Arp2/3 that was abolished upon mutation of Leu 470 to Ala; this C domain mutant was found to be defective in activation but not in its ability to bind Arp2/3 (41).

#### *The A domain*

The A domain is a stretch of about 20-25 residues that consists of an N-terminal group of acidic residues followed by an invariable tryptophan. The number of acidic residues is thought to augment the activity of the VCA region, with an increasing net charge giving rise to an increase in activation of the Arp2/3 complex. It was shown by

NMR that the acidic residues themselves do not bind directly to the complex. The current model for their role in activation is that they negate a stretch of very conserved basic residues along the Arp2 and Arp3 subunits but do not participate directly in making specific contacts with the complex. In fact, a number of activators from different species, especially from worms and fungi, have a neutral net charge. This species variation probably reflects the differences in the conservation of basic residues in the Arp2 and Arp3 subunits. The conserved tryptophan has been hypothesized to bind to a hydrophobic pocket on Arp3 based on homology modeling (42).

### **Mechanism of Activation of the Arp2/3 complex**

It has previously been proposed that when Arp2/3 binds to both a NPF and the side of an actin filament, the NPF also binds actin monomers through its WH2 domain and shuttles them to the actin-like Arp2 and Arp3, forming a nucleus for polymerization (4). While it is tempting to assume that activation relies only upon binding of the four components, multiple lines of evidence support the idea that further activation steps follow complex assembly. First, the crystal structure of the inactive Arp2/3 complex reveals that major conformational rearrangements must occur for Arp2 and Arp3 to form an actin-like dimer capable of nucleating a new filament (23). Second, no correlation was found between affinity of VCA mutants for actin and the Arp2/3 complex and actin nucleation (40,43). Lastly, mathematical modeling showed that an activation step only occurs after assembly of all components to the Arp2/3 complex (25). The nature of this activation step has remained elusive due to the number of components involved, the lack of a high-resolution structure of the activated state as well as the very short time scale in



which this step exists. Chemical crosslinking of VCA to Arp2/3 showed that VCA contacts subunits p21, Arp3, Arp2 and p40 (25). Recent electron microscopy studies suggest that the binding of the VCA peptides to Arp2/3 causes a large conformational change (44,45). It is thought that this change positions Arp2 and Arp3 in an actin-like dimer and that this conformational change is nucleation competent, since the yeast Arp2/3 complex has some activity in the absence of a NPF (44,46). Coronin, the only known inhibitor of the Arp2/3 complex, was shown to locate to the p35 subunit by EM and prevent the rigid body rotation needed to bring the Arps together, further supporting the idea that the conformational change induced by CA is biologically relevant. Both actin filaments and monomers are needed for maximal activation of the Arp2/3 complex and binding of each may contribute to the complexity of the activation step. Filamentous actin binding to the Arp2/3 complex is thermodynamically coupled to the binding of the VCA region and might serve to stabilize the conformational change caused by the VCA region (43,44). However, the Welch lab used a FRET assay to monitor the distance between YFP/CFP tagged p40 and p21 subunits and confirmed that there are major structural changes upon CA binding but saw no change in FRET signal upon titration of filaments (41). There are two interpretations of this result: first, the mother filament may serve only to stabilize the conformation brought upon by the CA region and increase its lifetime. On the other hand, the FRET assay is flawed in that it might not report on structural changes that change the orientation of the FRET pair with respect to the rest of the complex and not the absolute distance between them. It is not known whether the CA-induced conformational change represents the nucleation-competent 'transition state'. We believe that the incoming actin monomer plays a role in inducing the final

conformation as non-polymerizable actin monomers stimulate hydrolysis of ATP on Arp2 (47), a possible consequence of a conformational change during activation. If the model that Arp2 and Arp3 come together to form a short-pitch dimer is correct, our modeling suggests that an actin monomer presented to the Arp2/3 complex would add on in a long-pitch fashion, an orientation which is the most favorable in actin-nucleus formation (Fig. 4). A full understanding of the structural and kinetic basis for the role of monomeric actin is crucial to understanding the mechanism of activation of the Arp2/3 complex.

## Figure Legends

Fig. 1. Structure of ATP- and ADP- bound actin monomer. The polypeptide backbone is shown in gray ribbons, the nucleotide in multi-color stick figure representation, and the  $Mg^{2+}$  (purple) or  $Ca^{2+}$  (blue) ion. Each subdomain is designated by roman numerals. These structures were drawn from pdb entries 1ATN and 1J6Z, respectively.

Fig. 2. Structural polarity of the actin filament. The Holmes model of actin filament structure. Monomers across the filament helix are in a short-pitch orientation and those longitudinally along one protofilament are in the long-pitch orientation.

Fig. 3. Crystal structure of the Arp2/3 complex. A, Ribbon representation of the 2.0 Å resolution structure of the bovine Arp2/3 complex (1K8K). Residues from subdomains 1 and 2 of the Arp2 subunit were modeled using the structure of actin as a reference. B, Connolly surface representation of the structure. Note the horseshoe like appearance as seen by EM and analytical ultracentrifugation.

Fig. 4. Structural model of Arp2/3 activation. The structural changes necessary for Arp2 and Arp3 to form a short-pitch actin like dimer are illustrated. In addition, the two possible orientations for the first “daughter” monomer are shown. The “long-pitch” orientation is favored due to constraints of VCA crosslinking and electron microscopy. If the first monomer added to the complex in the “short-pitch” orientation, it would be impossible for the WH2 domain to bind the monomer and the C domain to bind to the p40 subunit at the same time.

Fig. 5. *A*, Domain layout of WASP/Scar proteins. EVH1, Ena/Vasp Homology 1 domain; B, basic region; GBD, GTPase binding domain; poly-proline, proline-rich region; SHD, Scar Homology domain; V, Verprolin-like or WASP Homology 2 domain; C, central or connecting domain; A, acidic domain. *B*, The structure of the ciboulot-actin complex (1SQK).

## References

1. Kabsch, W., and Vandekerckhove, J. (1992) *Annu Rev Biophys Biomol Struct* 21, 49-76
2. Amos, L. A., van den Ent, F., and Lowe, J. (2004) *Curr Opin Cell Biol* 16(1), 24-31
3. Otterbein, L. R., Graceffa, P., and Dominguez, R. (2001) *Science* 293(5530), 708-711
4. Pollard, T. D., and Borisy, G. G. (2003) *Cell* 112(4), 453-465
5. Sept, D., and McCammon, J. A. (2001) *Biophys J* 81(2), 667-674
6. Dominguez, R. (2004) *Trends Biochem Sci* 29(11), 572-578
7. Wear, M. A., and Cooper, J. A. (2004) *Trends Biochem Sci* 29(8), 418-428
8. Oda, T., Namba, K., and Maeda, Y. (2005) *Biophys J* 88(4), 2727-2736
9. Yarmola, E. G., Somasundaram, T., Boring, T. A., Spector, I., and Bubb, M. R. (2000) *J Biol Chem* 275(36), 28120-28127
10. Dunn, A. Y., Melville, M. W., and Frydman, J. (2001) *J Struct Biol* 135(2), 176-184
11. Baum, B., and Kunda, P. (2005) *Curr Biol* 15(8), R305-308
12. Otomo, T., Tomchick, D. R., Otomo, C., Panchal, S. C., Machius, M., and Rosen, M. K. (2005) *Nature* 433(7025), 488-494
13. Quinlan, M. E., Heuser, J. E., Kerkhoff, E., and Mullins, R. D. (2005) *Nature* 433(7024), 382-388
14. Warrior, R. (1994) *Dev Biol* 166(1), 180-194

15. Tsuda, M., Sasaoka, Y., Kiso, M., Abe, K., Haraguchi, S., Kobayashi, S., and Saga, Y. (2003) *Science* 301(5637), 1239-1241
16. Lankford, K. L., Cypher, C., and Letourneau, P. C. (1990) 2(1), 80-85
17. Machesky, L. M., Atkinson, S. J., Ampe, C., Vandekerckhove, J., and Pollard, T. D. (1994) *J Cell Biol* 127(1), 107-115
18. Welch, M. D., Iwamatsu, A., and Mitchison, T. J. (1997) *Nature* 385(6613), 265-269
19. Winter, D., Podtelejnikov, A. V., Mann, M., and Li, R. (1997) *Curr Biol* 7(7), 519-529
20. Rohatgi, R., Ma, L., Miki, H., Lopez, M., Kirchhausen, T., Takenawa, T., and Kirschner, M. W. (1999) *Cell* 97(2), 221-231
21. Mullins, R. D., Heuser, J. A., and Pollard, T. D. (1998) *Proc Natl Acad Sci U S A* 95(11), 6181-6186
22. Gournier, H., Goley, E. D., Niederstrasser, H., Trinh, T., and Welch, M. D. (2001) *Mol Cell* 8(5), 1041-1052
23. Robinson, R. C., Turbedsky, K., Kaiser, D. A., Marchand, J. B., Higgs, H. N., Choe, S., and Pollard, T. D. (2001) *Science* 294(5547), 1679-1684
24. Volkman, N., Amann, K. J., Stoilova-McPhie, S., Egile, C., Winter, D. C., Hazelwood, L., Heuser, J. E., Li, R., Pollard, T. D., and Hanein, D. (2001) *Science* 293(5539), 2456-2459
25. Zalevsky, J., Lempert, L., Kranitz, H., and Mullins, R. D. (2001) *Curr Biol* 11(24), 1903-1913

26. Nolen, B. J., Littlefield, R. S., and Pollard, T. D. (2004) *Proc Natl Acad Sci U S A* 101(44), 15627-15632
27. Machesky, L. M., and Insall, R. H. (1998) *Curr Biol* 8(25), 1347-1356
28. Welch, M. D., and Mullins, R. D. (2002) *Annu Rev Cell Dev Biol* 18, 247-288
29. Bompard, G., and Caron, E. (2004) *J Cell Biol* 166(7), 957-962
30. Higgs, H. N., Blanchoin, L., and Pollard, T. D. (1999) *Biochemistry* 38(46), 15212-15222
31. Hertzog, M., van Heijenoort, C., Didry, D., Gaudier, M., Coutant, J., Gigant, B., Didelot, G., Preat, T., Knossow, M., Guittet, E., and Carlier, M. F. (2004) *Cell* 117(5), 611-623
32. Demarest, S. J., Martinez-Yamout, M., Chung, J., Chen, H., Xu, W., Dyson, H. J., Evans, R. M., and Wright, P. E. (2002) *Nature* 415(6871), 549-553
33. Safer, D., Sosnick, T. R., and Elzinga, M. (1997) *Biochemistry* 36(19), 5806-5816
34. Toshima, J., Toshima, J. Y., Martin, A. C., and Drubin, D. G. (2005) *Nat Cell Biol* 7(3), 246-254
35. Cory, G. O., Cramer, R., Blanchoin, L., and Ridley, A. J. (2003) *Mol Cell* 11(5), 1229-1239
36. Prehoda, K. E., Scott, J. A., Mullins, R. D., and Lim, W. A. (2000) *Science* 290(5492), 801-806
37. Higgs, H. N., and Pollard, T. D. (2000) *J Cell Biol* 150(6), 1311-1320
38. Rohatgi, R., Ho, H. Y., and Kirschner, M. W. (2000) *J Cell Biol* 150(6), 1299-1310

39. Kim, A. S., Kakalis, L. T., Abdul-Manan, N., Liu, G. A., and Rosen, M. K. (2000) *Nature* 404(6774), 151-158
40. Panchal, S. C., Kaiser, D. A., Torres, E., Pollard, T. D., and Rosen, M. K. (2003) *Nat Struct Biol* 10(8), 591-598
41. Goley, E. D., Rodenbusch, S. E., Martin, A. C., and Welch, M. D. (2004) *Mol Cell* 16(2), 269-279
42. Beltzner, C. C., and Pollard, T. D. (2004) *J Mol Biol* 336(2), 551-565
43. Marchand, J. B., Kaiser, D. A., Pollard, T. D., and Higgs, H. N. (2001) *Nat Cell Biol* 3(1), 76-82
44. Rodal, A. A., Sokolova, O., Robins, D. B., Daugherty, K. M., Hippenmeyer, S., Riezman, H., Grigorieff, N., and Goode, B. L. (2005) *Nat Struct Mol Biol* 12(1), 26-31
45. Martin, A. C., Xu, X. P., Rouiller, I., Kaksonen, M., Sun, Y., Belmont, L., Volkmann, N., Hanein, D., Welch, M., and Drubin, D. G. (2005) *J Cell Biol* 168(2), 315-328
46. Wen, K. K., and Rubenstein, P. A. (2005) *J Biol Chem* 280(25), 24168-24174
47. Dayel, M. J., and Mullins, R. D. (2004) *PLoS Biol* 2(4), E91



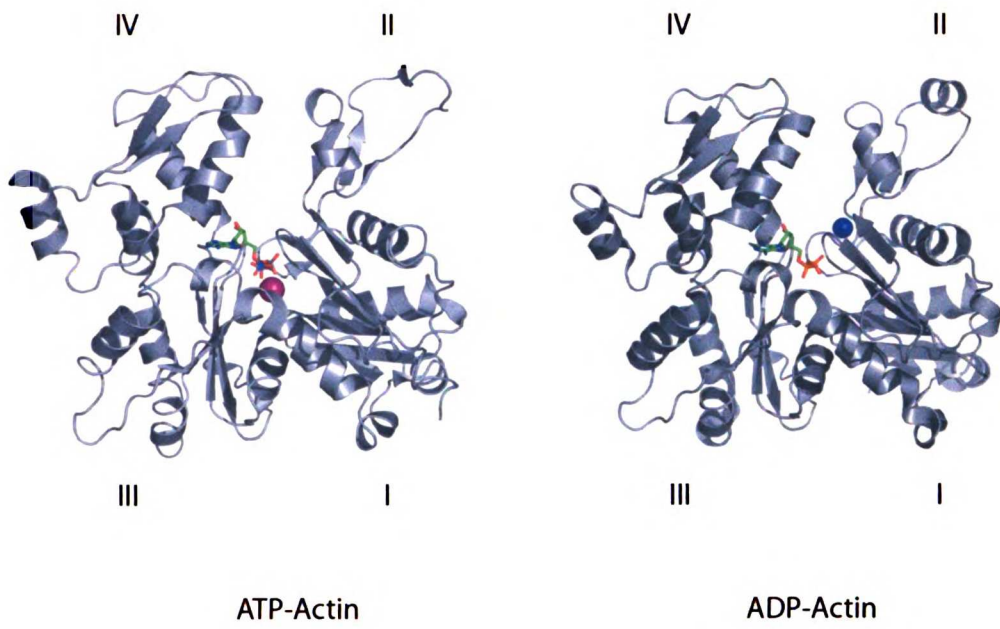


Figure 1

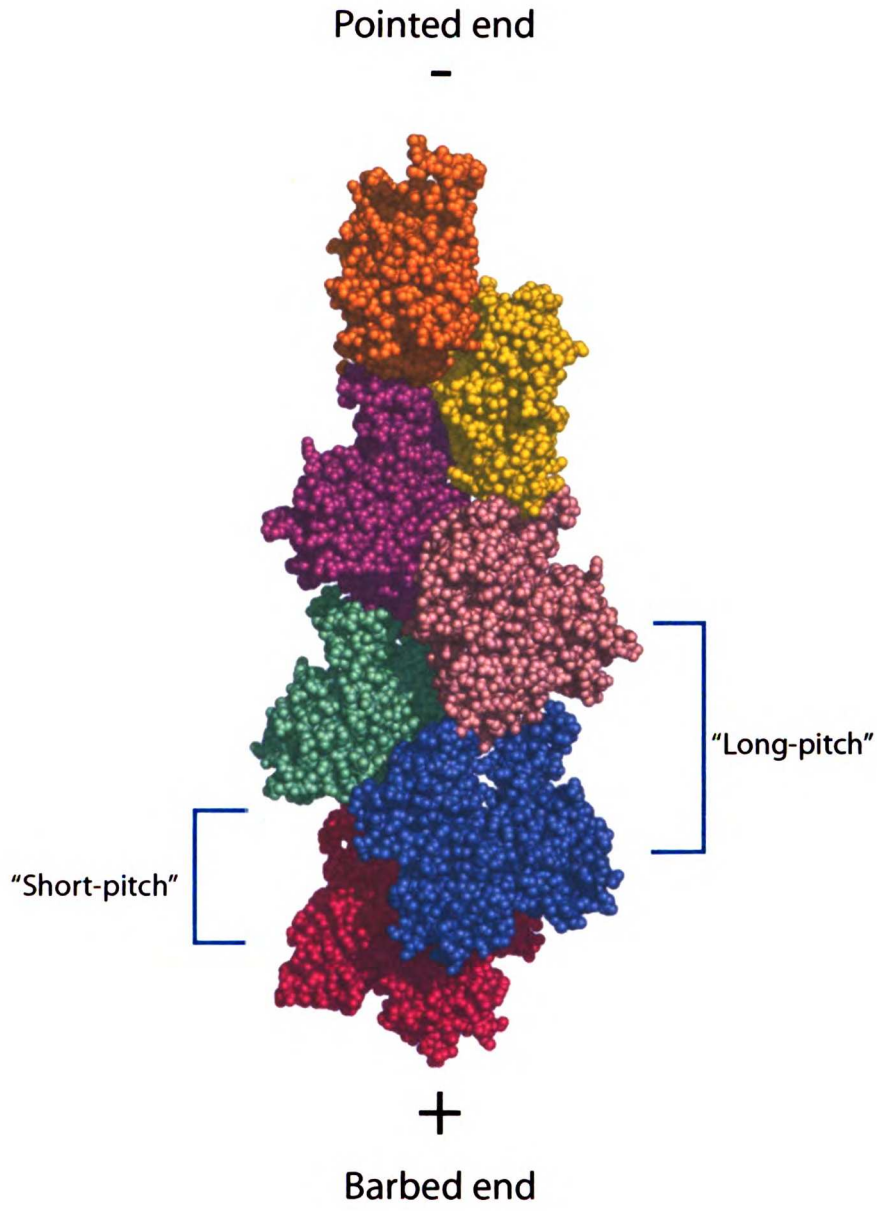


Figure 2

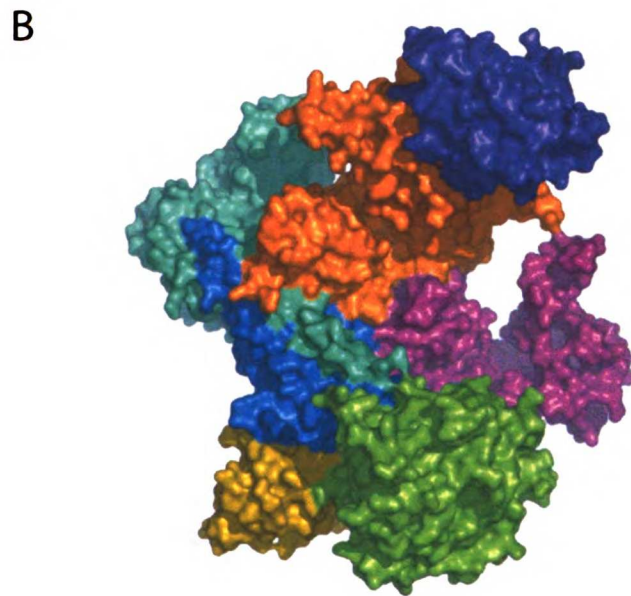
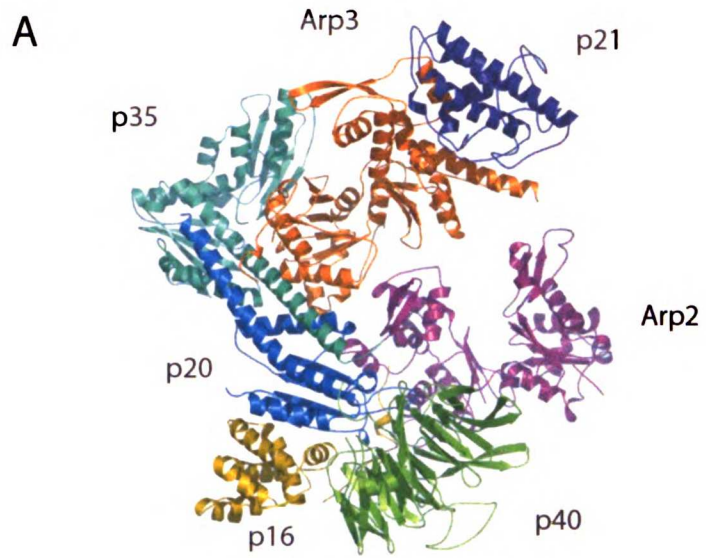


Figure 3

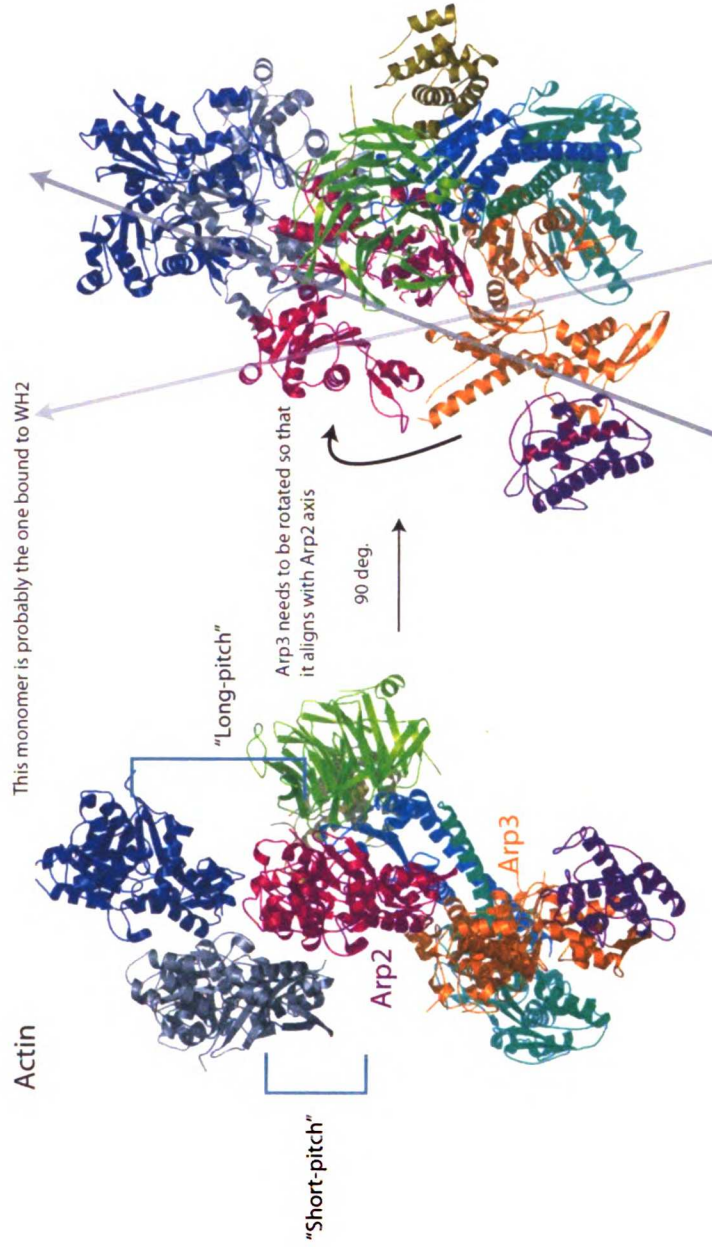
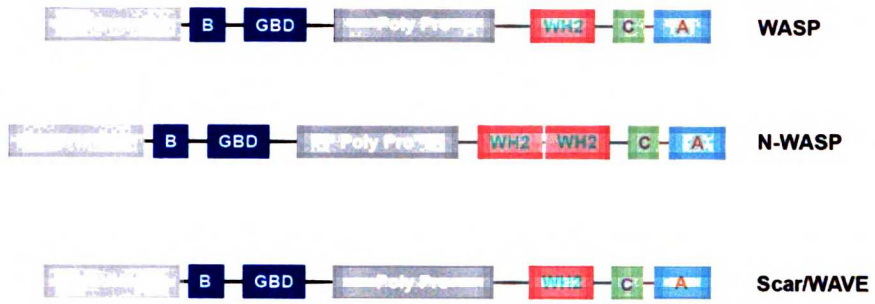


Figure 4

A



B

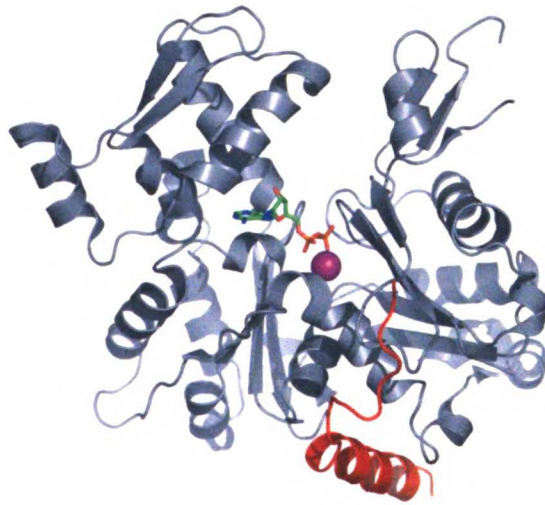


Figure 5

## Chapter 2

### **Actin Binding to the C Domain of WASP/Scar Proteins Plays a Critical Role in the Activation of the Arp2/3 Complex**

This work, currently in review for the *Journal of the Biological Chemistry*, demonstrates that a key step to activation of the Arp2/3 complex is the binding of an actin monomer to the C domain of WASp/Scar activator proteins. In addition, we have structurally defined the Scar WH2 domain and suggest a general mechanism of action for all WH2 containing proteins. The beginnings of the project date back to 1999 when Dyche Mullins, then a new professor at UCSF, came up to Volker Doetsch's lab looking for someone to work on the structure of the WH2 domain bound to actin. At the time, I was juggling five projects and was excited about this one because of my interest in the cytoskeleton. The structural work was made difficult due to the polymerization of actin and I had to work out a number of protocols to achieve high concentrations of monomeric actin suitable for NMR. The structural information we obtained, however, was not enough to answer the broader question of the role of the actin monomer in the activation of the Arp2/3 complex. I then moved to Dyche's lab where the work shifted to a more biochemical approach to get at the mechanism of activation. Initially, I figured out what actin was *not* doing. Due to work done in the past two years, however, we now have a better idea of the mechanism and together with the structural work is the basis of this chapter.

# **Actin Binding to the C Domain of WASP/Scar Proteins Plays a Critical Role in the Activation of the Arp2/3 Complex**

Alexander E. Kelly§, Heather Kranitz#, Volker Dötsch‡ and R. Dyche Mullins#

From the §Graduate Group in Biophysics and #Department of Cellular & Molecular Pharmacology, University of California San Francisco, San Francisco, CA 94143;

‡Institute for Biophysical Chemistry and Centre for Biomolecular Magnetic Resonance, University of Frankfurt, 60439 Frankfurt, Germany

This work was submitted to the *Journal of Biological Chemistry* on July 8<sup>th</sup>, 2005 and is currently under review.

## ABSTRACT

The WASP/Scar family of proteins directs actin filament assembly through the Arp2/3 complex – a multifunctional protein complex that nucleates and crosslinks actin filaments. The C-terminal portion of WASP/Scar proteins (the VCA domain) stimulates nucleation *in vitro* by binding both Arp2/3 and monomeric actin. The VCA domain is composed of an actin-binding WH2 domain (WASP homology 2 or V), an Arp2/3-binding central or connecting (C) and a C-terminal acidic domain (A). Here we describe the determinants for Arp2/3-mediated actin polymerization, and show that actin monomer binding to the C domain of WASP/Scar family proteins is essential for activation of the Arp2/3 complex. Structural analysis of the WH2 and C domains bound to an actin monomer reveals that the WH2-actin interaction is equivalent to the ciboulot-actin interaction previously observed with X-ray crystallography. Monomeric actin binds to the N-terminal half of the C domain, and mutation of conserved hydrophobic residues in the binding interface greatly diminishes Arp2/3-mediated actin polymerization. Furthermore, the C domain binds specifically but with less affinity to the p40 subunit of the Arp2/3 complex and this interaction is mutually exclusive with actin binding. These findings suggest that the C domain does not act as a static molecular bridge between actin and Arp2/3, but rather is in a dynamic equilibrium between the two bound states serving to initiate Arp2/3 complex activation.



## INTRODUCTION

The rapid assembly of actin filaments is necessary for many fundamental processes such as cell motility and endocytosis, as well as pathogenic invasion (1,2). Actin-based motility is mediated by the evolutionarily conserved, seven-subunit Arp2/3 complex, which nucleates the formation of new actin filaments. The Arp2/3 complex binds to the sides of pre-existing actin filaments, from which new filaments grow with a characteristic branch angle of 70 degrees optimal for force production (3,4).

*In vitro*, purified Arp2/3 complex has weak nucleating ability, and its activation requires four components: the Arp2/3 complex, a nucleation promoting factor (NPF), filamentous actin and monomeric actin (5,6). The NPFs include the WASP/Scar family of proteins WASP (Wiskott Aldrich Syndrome Protein), N-WASP (Neuronal-WASP) and Scar/WAVE (Suppressor of Cyclic AMP Receptor or Wiskott Aldrich Verprolin homologous protein) as well as the *S. cerevisiae* protein Bee1 and *Listeria monocytogenes* protein ActA (1,7). Many of these multi-domain proteins are regulated by small GTPases that serve to link the Arp2/3 complex to signaling cues. The C-terminal VCA region of WASP/Scar family proteins, which contain a verprolin homology (V) or WH2 (WASP homology 2) domain that binds actin monomers, and central (C) and acidic (A) regions that bind to Arp2/3, stimulate the actin-nucleating activity of the Arp2/3 complex (1) (Fig. 1). It has previously been proposed that when Arp2/3 binds to both a NPF and the side of an actin filament, the NPF also binds actin monomers through its WH2 domain and shuttles them to the actin-like Arp2 and Arp3, forming a nucleus for polymerization (1).

While it is tempting to assume that activation relies only upon binding of the four

components, multiple lines of evidence support the idea that further activation steps follow complex assembly. First, the crystal structure of the inactive Arp2/3 complex reveals that major conformational rearrangements must occur for Arp2 and Arp3 to form an actin-like dimer capable of nucleating a new filament (8). Second, no correlation was found between affinity of VCA mutants for actin and the Arp2/3 complex and actin nucleation (6,9). Lastly, mathematical modeling showed that an activation step only occurs after assembly of all components to the Arp2/3 complex (10). The nature of this activation step has remained elusive due to the number of components involved, the lack of a high-resolution structure of the activated state as well as the very short time scale in which this step exists. Chemical crosslinking of VCA to Arp2/3 showed that VCA contacts subunits p21, Arp3, Arp2 and p40 (10). Recent electron microscopy studies suggest that the binding of the VCA peptides to Arp2/3 causes a large conformational change (11,12). It is thought that this change positions Arp2 and Arp3 in an actin-like dimer and that this conformational change is nucleation competent, since the yeast Arp2/3 complex has some activity in the absence of an NPF (11,13). Both actin filaments and monomers are needed for maximal activation of the Arp2/3 complex and binding of each may contribute to the complexity of the activation step. Filamentous actin binding to the Arp2/3 complex is thermodynamically coupled to the binding of the VCA region and might serve to stabilize the conformational change caused by the VCA region (6,11). The role of monomeric actin, shown in WASP to bind to the CA region with low affinity (6) appears to be more complex, as non-polymerizable actin monomers stimulate hydrolysis of ATP on Arp2 (5), a possible consequence of a conformational change during activation (12). A full understanding of the structural and kinetic basis for the role

of monomeric actin is crucial to understanding the mechanism of activation of the Arp2/3 complex.

The C domain is an amphipathic peptide highly conserved among all NPFs and is a potential hotspot for regulation that translates upstream signals to activation of the Arp2/3 complex (9,14-17). Deletions and mutations in the C domain cause major defects in the nucleation promoting ability of Arp2/3 (6,9,17), while phosphorylation serves to augment Arp2/3 activity *in vitro* and *in vivo* (18). Furthermore, C domain binding to the GTPase binding domain (GBD) promotes autoinhibition of WASP and N-WASP (14-16), while *trans* inhibition may occur through the C domain in Scar proteins upon binding to the Nap125-Abi complex (9,19). The C domain adopts a helical conformation upon binding the GBD, with all conserved hydrophobic residues making important contacts (20). In context of the full-length VCA peptide, these same residues were shown by nuclear magnetic resonance (NMR) analysis to make multiple contacts with Arp2/3 (9). Additionally, there is no correlation between affinity for the Arp2/3 complex and nucleation promoting activity of C domain mutants. This further supports the model that there is an activation step subsequent to binding of the VCA peptide to the complex. A recent study suggested a role for C domain binding to the Arp2/3 complex, illustrating that the CA domain of WASP induced a conformational change on Arp2/3 that was abolished upon mutation of Leu 470 to Ala; this C domain mutant was found to be defective in activation but not in its ability to bind Arp2/3 (21).

Here we report a structural and biochemical analysis of the requirements of activation of Arp2/3 and the role of actin monomer binding in this mechanism. First, we define the C domain of WASP/Scar family proteins as a unique actin monomer binding

site that plays a key role in coordinating actin and Arp2/3. Second, we show that the WH2 domain is structurally related to the ciboulot actin binding domain. Lastly, we find that the C domain contacts the p40 subunit of Arp2/3 and this binding is mutually exclusive with actin binding, giving further insight into the activation mechanism of the Arp2/3 complex.

## MATERIALS AND METHODS

### *Plasmid Construction and Protein Purification*

All Scar1 and N-WASP plasmids were constructed by PCR using full-length human Scar1 (gift of Laura Machesky) and rat N-WASP (gift of Wendell Lim). All clones were verified by sequencing. Proteins were expressed in BL21 (pLysS) cells as C-terminal His<sub>6</sub>, N-terminal GST fusions or both, where indicated in the text. For uniform labeling with <sup>15</sup>N and <sup>2</sup>H, BL21 (pLysS) cells freshly transformed with Scar1 VC or VCA expression plasmids were grown in either Silantes [<sup>15</sup>N, <sup>2</sup>H] or [<sup>15</sup>N] OD2 media (Cambridge Isotope Laboratories, Cambridge, MA). For residue specific labeling, cells were grown in M9 minimal media containing uniformly labeled <sup>15</sup>N amino acid (lysine, arginine, alanine, isoleucine, leucine, valine) (Cambridge Isotope Laboratories). Expression of all proteins was induced by the addition of IPTG to a final concentration of 0.5 mM. After expression for 3 h, the cells were harvested by centrifugation, resuspended and disrupted by microfluidization and supernatants collected by centrifugation at 10,000 x g for 45 min. His<sub>6</sub> tagged proteins were isolated under either native or denaturing conditions on Ni-NTA resin. GST fusions were bound to

glutathione-agarose beads and cleaved off the column using either thrombin or PreScission Protease. All proteins were further purified by chromatography on MonoQ resin (Amersham Biosciences, Piscataway, NJ) and verified for molecular weight using MALDI-TOF mass spectrometry. Tag-free peptides were obtained from Synpep Corporation (Alameda, CA) and were >95% pure. Arp2/3 and actin were purified from *Acanthamoeba castellanii* (5,22) and was pyrene labeled as described (23).

#### *Fluorescent Labeling*

Purified proteins were exchanged into HEK buffer (50 mM KCl, 1 mM EDTA, 10 mM HEPES, pH 7.3) using a NAP-5 column, and incubated with a 4-7-fold molar excess of Alexa-488 C<sub>5</sub> maleimide (Molecular Probes, Eugene, OR) for 1 h at room temperature and overnight at 4°C. Samples were spun at 65,000 rpm, and the supernatant was chromatographed on a G-25 column to remove unreacted dye. MALDI-TOF was used to monitor percent labeling.

#### *Actin Polymerization*

All pyrene actin polymerization assays were performed with *Acanthamoeba* actin (6% pyrene labeled) in 50 mM KCl, 1 mM MgCl<sub>2</sub>, 1 mM EGTA, 10 mM HEPES, pH 7.0. Ca<sup>2+</sup>-actin was converted to Mg<sup>2+</sup>-actin prior to each polymerization reaction by a 2 minute incubation with 50 μM MgCl<sub>2</sub>, 200 μM EGTA. Fluorescence studies were conducted on the K2 Multifrequency Fluorometer. Data were analyzed using KaleidaGraph (Synergy Software, Reading, PA).

#### *Polarization Anisotropy*

Fluorescence studies were conducted on a K2 Multifrequency Fluorometer (ISS, Champagne, IL) at 25°C. The samples contained KMEH buffer (10 mM Na-HEPES, pH

7.0, 50 mM KCl, 1 mM EGTA and 1 mM MgCl<sub>2</sub>). For anisotropy measurements, fixed concentrations of Alexa-488-labeled Scar1 VCA, CA or C peptides were mixed with various concentrations of either the Arp2/3 complex, latrunculin-stabilized actin or both, and the data were fitted to a single-site binding isotherm to determine  $K_d$ . Alexa-488 was excited with polarized light at 493 nm and the emitted light was detected at 525 nm. Affinities of unlabeled peptides for either the Arp2/3 complex or actin were determined by competition with Alexa-488-labeled wild-type Scar1 VCA, CA or C peptides. Anisotropy data were fit to a full solution of the equilibrium competition binding equation using KaleidaGraph (6).

#### *Crosslinking*

Proteins were dialyzed into 50 mM KCl, 1 mM MgCl<sub>2</sub>, 1 mM EGTA, and 10 mM imidazole (pH 7.0) at 25°C to facilitate crosslinking. The indicated protein concentrations were mixed with freshly prepared 1-ethyl-3-(3-dimethylaminopropyl)-carbodiimide hydrochloride (EDC) and N-hydroxysuccinimide (NHS) for 30 min at room temperature. Samples were methanol/chloroform precipitated and analyzed by Western blotting with monospecific antibodies against the Arp2/3 complex subunits, or fluorescence imaging of Alexa-488 labeled C domain.

#### *NMR Spectroscopy*

NMR experiments were carried out at 30°C on Bruker DRX 500 MHz or 600 MHz spectrometers equipped with a triple-resonance Z-axis gradient CryoProbe. Unbound [<sup>15</sup>N]-VCA, residue selectively <sup>15</sup>N-labeled VC and [<sup>15</sup>N, <sup>2</sup>H]-VC samples each contained 400 μM protein in 90% H<sub>2</sub>O/10% D<sub>2</sub>O with modified G-actin buffer (buffer A: 50 mM d<sub>6</sub>-Na-HEPES (Cambridge Isotope Laboratories) pH 7.5, 100 μM CaCl<sub>2</sub>, 100 μM

ATP and 0.5 mM TCEP). For studies of actin bound peptides, 5 mLs ~50  $\mu$ M G-actin were exchanged into 2 mM  $d_6$ -Na-HEPES pH 7.5, 10  $\mu$ M ATP by Nap-5 chromatography and immediately lyophilized. The lyophilized powder was then resuspended in a solution containing 300  $\mu$ L of 400  $\mu$ M peptide in buffer A containing 600  $\mu$ M latrunculin B (Calbiochem). Samples were spun at 100,000 x g for 30 min resulting in a final actin concentration of 500  $\mu$ M. Assignments of residues in VC were obtained using a combination of [ $^{15}\text{N}$ , $^1\text{H}$ ]-HSQC (Heteronuclear Single Quantum Coherence), [ $^{15}\text{N}$ ,  $^1\text{H}$ ] TROSY-HSQC (Transverse Relaxation Optimized Spectroscopy), 3D [ $^{15}\text{N}$ , $^1\text{H}$ ] NOESY-HSQC, 3D [ $^{15}\text{N}$ , $^1\text{H}$ ] TROSY-NOESY-HSQC experiments (Nuclear Overhauser Effect Spectroscopy) (24) on [ $^{15}\text{N}$ ]-VCA, [ $^{15}\text{N}$ , $^2\text{H}$ ]-VCA, residue selectively  $^{15}\text{N}$ -labeled VC and [ $^{15}\text{N}$ , $^2\text{H}$ ]-VC samples bound to monomeric actin. NOESY mixing times were 80 ms and 120 ms. Data were processed using NMRPipe (25) and analyzed using XEASY (26).

## RESULTS

### *Secondary structure and interacting residues of the WH2-C-actin complex*

The binding of an actin monomer to a NPF and ultimately the Arp2/3 complex are essential steps involved in the mechanism of action of the Arp2/3 complex (1). As a first step towards understanding these events, we sought to define the minimal actin-binding region of the human Scar1 VCA peptide. Using a fluorescence polarization anisotropy competition assay, we measured the affinities of C-terminal truncation mutants of VCA for monomeric actin relative to that of the full-length labeled peptide (Table I). Removal of the A domain of Scar1 (VC) as well as removal of the last five residues of the C

domain (VCA5, residues 489-538) has no effect on actin binding. There is a 10-fold difference in binding affinities, however, for monomeric actin between the isolated WH2 domain and Scar1 VCA5 (3.1  $\mu\text{M}$  vs. 0.35  $\mu\text{M}$ , respectively). Therefore, we define the minimal actin-binding domain as VCA5 of human Scar1.

We then used NMR spectroscopy to determine the identity and secondary structure of  $^{15}\text{N}$ -labeled residues in Scar1 VC bound to an unlabeled actin monomer. VC was used instead of VCA5 because of its higher solubility. First, we used [ $^{15}\text{N}$ , $^1\text{H}$ ] TROSY-HSQC spectra to look for structural differences between free Scar1 VC and Scar1 VC bound to monomeric actin. Based on chemical shift dispersion, we found that 29 residues in Scar1 VC bind actin (Figs. 2A, 2B, S1). Changes in the chemical shift of a number of residues saturated at equimolar amounts of actin and Scar1 VC, consistent with formation of a 1:1 complex.

To better understand the structural changes that occur in VC upon binding actin, we collected [ $^{15}\text{N}$ , $^1\text{H}$ ] TROSY-NOESY spectra of VC bound to the 43 kDa actin monomer (Fig. 2C). Due to the high correlation time of the actin-VC complex, 100% deuteration of the VC peptide was required to reduce the relaxation time and produce NOEs with sharp linewidths, limiting information available to amide-amide intra-residue and inter-residue amide- $\text{H}\alpha$  NOEs. A combination of TROSY pulse sequences, 100% deuteration, buffer optimization (27) and use of a cryoprobe enabled us to acquire high-quality NOESY spectra at protein concentrations of 150-400  $\mu\text{M}$ . From the observed NOEs we determined direct connectivity of a number of residues. Consistent with previous reports (6,9), our data indicates that the VC domain by itself is unfolded and that about 60% of the VC peptide adopts a helical conformation upon binding actin.



We assigned the NOESY spectra and determined which residues of Scar1 VC contact actin by using residue-specific labeling strategies. Seven separate isotope-labeled samples of Scar1 VC were prepared each with a different  $^{15}\text{N}$ -labeled amino acid: alanine, valine, isoleucine, lysine, arginine, leucine, and glycine. The HSQC spectra of each labeled peptide alone and in complex with actin revealed which residues undergo significant chemical shift changes and line broadening upon binding actin (Fig. 2D). Such changes in the NMR spectra indicate the involvement of these amino acids in the binding interface. We correlated chemical shifts in the bound state with NOEs to partially assign the VC peptide. The entire WH2 domain (residues 498-522) was assigned using sequential NOEs and residue labeling. The presence of strong amide-amide NOEs indicates that the WH2 domain is helical. The intensity of the NOEs decreases dramatically at a position immediately C-terminal to the highly conserved Gly 512 and completely disappears at the C-terminal end of the canonical WH2 domain (Val 514), indicating that this region is either dynamic or in an ordered yet non-helical conformation (Fig. 2A). We observed two inter-residue amide-aliphatic NOEs between actin and Scar1 VC, one at residue Leu 502 and another at Arg 518. Both residues are highly conserved and are required for actin binding. As NOEs are short-range dipole-dipole interactions limited to distances of up to 5-7 Å, our data indicate that these residues in Scar1 VC are in direct contact with the actin monomer (Fig. 2A).

Consistent with our binding data above (Table I), a number of residues in the C domain undergo actin-induced chemical shift changes and line broadening (Fig. 2A). In addition, spectra of the isolated C domain show chemical shift changes and decreases in peak intensity upon binding actin (Fig. S1). Unlike the WH2 region, however, we detect

no amide-amide NOEs in the NOESY spectra of the C domain, either alone or together with the WH2 domain (Fig. 2A). The lack of NOEs between these residues indicates that the C domain is either non-helical or highly dynamic when bound to actin. Previous studies (9) found that the equivalent region in WASP becomes helical in the auto-inhibited state and suggested that the C domain is helical when bound to the Arp2/3 complex. We find no evidence that the C domain adopts a helical conformation when bound to actin but this does not exclude the possibility that a helix forms upon binding the Arp2/3 complex.

#### *Binding and activation properties of VCA truncations*

Based on our NMR data it appears that actin is binding to residues within the C domain that have previously been shown to be important for activation of the Arp2/3 complex (6,9,17). To confirm this, we tested whether the isolated C domain binds actin directly by fluorescence polarization anisotropy (Fig. 3A). A C-terminal cysteine was engineered into the isolated C domain and covalently linked to the fluorescent dye Alexa-488. Titration with actin caused a saturable increase in the anisotropy of the labeled C domain from 0.08 to 0.19. This increase is consistent with a single actin monomer binding to the C domain (Fig. 3A, inset). Fitting this curve to a single site hyperbola gave a  $K_d$  of 13.4  $\mu\text{M}$ . A competition assay for actin between unlabeled and labeled C domain yielded a  $K_d$  of 12.2  $\mu\text{M}$  for unlabeled peptide (data not shown), indicating that the dye has no significant effect on actin binding.

It has been previously reported that, under certain conditions, both the VC and CA domains of WASP can weakly stimulate Arp2/3 mediated actin polymerization

(6,28). Given the fact that both actin and Arp2/3 bind to residues in the C domain it is possible that these interactions allow the VC and CA peptides to retain some nucleation promoting activity. To this end, we measured the activities of multiple deletion constructs of Scar1 VCA (Table I) using pyrene-actin assembly assays. Removal of the WH2 domain from Scar1 VCA (Scar1 CA) significantly reduces the nucleation activity but does not completely abolish it, whereas removal of the acidic domain (Scar1 VC) abolishes nucleation activity entirely (Fig. 3B, Table I). Hufner et al. (28) previously reported that the VC domain of WASP fused to GST weakly promotes nucleation. In the present study, however, we used an untagged, monomeric version of the peptide. We believe the difference in results can be attributed to the dimerization of GST, which has been shown previously to artifactually increase the activity of VCA (29). Therefore, it appears that the CA region retains the minimal activating properties of Scar1 and that the WH2 domain serves to increase the stimulatory effects of the peptide *in vitro*. Consistent with this idea, insertion of flexible peptide linkers composed of glycine and serine residues (up to 8 Gly-Ser pairs) between the WH2 domain and the CA region of the VCA peptide had little effect on the kinetics of Arp2/3 mediated actin polymerization (Fig. 3C).

Addition of 150  $\mu$ M C domain peptide (~40:1 ratio of C domain:actin) inhibits the spontaneous polymerization of actin monomers but does not alter the polymer concentration as judged by pyrene fluorescence (Fig. 3D, data not shown). This agrees with previous data showing that VCA and WH2 peptides both inhibit spontaneous polymerization without sequestering actin monomers (30). Interestingly, the C domain increases the lag time of VCA/Arp2/3-mediated actin polymerization and, qualitatively,

appears to decrease the rate of ends generated in a dose dependent manner. Together, these results describe a new activity of the C domain, inhibition of spontaneous polymerization, and highlight its importance in Arp2/3 activation.

We next attempted to understand how the affinity of the V, C and A regions for actin and Arp2/3 each contribute to nucleation promoting activity. We measured the affinities of multiple deletion constructs of Scar1 VCA for actin and Arp2/3 using fluorescence anisotropy competition assays (Table I). Panchal et al. (9) reported that upon titration of a  $^{15}\text{N}$  labeled N-WASP VCA peptide with the Arp2/3 complex, residues within both the C and A domains undergo line-broadening indicative of binding to the complex (Fig. 2A). By both polarization anisotropy and tryptophan fluorescence, we find that the C domain alone binds very weakly to the Arp2/3 complex ( $K_d > 200 \mu\text{M}$ ) (Table I). By itself, the acidic domain (A) binds the Arp2/3 complex with micromolar affinity. Combining the A and C regions (CA) increases the affinity for the complex 8-fold compared to the isolated A region. This difference in binding energy is consistent with an affinity of the C domain for the Arp2/3 complex of approximately  $500 \mu\text{M}$ , indicating that C domain binding to the Arp2/3 complex is coupled to A domain binding. In our hands, the CA region is the smallest contiguous fragment that binds to both actin and the Arp2/3 complex and has the ability to stimulate the Arp2/3 complex.

#### *Actin and Arp2/3 bind to the C domain in a mutually exclusive manner*

One simple hypothesis for the role of the C domain in activation of the Arp2/3 complex is that it acts as a molecular bridge between monomeric actin and the Arp2/3 complex and positions the first monomer of the daughter filament in the proper

orientation on the complex. To test this “molecular bridge” hypothesis we used Alexa-488 labeled CA to monitor whether actin and Arp2/3 can bind simultaneously to the Scar1 C domain (Fig. 4A). We added 1  $\mu\text{M}$  Arp2/3 complex to 20 nM fluorescently labeled CA peptide (~50% bound) and then titrated in latrunculin-bound actin monomers up to high concentrations (100  $\mu\text{M}$ ). Addition of monomeric actin decreased anisotropy to a value between that of CA bound to Arp2/3 and CA bound to actin, as actin binding to the C-terminally labeled CA peptide does not greatly increase the anisotropy compared to peptide alone. This suggests that a significant fraction of the Arp2/3-bound CA is released (Fig. 4A). The Arp2/3 complex should still bind to the A domain, albeit with a lower affinity (Table I), due to its interaction with the highly conserved tryptophan in the A domain. Consistent with this idea, addition of excess unlabeled A peptide (40  $\mu\text{M}$ ) following the titration with monomeric actin caused a further saturable decrease in anisotropy to the level of actin plus CA alone. The apparent  $K_d$  calculated from the titration with actin is ~10  $\mu\text{M}$ , which agrees well with our direct binding measurements yielding an affinity of 12.2  $\mu\text{M}$  (Table I). These data are inconsistent with a role for the C domain in docking an actin monomer onto the Arp2/3 complex.

#### *C domain crosslinks to p40 of Arp2/3*

To better understand the interaction of the C domain with the Arp2/3 complex, we crosslinked Alexa-488 labeled C domain to the Arp2/3 complex using the zero-length crosslinker EDC in the presence of NHS. Crosslinked species were separated by SDS-PAGE and detected with a fluorescence imager (Fig. 4B). In the presence of the Arp2/3 complex EDC/NHS produces a single new fluorescent C domain-containing band of

about 45 kDa. Blotting with antibodies against Arp3, Arp2, p35 and p40 indicate that this band represents the C domain crosslinked to the p40 subunit of the complex. Addition of monomeric actin decreased crosslinking to p40, consistent with competition between actin and Arp2/3 for the C domain (Fig. S2). Finally, no new crosslinks were formed between the C domain and the Arp2/3 complex in the presence of phalloidin-F-actin, latrunculin-actin monomers or excess A peptide (Fig. S2, data not shown), further corroborating the finding that there is no Arp2/3-C-actin complex formed.

*Perturbation of C domain binding to actin, but not to Arp2/3, correlates with decreased nucleation promoting activity*

A comparison of the residue-specific data on Arp2/3, actin and GBD binding to the VCA peptide suggests that the binding sites for all three proteins overlap in the C domain (Fig. 2A). To understand the role of each binding event, we performed alanine scanning mutagenesis on the entire C domain and determined the ability of each mutant to activate the Arp2/3 complex (Figs. 5A, B; Table I). Several studies report that residues in the C domain are important for the activity of WASP/Scar family proteins (6,9,17). We find that every conserved hydrophobic residue in the C domain and both arginines at the C-terminal end are important for NPF activity (Figs. 2A, 5B).

Previous studies of similar mutants in the VCA region of N-WASP found no correlation between Arp2/3 activation and affinity for the Arp2/3 complex (9). Since many of the conserved residues in the Scar1 C domain involved in Arp2/3 activation also bind directly to actin monomers, we determined the affinities of mutants with the lowest activity for both actin and the Arp2/3 complex using fluorescence polarization anisotropy

(Table I, Fig. S3). Loss of nucleation activity correlated directly with perturbation of the affinity of the C domain for monomeric actin. The V531D mutation caused a 5-fold decrease in affinity for actin, while surprisingly, the L535A mutation caused a 3.5-fold increase in affinity for actin. Both mutations produce a 10-fold reduction in the number of filament ends generated in Arp2/3 complex activation assays. We observed no such correlation between nucleation promoting activity and affinity for the Arp2/3 complex, with neither mutation causing more than a two-fold decrease in affinity for the Arp2/3 complex. In addition, a C domain peptide containing the V531D mutation has no effect on spontaneous polymerization or VCA/Arp2/3 mediated actin polymerization (Fig. 3D).

## DISCUSSION

### *Structure and function of the WH2 domain*

The WH2 domain was originally identified as a sequence of approximately 25 residues at the C-terminal end of WASP family proteins that binds actin monomers with micromolar affinity. The WH2 domain binds monomers at the barbed-end and prevents spontaneous nucleation but does not alter their association with the fast-growing barbed end of existing filaments. This combination of activities makes the WH2 domain and related sequences a useful actin-binding module found in many different proteins (>30 proteins, SMART Database (31)) that alter cytoskeletal organization in different ways. Thymosin  $\beta$ 4 and tetra-thymosin  $\beta$ 4, for example, contain WH2-like sequences that help to sequester actin monomers and prevent filament assembly (32); ciboulot contains variant WH2 motifs that inhibit filament nucleation but promote filament elongation (33);

espin and MIM each contain WH2 sequences that promote formation and elongation of actin bundles (34,35); Spir-family proteins contain multiple WH2s that collaborate to nucleate new actin filaments (36); and finally, in WASP-family proteins the canonical WH2 motif plays a role in activating the Arp2/3 complex. Understanding the structure and function of this domain alone and in the context of nearby regulatory elements, therefore, will give us insight into several different classes of cytoskeletal regulatory mechanism.

Using NMR, we have shown that the Scar1 WH2 domain by itself is unfolded and that it acquires secondary structure upon binding monomeric actin. This disorder-to-order transition is advantageous in that it allows for high-specificity with micromolar affinity. Structurally, the Scar1 WH2 domain is defined by an N-terminal helix of 10-16 residues C-terminally capped by 2-5 helix breaking residues immediately followed by a four-residue L++ $\phi$  motif in an extended conformation (where L is a leucine, + an arginine or lysine and  $\phi$  any hydrophobic residue) (Fig. 2A). The helix is defined by a  $\phi\phi x\phi$  motif found in many other helical peptides that engage in protein-protein interactions, such as the nuclear hormone co-activator GRIP1 and transcriptional co-activator CBP/p300 (37). The helix-breaking residues are usually glycines (found in all WH2 domains from WASP/Scar1 proteins), prolines and aspartate. Comparing our data with the recent X-ray crystallographic structure of the ciboulot D1-actin complex and the NMR derived model of the thymosin  $\beta$ 4-actin complex reveals that both domains are structurally homologous to the WASP family WH2 domains (Fig. 6A) and use analogous residues to interact with actin. In particular we find that Leu 501 and Arg 512 in the Scar1 WH2 domain directly contact the actin monomer (Fig. 2A). The equivalent



residues in ciboulot (Val 14 and Lys 31) and thymosin (Met 6 and Lys 18) sit directly in the binding interface in their respective structural models (33,38,39).

Two factors appear to underlie the functional diversity of WH2-containing proteins: 1) the number of tandem WH2 sequences present, and 2) the structural and functional diversity of sequences adjacent to the WH2 domain, particularly on the C-terminal side. Spir, for example, contains four WH2 domains, linked by unstructured sequences. Individually each Spir WH2 domain potently inhibits spontaneous nucleation. Efficient filament nucleation requires at least two of the Spir WH2 domains to be linked in tandem. The third linker region of Spir (L3), however, can weakly nucleate new actin filaments on its own and is believed to stabilize actin dimers (36). These results illustrate that both the WH2 domain and its nearby residues are important for activity. Thymosin  $\beta$ 4 contains a single N-terminal WH2-like motif followed by a helical C-terminal region that binds the pointed-end of an actin monomer. This combination of barbed- and pointed-end binding effectively sequesters actin monomers and inhibits polymerization. It was proposed that for ciboulot and thymosin the WH2 domain consists of the secondary structure elements described above as well as the actin-binding peptides C-terminal to the  $L++\phi$  motif. Mutation of residues 20, 21, 35, and 36 of thymosin  $\beta$ 4 changed the activity of the peptide from G-actin sequestration to allowing polymerization from the barbed-end of a filament (33). This change correlated to a much weaker binding of the C-terminal extension to the actin monomer, effectively leaving the WH2 domain as the primary binding determinant. The primary structures and binding modes of the C-terminal extensions of all WH2 domain-containing proteins are not conserved (Fig. 6B), giving rise to diverse activities.

WASP family proteins contain either one or two WH2 domains but there is no strong correlation between nucleation promoting activity and number of WH2 domains present. Rather, it is the sequence on the C-terminal side of the WH2 domain – the C domain - that appears to determine its role in Arp2/3 activation. As we have shown, the C domain plays a crucial role in actin nucleation.

*Actin and Arp2/3 binding by the C domain*

Three lines of evidence suggest a critical role for the C domain in the activation of the Arp2/3 complex: 1) The region is highly conserved in all WASP-family proteins; 2) Mutation of conserved residues decreases nucleation promoting activity; and 3) in WASP and N-WASP, interaction of the GBD with the C domain strongly inhibits nucleation-promoting activity. Despite its importance, however, the role of the C domain in Arp2/3 activation is not well understood. We find that both actin monomers and the Arp2/3 complex bind to the C domain and we propose that it may coordinate their interaction.

Previous results indicated that residues in the WASP/Scar family C domain interact directly with, and promote a conformational change within the Arp2/3 complex. The crystal structure of the inactive Arp2/3 complex reveals that major conformational rearrangements must occur for Arp2 and Arp3 to form an actin-like dimer capable of nucleating a new filament (8). In lower-resolution structural models based on electron microscopy, the Arp2/3 complex appears in at least three conformations: open, intermediate, and closed (11,12). Binding of full-length WASP promoted appearance of the closed state of the Arp2/3 complex. Moreover, a FRET assay demonstrated that a wild-type CA peptide from N-WASP induces a conformational change in the Arp2/3

complex that brings the p40 and p21 subunits (and presumably the Arp2 and Arp3 subunits to which they are connected) into closer proximity (21). These authors also found that mutation of a conserved hydrophobic residue in the C domain, L470A (equivalent to V531D in Scar1 (9)), abolishes the ability of the construct to induce a conformational change. This result is consistent with a report that residues in the C domain directly interact with the Arp2/3 complex (9). This C domain-dependent conformational change may correspond to the rate-limiting 'activation' step in Arp2/3-dependent nucleation (10).

There is at present no high-resolution structural model for the interaction between VCA domains and the Arp2/3 complex. We showed previously that WASP-family CA domains crosslink to multiple subunits of the Arp2/3 complex: p40, Arp2, Arp3 and p21 (10). Here, we find that zero-length chemical crosslinkers crosslink the C domain to the p40 subunit. The p40 subunit contains multiple WD40-like repeats. These repeats are found in many signaling proteins and mediate numerous types of protein-protein interactions, particularly with highly conserved disordered regions. Previously it was shown that within the yeast Arp2/3 complex, the p40 subunit provides most of the binding energy for the CA peptide, and isolated p40 binds VCA with near wild-type affinity (40). This model is not consistent with previous crosslinking studies or our data showing that the C domain provides little binding energy for the Arp2/3 complex. The recent EM model of full length yeast WASP bound to the Arp2/3 complex shows a large mass located at the junction between p40, Arp2 and Arp3 (11,12). In addition to these results, Weaver et al. (41) provide evidence that the highly-conserved tryptophan found in the C-terminal portion of the A domain of all Arp2/3 activators interacts with the Arp3

subunit. From these results we propose an orientation for the CA peptide on the Arp2/3 complex (Fig. 7). The N-terminal region interacts specifically with the p40 subunit and the A domain stretches from this site on p40 to Arp3, where the conserved tryptophan in the acidic domain might fit into a hydrophobic pocket (42).

Our NMR studies identify residues in the N-terminal half of the C domain that directly contact actin (Figs. 2A, S1, Table I) and also indicate that the C domain binds monomeric actin in an extended, non-helical conformation and that the C and WH2 domains bind simultaneously. Furthermore, we find that the C domain inhibits the spontaneous nucleation of actin monomers, an activity that is similar to that of the VCA region and the canonical WH2 domain (30). The WH2 domain sterically blocks the formation of a nucleus by binding to a cleft between subdomains 1 and 3 of actin but allows for barbed-end elongation from preformed filaments. Therefore, it is likely that the C domain inhibits spontaneous nucleation by binding near the barbed-end of a monomer. This activity is distinct from that of the C-terminal extension of the thymosin  $\beta$ 4 WH2 domain, which binds the pointed-end and helps to sequester actin. We also find that the C domain can inhibit VCA/Arp2/3 mediated actin polymerization in a dose dependent manner. It does not appear that this is caused by directly perturbing the VCA/Arp2/3 interaction, as our results indicate that the C domain interacts very weakly with the Arp2/3 complex ( $K_d > 200 \mu\text{M}$ ) and at the maximal concentration tested (150  $\mu\text{M}$ ), could not act as a competitive inhibitor. The C domain interacts more strongly ( $>20$  fold) with monomeric actin ( $K_d \sim 10 \mu\text{M}$ ), however, and inhibition may be a consequence of both preventing the interaction of a monomer with the C domain of VCA, as well as inhibition of spontaneous nucleation. In addition, mutations V531D and L535A, which

severely impair the activity of the Scar1 VCA domain, have no effect on affinity for the Arp2/3 complex. Both mutations, however, significantly perturb actin binding either by strengthening (L535A) or weakening (V531D) it. Furthermore, a C domain peptide containing the V531D mutation inhibited neither spontaneous actin polymerization nor VCA/Arp2/3 mediated actin polymerization. We propose, therefore, that actin binding to the C domain plays a significant role in the first steps to activating the Arp2/3 complex.

#### *Models for Arp2/3 activation*

A realistic model for activation of the Arp2/3 complex must take into account four observations: 1) Binding of the CA region to the Arp2/3 complex induces a conformational change that is probably required for nucleation (11,12,21). 2) In the presence of the VCA domain, monomeric actin induces a further conformational change that results in hydrolysis of ATP on the Arp2 subunit (5). 3) The C domain binds even more tightly to monomeric actin than to the Arp2/3 complex and mutations that perturb affinity for actin also perturb Arp2/3 activation. 4) Binding of actin and the Arp2/3 complex to the C domain is mutually exclusive.

The simplest model for Arp2/3 activation is that the C domain acts as a “molecular bridge”, directly contacting both actin and the Arp2/3 complex and acting as a template for their interaction. This interaction could cause further conformational changes in the complex resulting in ATP hydrolysis by the Arp2 subunit and formation of a stable nucleus. This model is consistent with all available data except the observation that binding of actin and the Arp2/3 complex to the C domain is mutually exclusive. To account for this fact we propose that the C domain exists in dynamic equilibrium between

binding actin and the Arp2/3 complex (Fig. 7). When bound to the Arp2/3 complex the C domain induces a relatively stable conformational change that brings Arp2 and Arp3 into proximity. The C domain then dissociates; binds to the actin monomer tethered to the WH2 domain; and orients the monomer for proper interaction with Arp2. If the monomer makes correct contact before the complex returns to its inactive state, it triggers creation of a stable hetero-trimeric nucleus composed of Arp2, Arp3 and actin that seeds the formation of a daughter filament. During this event, Arp2 ATP hydrolysis causes release of the CA region from the Arp2/3 complex (5). This “dynamic interaction and conformational memory” model would account for the coupling of actin binding and filament nucleating activities as well as the mutually exclusive interaction. The relatively weak affinities of the C domain for both actin and the Arp2/3 complex seen here indicate that the C domain is, in fact, in dynamic equilibrium between the two proteins. Furthermore, both strengthening and weakening the interaction of the C domain with actin result in nearly complete ablation of NPF activity. This suggests that the off- and on-rates of the C domain for actin and the Arp2/3 complex are tuned to optimal values. Future experiments detailing the kinetics of the C domain/actin and C domain/Arp2/3 interactions as well as high-resolution structural information of the Arp2/3 complex bound to VCA, F-actin and monomeric actin are needed to fully resolve the mechanisms of activation of the Arp2/3 complex.

## REFERENCES

1. Pollard, T. D., and Borisy, G. G. (2003) *Cell* **112**(4), 453-465

2. Engqvist-Goldstein, A. E., and Drubin, D. G. (2003) *Annu Rev Cell Dev Biol* **19**, 287-332
3. Volkmann, N., Amann, K. J., Stoilova-McPhie, S., Egile, C., Winter, D. C., Hazelwood, L., Heuser, J. E., Li, R., Pollard, T. D., and Hanein, D. (2001) *Science* **293**(5539), 2456-2459
4. Mullins, R. D., Heuser, J. A., and Pollard, T. D. (1998) *Proc Natl Acad Sci U S A* **95**(11), 6181-6186
5. Dayel, M. J., and Mullins, R. D. (2004) *PLoS Biol* **2**(4), E91
6. Marchand, J. B., Kaiser, D. A., Pollard, T. D., and Higgs, H. N. (2001) *Nat Cell Biol* **3**(1), 76-82
7. Gouin, E., Welch, M. D., and Cossart, P. (2005) *Curr Opin Microbiol* **8**(1), 35-45
8. Robinson, R. C., Turbedsky, K., Kaiser, D. A., Marchand, J. B., Higgs, H. N., Choe, S., and Pollard, T. D. (2001) *Science* **294**(5547), 1679-1684
9. Panchal, S. C., Kaiser, D. A., Torres, E., Pollard, T. D., and Rosen, M. K. (2003) *Nat Struct Biol* **10**(8), 591-598
10. Zalevsky, J., Lempert, L., Kranitz, H., and Mullins, R. D. (2001) *Curr Biol* **11**(24), 1903-1913
11. Rodal, A. A., Sokolova, O., Robins, D. B., Daugherty, K. M., Hippenmeyer, S., Riezman, H., Grigorieff, N., and Goode, B. L. (2005) *Nat Struct Mol Biol* **12**(1), 26-31
12. Martin, A. C., Xu, X. P., Rouiller, I., Kaksonen, M., Sun, Y., Belmont, L., Volkmann, N., Hanein, D., Welch, M., and Drubin, D. G. (2005) *J Cell Biol* **168**(2), 315-328

13. Wen, K. K., and Rubenstein, P. A. (2005) *J Biol Chem* **280**(25), 24168-24174
14. Prehoda, K. E., Scott, J. A., Mullins, R. D., and Lim, W. A. (2000) *Science* **290**(5492), 801-806
15. Higgs, H. N., and Pollard, T. D. (2000) *J Cell Biol* **150**(6), 1311-1320
16. Rohatgi, R., Ho, H. Y., and Kirschner, M. W. (2000) *J Cell Biol* **150**(6), 1299-1310
17. Rohatgi, R., Ma, L., Miki, H., Lopez, M., Kirchhausen, T., Takenawa, T., and Kirschner, M. W. (1999) *Cell* **97**(2), 221-231
18. Cory, G. O., Cramer, R., Blanchoin, L., and Ridley, A. J. (2003) *Mol Cell* **11**(5), 1229-1239
19. Eden, S., Rohatgi, R., Podtelejnikov, A. V., Mann, M., and Kirschner, M. W. (2002) *Nature* **418**(6899), 790-793
20. Kim, A. S., Kakalis, L. T., Abdul-Manan, N., Liu, G. A., and Rosen, M. K. (2000) *Nature* **404**(6774), 151-158
21. Goley, E. D., Rodenbusch, S. E., Martin, A. C., and Welch, M. D. (2004) *Mol Cell* **16**(2), 269-279
22. MacLean-Fletcher, S., and Pollard, T. D. (1980) *Cell* **20**(2), 329-341
23. Mullins, R. D., and Machesky, L. M. (2000) *Methods Enzymol* **325**, 214-237
24. Riek, R., Fiaux, J., Bertelsen, E. B., Horwich, A. L., and Wuthrich, K. (2002) *J Am Chem Soc* **124**(41), 12144-12153
25. Delaglio, F., Grzesiek, S., Vuister, G. W., Zhu, G., Pfeifer, J., and Bax, A. (1995) *J Biomol NMR* **6**(3), 277-293



26. Bartels, C., Xia, T. H., Billeter, M., Guntert, P., and Wuthrich, K. (1995) *J. Biomol. NMR* **6**(1), 1-10
27. Kelly, A. E., Ou, H. D., Withers, R., and Dotsch, V. (2002) *J Am Chem Soc* **124**(40), 12013-12019
28. Hufner, K., Higgs, H. N., Pollard, T. D., Jacobi, C., Aepfelbacher, M., and Linder, S. (2001) *J Biol Chem* **276**(38), 35761-35767
29. Higgs, H. N., Blanchoin, L., and Pollard, T. D. (1999) *Biochemistry* **38**(46), 15212-15222
30. Higgs, H. N., and Pollard, T. D. (1999) *J Biol Chem* **274**(46), 32531-32534
31. Letunic, I., Copley, R. R., Schmidt, S., Ciccarelli, F. D., Doerks, T., Schultz, J., Ponting, C. P., and Bork, P. (2004) *Nucleic Acids Res* **32**(Database issue), D142-144
32. Safer, D., Sosnick, T. R., and Elzinga, M. (1997) *Biochemistry* **36**(19), 5806-5816
33. Hertzog, M., van Heijenoort, C., Didry, D., Gaudier, M., Coutant, J., Gigant, B., Didelot, G., Preat, T., Knossow, M., Guittet, E., and Carlier, M. F. (2004) *Cell* **117**(5), 611-623
34. Mattila, P. K., Salminen, M., Yamashiro, T., and Lappalainen, P. (2003) *J Biol Chem* **278**(10), 8452-8459
35. Loomis, P. A., Zheng, L., Sekerkova, G., Changyaleket, B., Mugnaini, E., and Bartles, J. R. (2003) *J Cell Biol* **163**(5), 1045-1055
36. Quinlan, M. E., Heuser, J. E., Kerkhoff, E., and Mullins, R. D. (2005) *Nature* **433**(7024), 382-388

37. Demarest, S. J., Martinez-Yamout, M., Chung, J., Chen, H., Xu, W., Dyson, H. J., Evans, R. M., and Wright, P. E. (2002) *Nature* **415**(6871), 549-553
38. Domanski, M., Hertzog, M., Coutant, J., Gutsche-Perelroizen, I., Bontems, F., Carlier, M. F., Guittet, E., and van Heijenoort, C. (2004) *J Biol Chem* **279**(22), 23637-23645
39. Irobi, E., Aguda, A. H., Larsson, M., Guerin, C., Yin, H. L., Burtnick, L. D., Blanchoin, L., and Robinson, R. C. (2004) *Embo J*
40. Pan, F., Egile, C., Lipkin, T., and Li, R. (2004) *J Biol Chem* **279**(52), 54629-54636
41. Weaver, A. M., Heuser, J. E., Karginov, A. V., Lee, W. L., Parsons, J. T., and Cooper, J. A. (2002) *Curr Biol* **12**(15), 1270-1278
42. Beltzner, C. C., and Pollard, T. D. (2004) *J Mol Biol* **336**(2), 551-565
43. Vinson, V. K., De La Cruz, E. M., Higgs, H. N., and Pollard, T. D. (1998) *Biochemistry* **37**(31), 10871-10880

#### FOOTNOTES

We are extremely grateful to members of the Mullins, Dötsch and Vale labs for providing helpful discussions, valuable reagents and technical expertise. We thank Orkun Akin for assistance with MATLAB, Kevin Slep for advice, Brian Kelch for initial experiments and Brian Volkman for use of NMR facilities. This work was supported by a National Institutes of Health (NIH) R01 Grant #: GM61010.

<sup>1</sup>The abbreviations used are: NPF, nucleation promotion factor; WASP, Wiskott Aldrich Syndrome Protein; Scar, Suppressor of Cyclic AMP Receptor; WAVE, Wiskott Aldrich Verprolin homologous protein; WH2, WASP homology 2; GBD, GTPase binding domain; NMR, nuclear magnetic resonance; EDC, 1-ethyl-3-[3-dimethylaminopropyl] carbodiimide hydrochloride; NHS, N-hydroxysulfosuccinimide; HSQC, heteronuclear single quantum coherence; TROSY, transverse relaxation optimized spectroscopy; NOESY, nuclear Overhauser effect spectroscopy.

## FIGURE LEGENDS

**Fig. 1.** Domain layout of WASP/Scar proteins. EVH1, Ena/Vasp Homology 1 domain; B, basic region; GBD, GTPase binding domain; poly-proline, proline-rich region; SHD, Scar Homology domain; V, Verprolin-like or WASP Homology 2 domain; C, central or connecting domain; A, acidic domain.

**Fig. 2.** Secondary structure and interacting residues of the VC-actin complex. *A*, Alignment of human Scar1, WASP, and N-WASP VCA regions. Structural information from Fig. 2B-D is displayed above the alignment. Actin binding residues were determined by line-broadening and NOEs. Secondary structure was determined by the presence and strength of amide-amide NOEs. Arp2/3 interacting residues were determined by line-broadening experiments (9). The autoinhibitory helix denotes the structure of the C domain bound to the GBD of WASP (20). *B*,  $^1\text{H}$ - $^{15}\text{N}$  TROSY-HSQC spectrum of [ $^{15}\text{N}$ , $^2\text{H}$ ]-Scar1 VC (residues 489-538) bound to  $\text{Ca}^{2+}$ -ATP-actin with latrunculin B at 25°C. The assignment of residues in the bound state is shown. *C*, Selected regions of the 3D [ $^{15}\text{N}$ , $^1\text{H}$ ] TROSY-NOESY-HSQC spectra of [ $^{15}\text{N}$ ,  $^2\text{H}$ ] VC bound to  $\text{Ca}^{2+}$ -ATP-Actin showing intramolecular amide-amide NOEs. Crosspeaks are shown in red, intramolecular NOEs shown in black. Text denotes connecting residue. *D*, overlay of the [ $^{15}\text{N}$ ,  $^1\text{H}$ ] HSQC spectra of the free [ $^{15}\text{N}$ -Lys] VC (black) and the [ $^{15}\text{N}$ -Lys] VC-actin complex (red).

**Fig. 3.** Binding and activation properties of VCA truncations. *A*, C domain binds actin monomers. Conditions: 10 mM HEPES pH 7.0, 50 mM KCl, 1 mM EGTA and 1mM MgCl<sub>2</sub>, 200 μM latrunculin B. Equilibrium binding of the C domain labeled with Alexa-488 (0.2 μM) to monomeric actin measured by fluorescence anisotropy. Curve is best fit of data to binding quadratic (43) yielding equilibrium constant of 13.4 μM (see Table I). Scatchard plot (inset) indicates a 1:1 stoichiometry. *B*, Time course of pyrene-actin polymerization for VCA truncations. Mg-ATP-actin monomers (4 μM 5% pyrene-labelled) and 10 nM Arp2/3 complex were polymerized in 10 mM HEPES pH 7.0, 50 mM KCl, 1 mM EGTA and 1 mM MgCl<sub>2</sub> at 22°C, either alone or with 0.5 μM Scar1 VCA (residues 489-559), 4 μM Scar1 CA (residues 523-559), 4 μM Scar1 VC (residues 489-543). *C*, Activities of Gly-Ser insertions. Mg-ATP-actin monomers (2 μM 6% pyrene-labeled) and 10 nM Arp2/3 complex were polymerized either alone or with 0.5 μM of indicated construct. Scar CA was used at 4 μM. The number of Gly-Ser pairs is indicated by n. The placement of the Gly-Ser pairs in the VCA sequence is illustrated. *D*, The C domain inhibits spontaneous actin polymerization. Time course of pyrene-actin (4 μM, 5% pyrene-labeled) polymerization in the presence of 150 μM and 75 μM C and C-V531D peptides alone or with 10 nM Arp2/3 complex and 0.25 μM Scar1 VCA peptide.

**Fig. 4.** Interaction of the C domain with Arp2/3 and actin. *A*, Actin competes with Arp2/3 complex for binding to the C domain. Equilibrium binding of the CA domain labeled with Alexa-488 (0.02 μM) to monomeric actin in the presence of 1 μM Arp2/3 complex measured by fluorescence anisotropy. Anisotropies of different bound states are given on the right side of the graph. At 95 μM actin, 40 μM A domain (544-559) was added to the sample. *B*, EDC/NHS crosslinking of Alexa488 labelled C domain (522-

543) to the Arp2/3 complex. Each reaction was immunoblotted with antibodies to the four highest molecular weight subunits of Arp2/3. The coomassie (c), fluorescence (f) and immunoblot (ib) signals for each condition are shown. The only subunit of Arp2/3 that crosslinks to the C domain, p40, is shown in the red box. Asterisks denote the full-length C peptide and its degradation product. This degradation product is missing residues 522-527 of Scar1 as measured by MALDI-TOF spectrometry. Crosslinking reaction conditions: 2 mM EDC/NHS (50 mM KCl, 1 mM MgCl<sub>2</sub>, 1 mM EGTA, 1 mM DTT, 0.2 mM ATP, and 10 mM imidazole [pH 7.0]) was added to 8 μM Arp2/3 complex alone or with 25 μM Scar1 C for 45 minutes at room temperature.

**Fig. 5.** Effect of C domain mutations on activation of the Arp2/3 complex. *A*, Plot of the concentration of ends versus time for each mutant in the C domain of Scar1 VCA [489-559] peptides. Curves were generated from time-courses of pyrene-actin polymerization for each mutant (0.5 μM) in the presence of 10 nM Arp2/3 complex, 2 μM actin in KMEH at 22°C. *B*, Relative maximum concentration of ends for each mutant, normalized to wild-type Scar1 VCA. Residues shown to bind actin in Fig. 2A are indicated in red.

**Fig. 6.** Regions C-terminal to the WH2 domain dictate function. *A*, Structural alignment of WH2 domains. Scar1 WH2 [498-514], ciboulot D1[10-33], thymosin β4 [2-20], and Spir C [432-448] are shown. Residues directly facing actin are in red, extended motif in gray. Actin-binding residues are predicted for Spir. *B*, Residues C-terminal to the WH2 domain dictate the function of the protein. Domain layout of selected WH2 domain-containing proteins.

Fig. 7. Role of the C domain-actin interaction in Arp2/3 activation. Model of the steps leading to activation of the Arp2/3. Actin is shown in gray, WH2 in red, C in green, A in blue, the Arp2/3 complex in orange and brown. We propose the following steps to activation of the Arp2/3 complex: 1. The C domain of the VCA peptide binds to the Arp2/3 complex and an actin monomer in a mutually exclusive manner and exists in a dynamic state. Binding of the C domain to the Arp2/3 complex occurs through the p40 subunit and the A domain is modeled to bind to Arp2 and Arp3 based on previous results (10,41,42). The VC region binds to the barbed-end of an actin monomer. 2. The CA region induces a conformational change of the Arp2/3 complex bringing p21, Arp3, Arp2 and p40 in closer proximity to each other (11,12,21). 3. The C domain then binds the actin monomer and with the WH2 domain positions it on the Arp2/3 complex. The monomer binds the actin-like Arp2 and Arp3 subunits, forming a nucleus for polymerization and formation of a daughter filament. The addition of the monomer triggers ATP hydrolysis on Arp2. 4. The WH2-actin contact is lost due to filament formation and Arp2 ATP hydrolysis lowers the affinity for the CA region such that VCA is released (5).

TABLE I

**Affinities and activities for all Scar1 VCA mutations**

Construct	K <sub>d</sub> for Actin (μM) <sup>a</sup>	K <sub>d</sub> for Arp2/3 (μM) <sup>a</sup>	Activity <sup>b</sup>
Scar VCA	0.32	0.88	1.0
VC	0.40	>200 <sup>d</sup>	0.0
VCAΔ5	0.35	n.d.	n.d.
V	3.10	n.d.	0.0
CA	11.50	0.92	0.08
C	12.20	>200 <sup>d</sup>	0.0 <sup>c</sup>
A	n.d.	7.30	0.0 <sup>c</sup>
VCA V531A	0.93	1.30	0.5
VCA V531D	1.69	1.90	0.1
VCA L535A	0.09	1.10	0.2
VCA T533D	0.34	0.74	1.1

<sup>a</sup>Affinities were measured by competition with Alexa-488 Scar1 VCA or Alexa-488 Scar1 C using fluorescence polarization anisotropy.

<sup>b</sup>Activity is calculated by dividing the maximum number of ends generated for the specified construct by the number of ends generated by wild-type VCA.

<sup>c</sup>Inhibits at high concentrations.

<sup>d</sup>Binding was determined by monitoring tryptophan fluorescence of the Arp2/3 complex upon titration of Scar C and polarization anisotropy of a Alexa-488 labeled C domain.

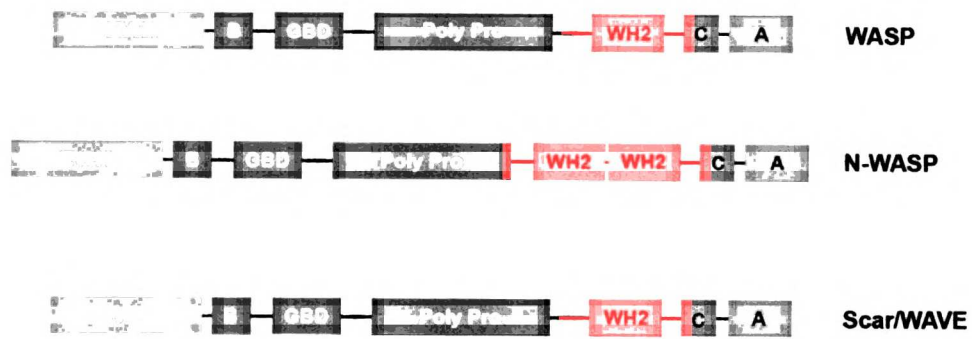


Figure 1



A

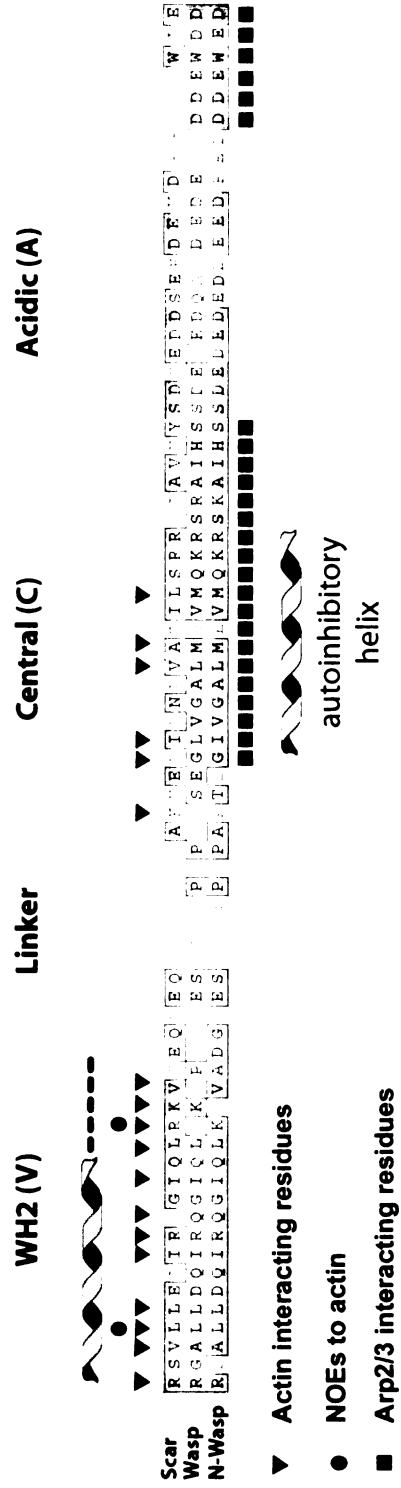


Figure 2

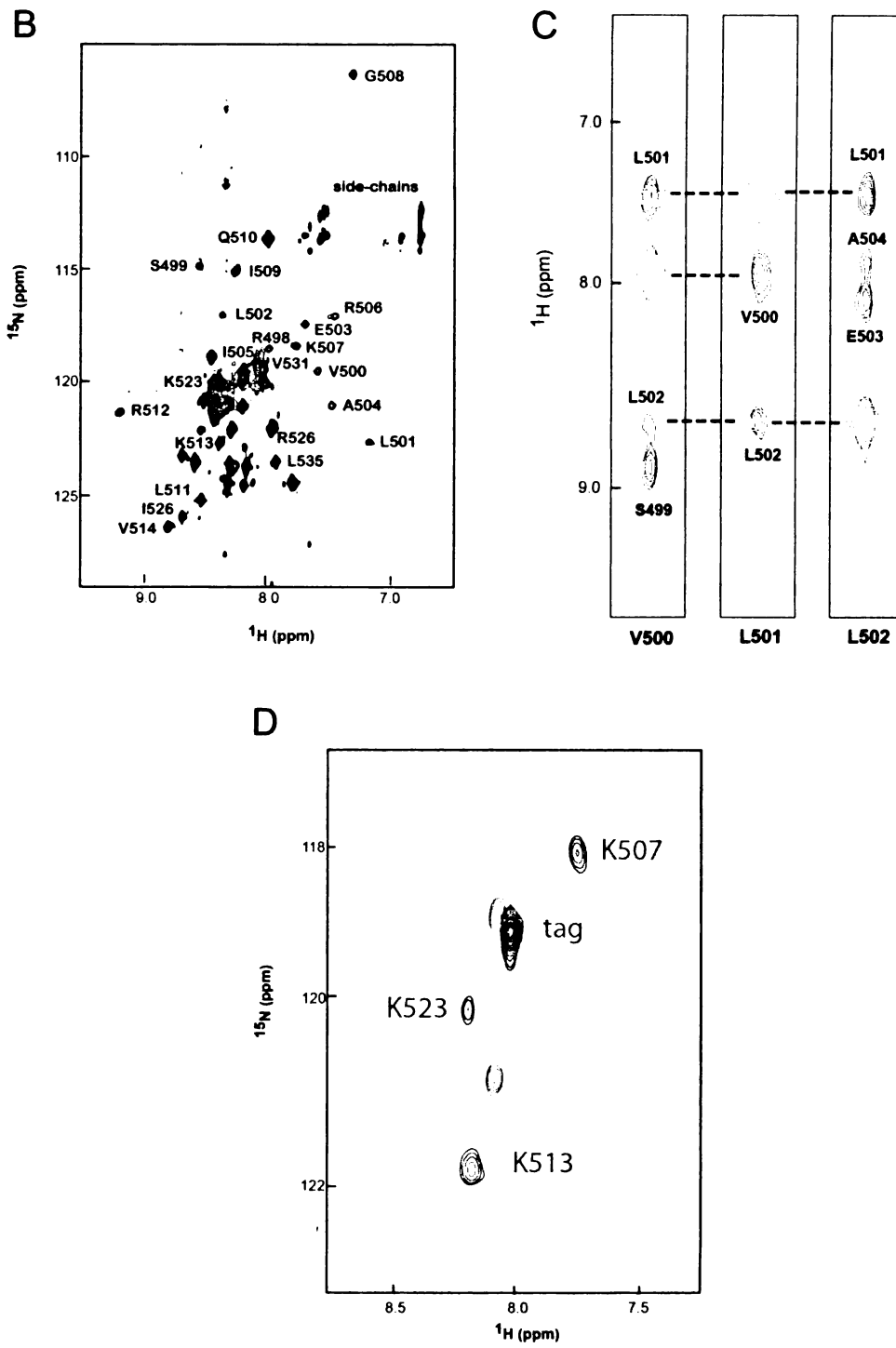


Figure 2

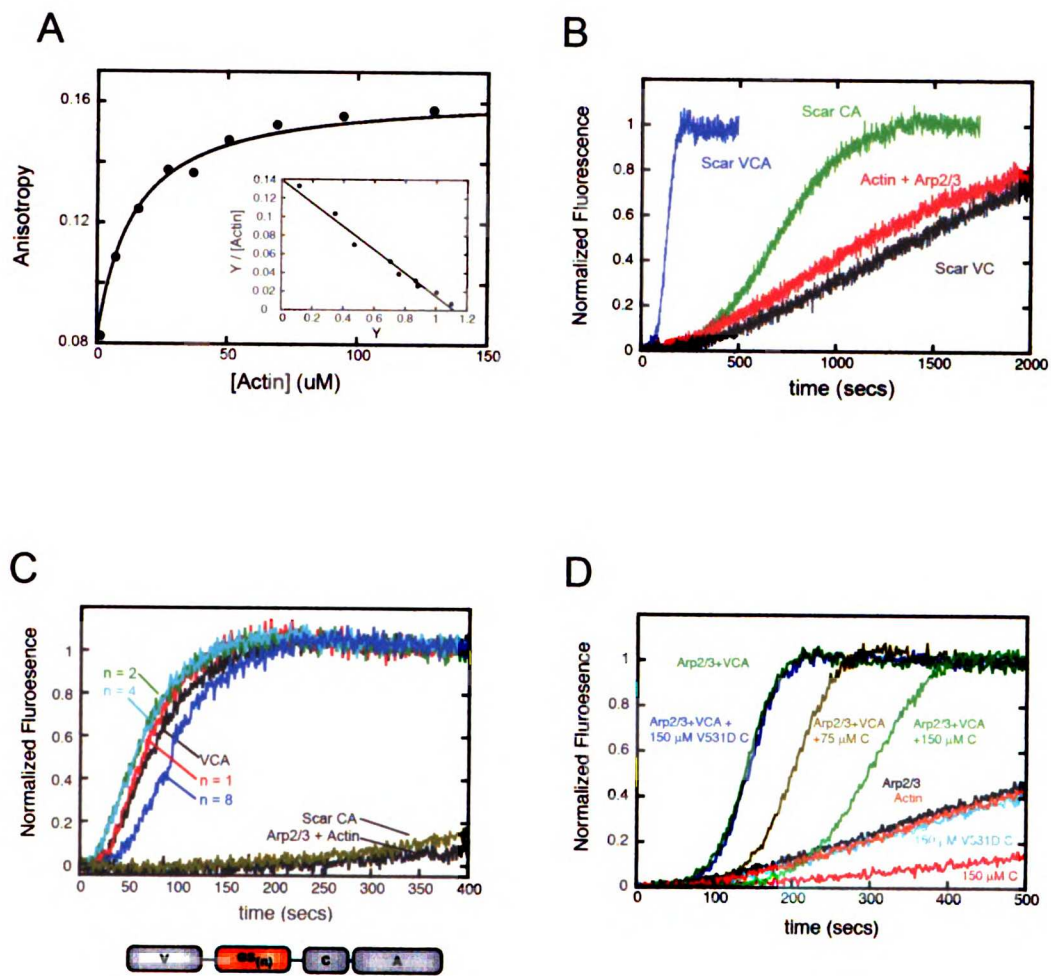


Figure 3

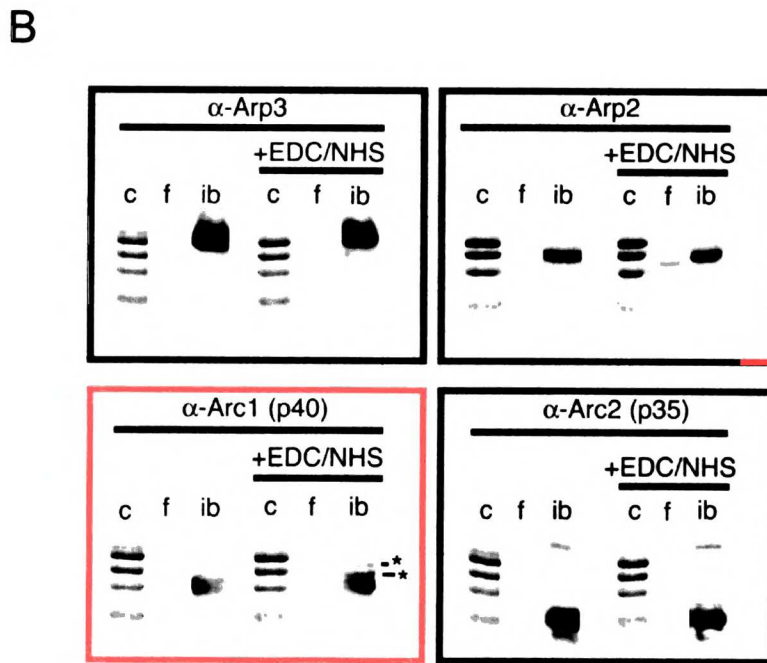
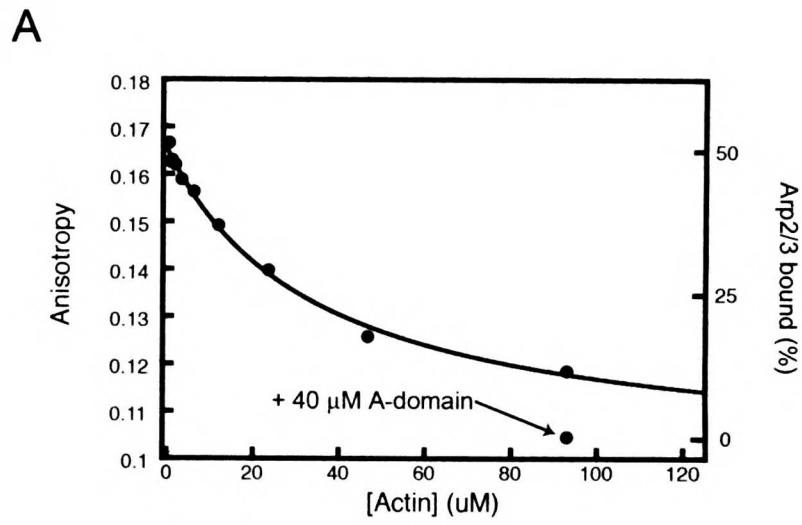
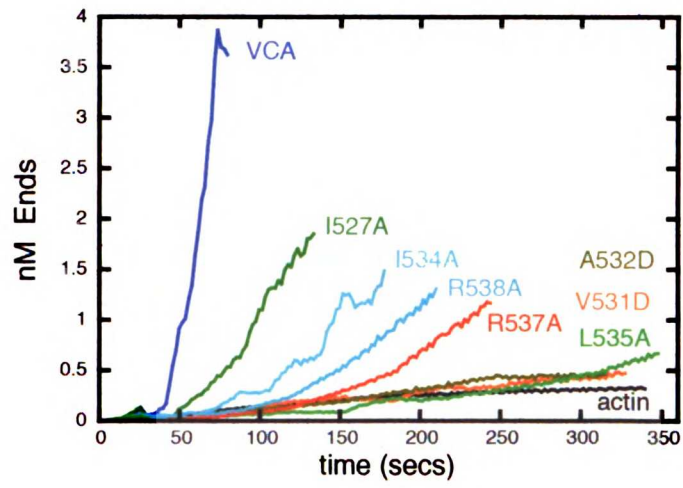


Figure 4

A



B

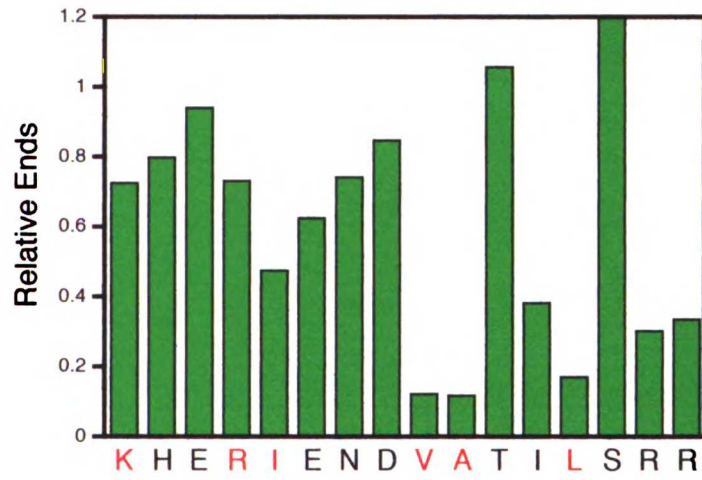


Figure 5

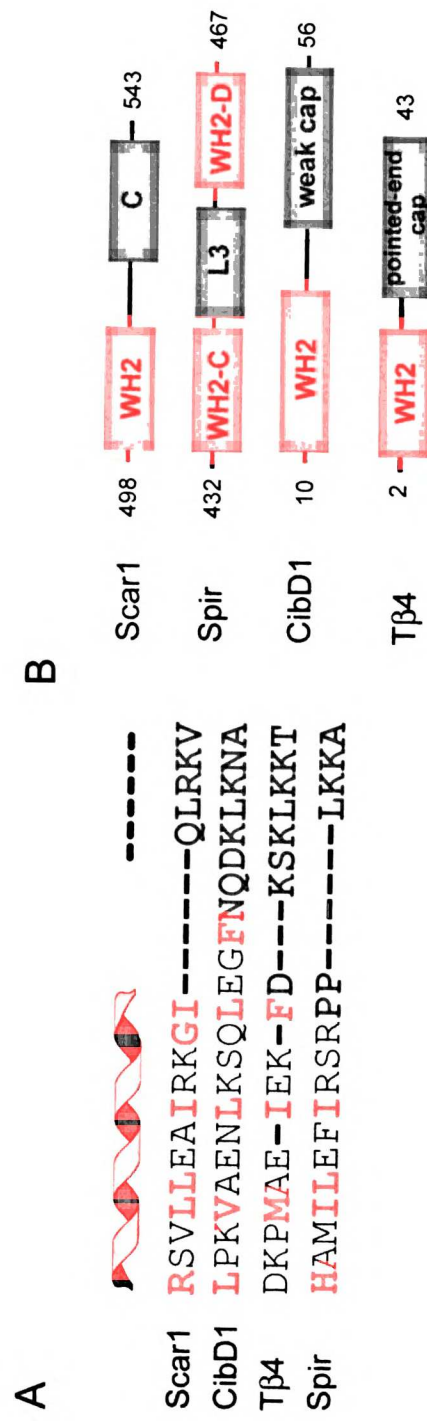


Figure 6

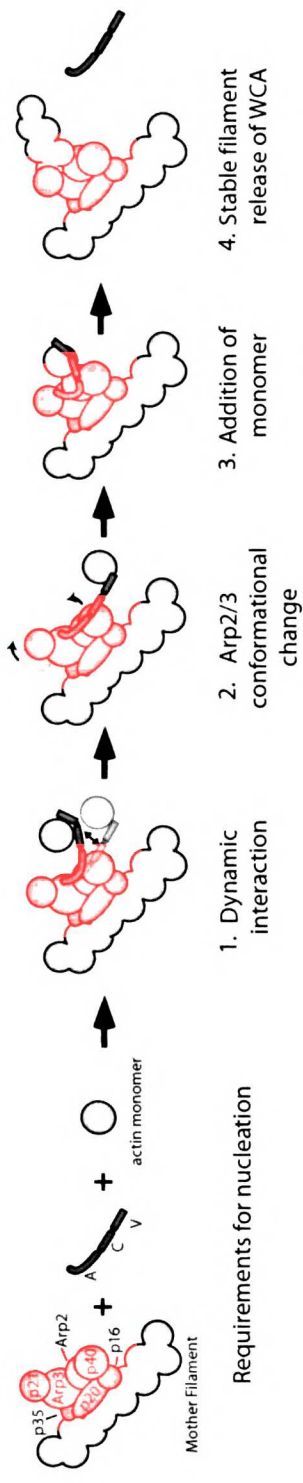


Figure 7

## SUPPLEMENTARY DATA

### **Fig. S1. HSQC spectra of Scar1 VCA truncations with and without actin.**

A, Overlay of the  $^1\text{H}$ - $^{15}\text{N}$  TROSY-HSQC spectrum of [ $^{15}\text{N}$ , $^2\text{H}$ ]-Scar1 VC bound to  $\text{Ca}^{2+}$ -ATP-actin (shown in red) with  $^1\text{H}$ - $^{15}\text{N}$  HSQC spectra of [ $^{15}\text{N}$ , $^2\text{H}$ ]-Scar1 VCA free (shown in gray) and bound to  $\text{Ca}^{2+}$ -ATP-actin (shown in green), at 25.0°C. Circles denote residues Gly 508 and Trp 557. Gly 508 shifts upon actin-binding (arrow) whereas Trp 557 in the A domain does not. Conditions were the same as described in “Materials and Methods”. B, Overlay of the  $^1\text{H}$ - $^{15}\text{N}$  HSQC spectra of 200  $\mu\text{M}$  [ $^{15}\text{N}$ , $^1\text{H}$ ]-Scar1 C free (shown in black) and bound to 200 $\mu\text{M}$  Ca-ATP-actin (shown in red) at 25.0 °C in “buffer A” as defined in “Materials and Methods”. Circles denote resonances that significantly broaden upon addition of actin and arrows denote resonances that shift upon addition of actin.

### **Fig. S2. Crosslinking of the C domain to the Arp2/3 complex in the presence of actin and F-actin.**

EDC/NHS crosslinking of 8  $\mu\text{M}$  Alexa-488 labeled C domain (522-543) to 5  $\mu\text{M}$  Arp2/3 complex in the presence of 20  $\mu\text{M}$  monomeric actin labeled with Alexa-648 (Molecular Probes) and/or 8  $\mu\text{M}$  unlabeled phalloidin-stabilized F-actin. The coomassie, Alexa-648 fluorescence (a648 actin) and Alexa-488 fluorescence (a488 C) signals for each condition are shown. All lanes shown are after completion of crosslinking except for the 1<sup>st</sup> lane of the group “Arp2/3”, showing 5  $\mu\text{M}$  Arp2/3 before crosslinking. The positions of the C domain, actin, Arp2/3, actin-C crosslink, and p40-C crosslink are shown. No Actin-C-Arp2/3 crosslinks were observed. Crosslinking conditions were the same as in “Materials and Methods”.



**Fig. S3. Binding of Scar1 VCA mutants to actin and the Arp2/3 complex.**

A, Competition between unlabeled Scar1 VCA (green squares), V531D VCA (black circles) and L535A VCA (blue squares) peptides with 0.02  $\mu\text{M}$  Alexa-488 N-terminal labeled Scar1 VCA for binding to 0.4  $\mu\text{M}$  monomeric actin as measured by fluorescence anisotropy. Black lines are best fits to a full solution of the equilibrium competition binding equation using KaleidaGraph (1). Conditions were as described in “Materials and Methods”. B, Competition between unlabeled Scar1 VCA (green triangles), V531D VCA (black circles) and L535A VCA (blue squares) peptides with 0.02  $\mu\text{M}$  Alexa-488 C-terminal labeled Scar1 CA for binding to 1  $\mu\text{M}$  Arp2/3 complex as measured by fluorescence anisotropy. Black lines are best fits to a full solution of the equilibrium competition binding equation using KaleidaGraph (1). Conditions were as described in “Materials and Methods”.

1. Marchand, J. B., Kaiser, D. A., Pollard, T. D., and Higgs, H. N. (2001) *Nat Cell Biol* 3(1), 76-82

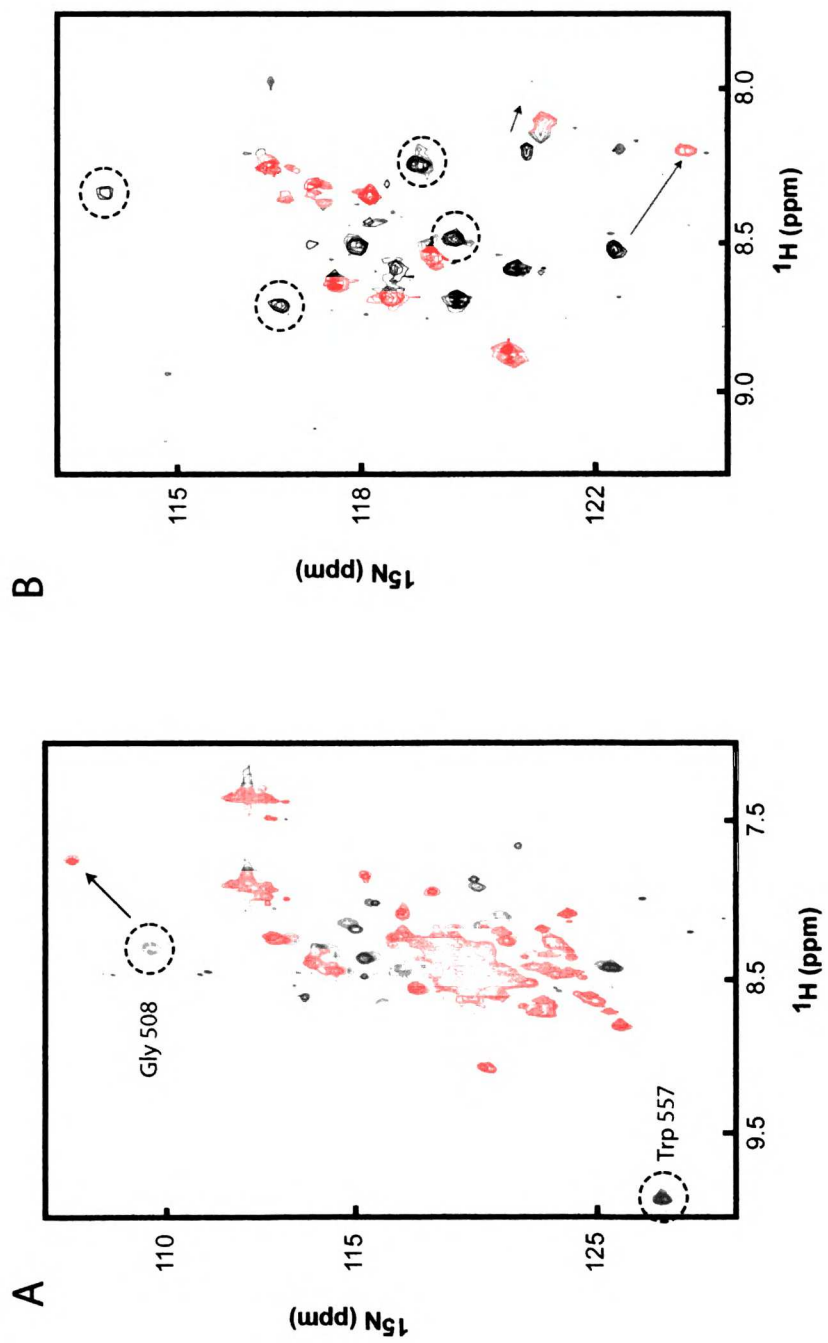
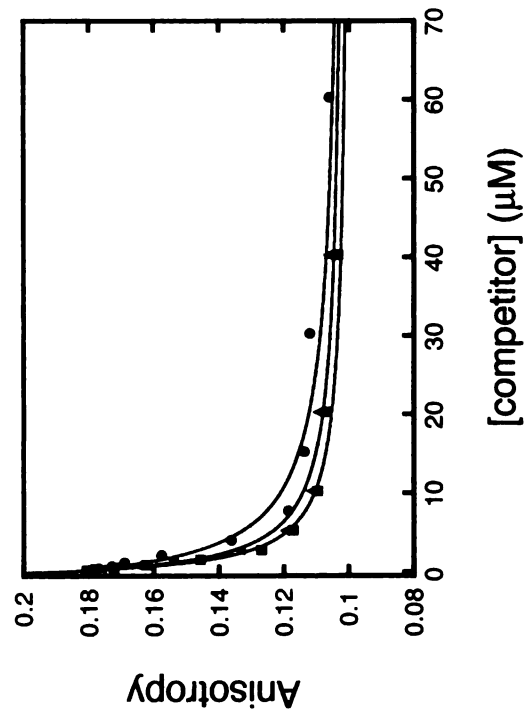


Figure S1



B



A

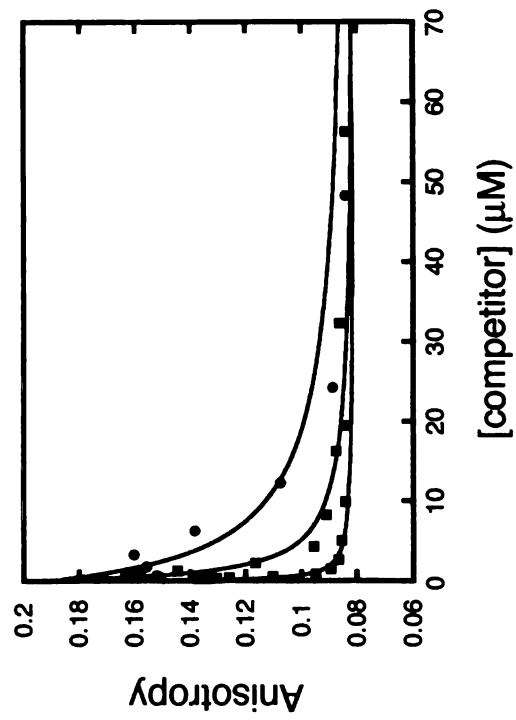


Figure S3

## Chapter 3

### Low-conductivity buffers for high-sensitivity NMR measurements

This work, published in the *Journal of the American Chemical Society* in 2002, was born out of necessity. Our work on the structure of the WH2-actin complex by NMR (**Chapter 2**) was not initially possible due to the low solubility of the complex, its short lifetime and the poor signal to noise of room temperature NMR probes. We received a CryoProbe in 2001 which has the advantage of increasing the signal to noise ratio by 3-5 fold compared to that of a normal probe. With this technology, it is possible to acquire high-quality spectra of proteins below 300  $\mu\text{M}$ . However, the high concentration of salt and buffer required for the stabilization of the complex essentially removes this advantage. In addition, the resistance caused by the high-conductivity of the samples causes heating and T1 noise, both of which hinder the acquisition of lengthy three-dimensional NMR spectra. Therefore, we sought to design a set of buffers that would allow for stabilization of the complex and retain the high-sensitivity of the CryoProbe. This technology will become more important as sensitivity losses increase with the square of the field strength. It appears that the field has embraced these buffer systems, with Cambridge Isotope Laboratories now offering the highest-sensitivity buffers in deuterated form (at substantial cost, of course).

## Low-conductivity buffers for high-sensitivity NMR measurements

Alexander E. Kelly§, Horng D. Ou§, Richard Withers‡ and Volker Dötsch#

§ Graduate Group in Biophysics, University of California San Francisco, San Francisco, CA 94143, USA,

‡ Bruker Biospin Corporation, 47697 Westinghouse Drive, Fremont, CA 94539, USA,

# Departments of Pharmaceutical Chemistry and Cellular & Molecular Pharmacology, University of California San Francisco, San Francisco, CA-94143, USA

Reproduced with permission from the *Journal of the American Chemical Society* **124**, 12013-12019 (2002). Copyright 2002 American Chemical Society [refer to Appendix C].

## **Abstract**

The sensitivity of nuclear-magnetic-resonance (NMR) probes, especially the recently introduced cryogenic probes, can be substantially reduced by the electrical noise generated by conductive samples. In particular, samples of biological macromolecules, which usually contain salts to keep the pH constant and to prevent aggregation can experience a significant reduction in sensitivity. So far this dependence has forced researchers to minimize the salt concentrations in their samples. Here we demonstrate that the decisive factor is not the salt concentration itself but the conductivity which is a function of both the concentration and the mobility of the ions in solution. We show that, by choosing buffers with low ionic mobility, the sample conductivity can be dramatically reduced and the sensitivity substantially enhanced compared to the same measurement with an equal concentration of a standard NMR buffer such as phosphate. We further show that the highest sensitivity gain of one buffer over another is equal to the square root of the ratio of their ion mobilities and describe a simple method to evaluate the effect of a certain buffer on the sensitivity.

## Introduction

Compared to other spectroscopic techniques NMR spectroscopy is a relatively insensitive method, requiring concentrations in the micro- to millimolar range. However, NMR provides an enormous amount of detail about the chemical organization and the structure of compounds that - with the exception of x-ray crystallography - cannot be obtained by any other method. Arguably, NMR has become the most important analytical tool in organic chemistry and a very important one in structural biology and biochemistry. Based on this importance, improving the sensitivity of NMR experiments has been a major goal for many research groups over the last thirty years. The introduction of pulsed Fourier techniques <sup>1</sup>, stronger magnets, better preamplifiers and probes, and pulse sequences such as the sensitivity enhancement method <sup>2-4</sup> have all contributed to an enormous increase in sensitivity. One of the most important contributions has been the recent introduction of cryogenic probes <sup>5-11</sup>. These probeheads increase the sensitivity of NMR experiments three- to fourfold relative to conventional probeheads <sup>12-14</sup>. This sensitivity increase is achieved by cooling the radio frequency (RF) receiver coils to temperatures of 15 to 30 K. At these temperatures, the coils have lower resistance, allowing for higher quality factors (Q) (and therefore increased signal amplitude), and lower thermal noise. Both higher Q and lower noise result in an increase in the signal-to-noise (S/N) ratio and hence sensitivity.

This full sensitivity increase of cryogenic probes, however, is realized only if the sample under study is electrically insulating, like organic solvents. An electrically conductive such as a buffered solution used in protein structure determinations, will add a



resistance to the coil, which can significantly reduce the signal-to-noise ratio. Many biological macromolecules must be studied in buffered solutions to keep the pH constant and the molecule in a defined protonation state. Moreover, in many cases additional salts must be added to increase the solubility and to prevent aggregation of the biomolecule of interest. It has been shown by numerous researchers that salt concentrations of 100 to 150 mM, which are typical for many biological samples, decrease the sensitivity advantage of a cryogenic probe to about a factor of two better than that of a conventional probe with the same sample<sup>9,15</sup>. Usually, several different buffers and salts can be used to obtain good solution conditions, providing the NMR spectroscopist with a few options. So far, buffers are mainly chosen to minimize interference of their NMR signals with the signals of the biological macromolecules. A recent survey of buffer conditions used for NMR structure determinations showed that 27% of all structures were determined in unbuffered (or auto-buffered) solutions, 50% in phosphate, 10% in acetate buffer and 9% in Tris buffer<sup>16</sup>. These buffers either do not contain protons or are commercially available in deuterated forms.

With the introduction of cryogenic probes, optimization of sensitivity has emerged as another criterion for buffer selection. To achieve the highest possible sensitivity and to optimize the advantages of cryogenic probes, the laboratory of Joshua Wand has designed a very powerful method that is based on encapsulating proteins in reverse micelles which are themselves dissolved in organic solvents of low viscosity<sup>15,17-19</sup>. Such samples not only show sharper resonance lines due to faster tumbling rates of the proteins, but also nearly eliminate the sample noise contribution, thus providing the

highest possible sensitivity. Unfortunately, however, this method requires time-consuming sample preparation and is not applicable to all proteins.

Designing buffers that are easily prepared, work with most proteins, are adjustable to the required pH and preserve the sensitivity of cryogenic probes would be very attractive. To date, the optimization of buffer conditions for achieving high sensitivity has focused on reducing the total salt concentration which must be balanced against the need to maintain the conformation and solubility of the macromolecule. However, as we show here, the sensitivity depends on the conductivity of a sample, which is a function of both the ion concentration and ion mobility. Using NMR buffers made of ions with low ion mobility should provide a way to improve the sensitivity of NMR experiments even if high salt concentrations are necessary, such as to prevent aggregation. We show that such buffers can indeed be designed and that they can increase the sensitivity significantly relative to the currently most widely used buffers.

## **Experimental section**

### **Preparation of Buffers**

To investigate the influence of different buffers on the sensitivity of NMR experiments, salt solutions were prepared with varying predicted conductivities based on ion type. All solutions were made with 0.22  $\mu\text{m}$  filtered, deionized-distilled  $\text{H}_2\text{O}$  and the highest-grade reagents available (Sigma or Fluka). All buffers in Table 1 were made to a concentration of 200 mM without adjustment of the pH. For the design of buffers at a specific pH, selected salts from Table 1 were titrated with concentrated solutions of different bases or acids as indicated in Table 2. All buffers had a final concentration of the compound

indicated in column 1 of 200 mM. The phosphate buffer was prepared by mixing  $\text{Na}_2\text{HPO}_4$  and  $\text{NaH}_2\text{PO}_4$  solutions according to published tables<sup>20</sup> to a final phosphate concentration of 200 mM. All pH measurements were made with a Mettler-Toledo MP 220 pH meter.

#### Measurement of the Quality Factor

To determine the RF quality factor (Q) of the cryogenic probe loaded with different samples, we connected the probe to a network analyzer. A volume of 700 ml of each solution was placed in a standard 5mm NMR sample tube and loaded into the cryogenic probe (Bruker 500 MHz TXI CryoProbe<sup>TM</sup>). The probe was, for each sample, matched to an HP8752C vector network analyzer and the Q of its <sup>1</sup>H channel was measured. Measurement errors for the  $R_s/R_c$  values were estimated from  $D(R_s/R_c) = [(DQ/DQ_0)^2 + (DQ_0/Q^2)^2]^{0.5}$ , where  $Q_0$  is the Q of the empty probe. Experimental errors of the Q-factor measurements were determined by performing individual measurements in triplicate.

#### Conductivity Measurements

The conductivities of all solutions listed in Tables 1 and 2 were determined using an Amber Science Inc. (Eugene, Oregon) Model 1056 conductivity meter at room temperature. The meter was calibrated before each measurement using a 0.005N solution of KCl ( $718 \mu\text{S}/\text{cm} \pm 1$  at 25°C) as a standard.

#### Signal-to-Noise Measurements

Signal-to-Noise measurements were performed on 200mM solutions of HEPES-NaOH (pH 7.0), Tris-HCl (pH 7.0), sodium phosphate (pH 7.0), sodium chloride, and pentasodium tripolyphosphate at 25°C containing 2mM para-aminobenzoic acid (PABA) as a reference. 500  $\mu$ L of each solution were loaded into standard 5 mm NMR tubes and one-dimensional (1D) spectra were acquired with 4 scans. Signal-to-Noise ratios of the most downfield doublet of PABA were calculated using the program XWINNMR (Bruker). Relative peak intensities were also determined on 500  $\mu$ L, 50mM solutions of MES/Bis-Tris (pH 6.0), HEPES-NaOH (pH 7.0), MOPS/Bis-Tris propane (pH 7.0), and sodium phosphate (pH 7.0) containing 1 mM lysozyme (Sigma) with 4 scans and processed using XWINNMR. The lysozyme was extensively dialyzed against deionized-distilled H<sub>2</sub>O prior to sample preparation. All measurements were carried out on a 500 MHz Bruker DRX NMR instrument equipped with a TXI CryoProbe™.

## Results and Discussion

The signal-to-noise ratio (S/N) or sensitivity of NMR experiments depends on many different factors that include sample specific parameters such as concentration and parameters linked to the individual pulse sequence and the hardware used during the experiment. The most important hardware components that influence the sensitivity are the probe and the preamplifier. Their contribution depends on the temperature of the coil,  $T_c$ , its resistance,  $R_c$ , the temperature of the sample,  $T_s$ , the resistance added to the coil by the sample,  $R_s$  (henceforth referred to as the “sample resistance”) and the noise temperature of the preamplifier,  $T_a$ . This dependence can be written in the following equation<sup>21-24</sup>:

$$S/N \sim (T_c R_c + T_a |R_c + R_s| + T_s R_s)^{-0.5} \quad (1)$$

In cryogenic probes the temperature of the coil is in the range of 15K to 30K, the preamplifier noise temperature is in the range of 10K to 15K and the coil resistance is small compared to the resistance of conventional room temperature probes. This makes the first and second term in Equation 1 small and is the basis for the higher sensitivity of cryogenic probes relative to probes with the coil and preamplifier at room temperature. The third term, however, is similar for conventional and cryogenic probes since it depends primarily on the sample temperature and sample resistance. From Equation 1 it is easy to see that an increase in the third term decreases the sensitivity. Equation 1 also predicts that the relative influence of the third term is stronger for cryogenic probes because the first two terms are much smaller for cryogenic probes than for conventional probes. As we will show below,  $R_s$  is proportional to the sample conductivity, which explains why samples of high conductivity have a stronger impact on the sensitivity of cryogenic probes than on room temperature probes. (However, one should point out that the absolute sensitivity of a cryogenic probe is always higher than that of a conventional probe). For most biological and many chemical applications the sample temperature can only be changed within a narrow range of roughly 30K or ~10% of the value of  $T_s$ . On the other hand, the sample resistance  $R_s$  depends on the exact buffer and salt conditions used in the sample. Salt concentrations in biological NMR samples vary from millimolar to molar (or 2-3 orders of magnitude). Based on this large variation, the sample resistance  $R_s$  becomes one of the most critical parameters in determining the sensitivity of

NMR experiments with cryogenic probes. This sample resistance is the result of the inductive coupling between the sample and the coil. The value of this resistance can be calculated from the energy dissipated in the sample by currents induced in the sample by the RF field. Gadian and Robinson calculated this to be, for a solenoidal coil of radius  $a$  and  $n$  turns <sup>23</sup>:

$$R_s = \frac{\pi \omega^2 \mu^2 \sigma n^2 b^4 L}{32 (a^2 + (L/2)^2)} \quad (2)$$

where  $\omega$  is the angular frequency of operation,  $\mu$  is the permeability of free space, and  $\sigma$ ,  $b$  and  $L$  are the conductivity, the radius, and the length of the sample, respectively <sup>25</sup>.

The dependence of the sensitivity of an NMR experiment on the salt concentration has been recognized for a long time and much attention has focused on minimizing the salt concentration of NMR samples. However, as shown in Equation 2 the sample resistance is proportional to the conductivity  $\sigma$  of the sample which in turn is proportional not only to the ionic concentration  $c$ , but also to the mobility  $\lambda$  of the ions in solution and their respective charge  $q$ . For a solution containing different types of ions, their individual contributions are summed up:

$$R_s \sim \sigma = \sum c_i q_i \lambda_i \quad (3)$$

where the index  $i$  covers all of the ionic species present. This equation predicts that choosing buffers with low ion mobility  $\lambda$  should allow us to preserve the high sensitivity of cryogenic probes even in the presence of high salt concentrations.

To test this hypothesis we have investigated the influence of several different salt solutions on the sensitivity of a cryogenic probe by measuring the Q of the proton channel of a triple resonance cryogenic probe on our 500 MHz Avance Bruker NMR instrument. Measurements of the individual quality-factors and of  $Q_0$ , the quality-factor of the empty, unloaded probe allows us to calculate the ratio of sample resistance,  $R_s$  to the coil resistance  $R_c$ :

$$R_s/R_c = Q_0/Q - 1 \quad (4)$$

In turn, this ratio can be used to calculate the sensitivity factor L, defined as the ratio of the sensitivity of the loaded probe and the unloaded probe:

$$L = \frac{(S/N)_{\text{loaded}}}{(S/N)_{\text{unloaded}}} = \sqrt{\frac{R_c(T_c + T_a)}{R_c T_c + T_s R_s + T_a(R_c + R_s)}} = \left(1 + \frac{R_s(T_s + T_a)}{R_c(T_c + T_a)}\right)^{-0.5} \quad (5)$$

The factor L can vary between 0 and 1 with 1 being the highest achievable sensitivity, *i.e.* that of a probe with a nonconductive sample, which does not reduce the sensitivity from that of an empty probe. With the temperatures  $T_s$  set to 298K,  $T_c$  to 27K and  $T_a$  to 15K this equation can be simplified to:

$$L = \left(1 + 7.45 \frac{R_s}{R_c}\right)^{-0.5} \quad (6)$$

Table 1 lists the  $R_s/R_c$  ratios and the expected sensitivity factors  $L$  for all investigated samples. All solutions were at a concentration of 200 mM in order to increase the accuracy of the RF measurement. Also shown are the DC conductivities measured for each sample. The results in Table 1 demonstrate that huge differences in the  $R_s/R_c$  ratios exist, ranging from 2.71 for pentasodium tripolyphosphate to 0.02 for Bis-Tris. These differences in the  $R_s/R_c$  values predict sensitivity differences between the best and the worst solutions of more than a factor of 4, showing a strong influence of the nature of the salt in the sample on the sensitivity. The results suggest that the detrimental effect of high salt concentrations can be counterbalanced by low ion mobilities. However, the conductivity of the sample depends also on the protonation state of the individual buffer. Weak acids for example are mainly protonated and uncharged. The results in Table 1 should therefore be used only for rough guidance for the creation of buffers that preserve the high sensitivity of cryogenic probes. However, these results also clearly demonstrate the effect of the ion mobility on the sensitivity. Comparison of the results obtained with NaCl and KCl shows that their conductivity and sensitivity factors differ despite both having the exact same ionic concentration (and ionic strength). The sodium salt achieves a higher sensitivity than the potassium salt, in accordance with their relative ion mobilities<sup>26,27</sup>. Stronger effects are seen in a comparison of the phosphate salts: the highest sensitivity is achieved by tetrabutylammonium, followed by sodium and potassium, again following the relative mobilities of these ions<sup>26,27</sup>.

The solutions used in the experiments described above were not adjusted to a particular pH. Most biological and chemical NMR applications, however, require a particular pH value to keep the solute in a defined protonation state. Typically, specific pH values are



achieved by titrating a solution of a weak acid or weak base with a strong base or strong acid, usually hydrochloric acid and sodium hydroxide (or alternatively, specific pH values are achieved by mixing the appropriate amounts of an acid and its conjugate base according to the Henderson-Hasselbalch equation <sup>28</sup>). These titrations, however, add additional ions to the solution. Since the conductivity of the entire sample is the sum of the contributions of the individual ion species, adding ions with a high mobility can have a detrimental effect on the sensitivity. This effect can be seen in the data of Table 1. The sodium and chloride salts of several organic buffers with low ion mobilities of the organic component show a high conductivity and a low sensitivity due to the presence of the sodium or chloride ions with high mobility. This problem can be avoided if an acid or base with low ion mobility is added. Unfortunately, most acids and bases with low ion mobilities are weak and the titration of a weak acid with a weak base does not necessarily produce a good buffer. However, if the pKa values of both involved compounds are very similar, solutions with good buffer capacities can be produced. Examples are combinations of the base Bis-Tris propane (pKa 6.8) with the acids PIPES (pKa 6.8) or MOPS (pKa 7.2) and Tris base (pKa 8.1) with bicine (pKa 8.3). Based on the results shown in Table 1 we have selected some of the best compounds and titrated them either with hydrochloric acid or sodium hydroxide or, if the pKa values of a weak acid and a weak base are close, we also tested those combinations. Table 2 summarizes our results. Clearly, certain combinations show significantly higher predicted sensitivities than others. In particular, the combination of MOPS and Bis-Tris Propane at pH 7 as well as bicine and Tris base or NaOH at pH 8 should achieve high sensitivities.

Equation 3 shows that the conductivity of a certain buffer also depends on the charge of its ions. At the same molarity, a buffer with multiple charges such as phosphate reduces the sensitivity more than a buffer with a single charge and similar ion mobility. To predict the effect of a certain buffer on the sensitivity, the protonation state of its ions must also be considered. At pH values  $\sim 2$  the main species of a phosphate buffer are  $\text{H}_3\text{PO}_4$  and  $\text{H}_2\text{PO}_4^-$ , while at the more biological relevant pH of 7,  $\text{H}_2\text{PO}_4^-$  and  $\text{HPO}_4^{2-}$  are dominant and a further decrease of the sensitivity due to the increased charge is expected. In addition, increased charge is also linked to an increase in the counterion concentration. In particular, if the counterions have a high mobility they can significantly further decrease the sensitivity. One example is pentasodium tripolyphosphate, which we have included in our investigation as an example of a compound with high conductivity. As mentioned above, all buffer concentrations for the experiments reported in Tables 1 and 2 were 200mM. We have used this molarity-based comparison and not a normality-based one (normalized to the same amount of charge) in order to compare buffers with similar buffering capacities.

To further investigate if the differences in buffer sensitivities predicted by the data shown above can be detected in real NMR experiments we prepared 2 mM solutions of para-aminobenzoic-acid (PABA) in 200 mM solutions of HEPES/NaOH (pH 7.0), Tris base/HCl (pH 8.0), NaCl, sodium phosphate (pH 7.0) and pentasodium tripolyphosphate (unadjusted pH) and measured one-dimensional proton spectra of these samples (Figure 1). These spectra confirm that the type of buffer has a dramatic effect on the sensitivity of NMR experiments. Furthermore, comparison of the relative intensities in the spectra

with the predicted sensitivity factors  $L$  of the buffers used demonstrates a good correlation.

All experiments described above have been carried out at salt concentrations of 200 mM. However, most NMR experiments are performed at different ion concentrations and the relative sensitivity gain of a specific buffer over another type of buffer also depends on the concentration. The dependence of the relative sensitivity of two buffers can be calculated from the ratio of their sensitivity factors  $L_1$  and  $L_2$ :

$$\frac{L_1}{L_2} = \sqrt{\frac{(1 + 7.45 \frac{R_{s2}}{R_c})}{(1 + 7.45 \frac{R_{s1}}{R_c})}} \quad (7)$$

For low buffer concentrations the sample resistance of the two buffers,  $R_{s2}$  and  $R_{s1}$  decreases. In the limit of very low concentrations the factor  $7.45R_{s2}/R_c$  becomes small relative to 1 and can be neglected. In this case, the ratio of  $L_1/L_2$  is equal to 1 and the sensitivity is independent of the nature of the buffer. At high salt concentrations, the sample resistance becomes the dominant factor in Equation 7. In this case the factor  $7.45R_s/R_c$  becomes large relative to 1 and, in combination with Equation 3, equation 7 can be simplified (ignoring the effect of the counterion in the sum):

$$\frac{L_1}{L_2} = \sqrt{\frac{\lambda_2}{\lambda_1}} \quad (8)$$

This result shows that for high salt concentrations, the gain in sensitivity of a particular buffer over another becomes independent of the actual ion concentration and reaches a maximum that is equal to the square root of the ratio of the individual ion mobilities.

The results summarized in Tables 1 and 2 show some examples of buffers that can be used to achieve high sensitivity. However, many more potentially interesting buffers exist that remain to be tested. Furthermore, biological samples often require mixtures of different buffers and salts to keep the pH stable and to prevent aggregation. In principle, the measurement of the quality factor of a probe loaded with a specific buffer can be used to calculate the sensitivity factor, which allows us to evaluate the usefulness of a particular buffer. However, in most cases a network analyzer to measure the Q will not be readily available. On the other hand, Equations 3 and 4 predict a linear relationship between the  $R_s/R_c$  ratio and the DC conductivity of the sample. A calibration curve that links the measured conductivity to the  $R_s/R_c$  ratio can be used with Equation 6 to calculate the sensitivity factor L. We have used pentasodium tripolyphosphate and NaCl solutions ranging in concentration from 8 mM to 200 mM to measure both the quality factor of the probe loaded with these solutions and their conductivity (Figure 2, inset). From a linear regression analysis we obtained the following equation with C being the conductivity of the sample measured in mS/cm:

$$R_s/R_c = 0.087 \text{mS}^{-1} \text{cm C} \quad (9)$$

To investigate if Equation 9 can be used to calculate the sensitivity factor L of a certain buffer we have used it to calculate  $R_s/R_c$  values for all buffers and salt solutions in

Tables 1 and 2 based on their conductivity. A plot of the measured  $R_s/R_c$  values versus the calculated ratios exhibits a good correlation, indicating that conductivity measurements can be used to determine the sensitivity of buffers in NMR experiments (Figure 2). Some deviations from the theoretical line exist, mainly in the region with low conductivity buffers. In particular HEPES buffers demonstrate a linear correlation with a different y-axis intercept. This behavior is due to systematically smaller conductivity values measured by the conductivity meter. We interpret this result as likely being caused by interaction between the HEPES buffer and the electrode used during these measurements. For buffers that show such deviations, an additional calibration curve with this buffer can be determined.

The exact form of Equation 9 will also depend on the specific probe. However, a calibration curve could easily be determined with the help of a network analyzer as part of the installation procedure of the probe. Once such a calibration curve is available, the relationship between the conductivity and the  $R_s/R_c$  value can be used to optimize buffer conditions that preserve the high sensitivity of cryogenic probes.

Most biological NMR experiments are carried out at buffer concentrations of approximately 50 mM. To investigate the sensitivity gain of two of our best buffers at pH 7.0, MOPS/Bis-Tris propane and HEPES/NaOH, over the most commonly used NMR buffer, sodium phosphate, we prepared solutions of 1mM lysozyme in all 3 buffers and measured one-dimensional experiments (Figure 3). To avoid problems with differences in the amide proton exchange rates and overlap with buffer resonances only the extreme high-field end of the spectra were used for an analysis of the relative sensitivities. The sensitivity in the MOPS- and the HEPES-buffered spectra is virtually the same, which is

in agreement with theoretical values for both buffers at a 50 mM concentration. The conductivities for the 50 mM HEPES/NaOH and MOPS/Bis-Tris propane buffers are 0.693 mS/cm and 0.83 mS/cm, respectively. After correcting the HEPES conductivity for its systematic offset and using Equation 9 to calculate the  $R_s/R_c$  values and the corresponding sensitivity factors, the predicted sensitivity of the MOPS-based to the HEPES-based buffer is 1.09:1.0. In contrast, a significant difference exists between these two spectra and the phosphate-buffered spectrum. Using the most high-field shifted resonances, the peak intensity (at equal noise level) is approximately 1.5 times higher in the spectrum with the HEPES and MOPS buffers than in the phosphate buffer spectrum. Based on the conductivity of the 50 mM phosphate buffer of 5.71 mS/cm even higher gains in sensitivity of 1.6 with HEPES and 1.7 with MOPS are predicted. These values are not fully achieved due to the presence of counterions from the protein that lead to a slightly reduced sensitivity gain. This 50% increase in sensitivity relative to the most often used NMR buffer demonstrates that careful buffer selection can lead to significant sensitivity gains even under conditions typical for NMR experiments with biological samples.

Many NMR experiments with protein samples are carried out at slightly acidic pH in order to reduce the chemical exchange rate of the amide protons with water. A potential useful buffer in the pH range of 5.5 to 6.5 is MES which has a pKa of 6.1. To investigate its effect on the sensitivity of NMR experiments we have titrated a 200 mM sample of MES with sodium hydroxide and with Bis-Tris to a pH of 6.0. The conductivity of the MES sample titrated with NaOH was 4.65 mS/cm and of the sample titrated with Bis-Tris was 2.85 mS/cm. These values predict a sensitivity of the MES/Bis-Tris buffer close to

that of the MOPS/Bis-Tris propane buffer. To test this, we have prepared a 1 mM sample of lysozyme in 50 mM MES/Bis-Tris, pH 6.0 and compared the spectrum to the lysozyme spectra measured in the other buffers (Figure 3). The sensitivity of the MES/Bis-Tris sample is very similar to the sensitivity obtained with the MOPS/Bis-Tris propane sample and considerably higher than the sensitivity achieved with the phosphate sample, demonstrating that MES-based buffers are excellent buffers in the slightly acidic pH range.

Although we have tested conductivity, sample resistance and sensitivity in a small pH range, we expect that similar high-sensitivity buffers can be identified and used at pH values over a range of at least 3 to 11. Over this range the hydrogen and hydroxyl ion concentrations are equal to or less than 1 mM and hence, in spite of their relatively high mobilities, would not substantially increase the conductivity of the sample. As an aid in identifying candidate high-sensitivity buffers, one should note that ion mobility  $\lambda$  and diffusion coefficient  $D$  are related by the Einstein relation:

$$\frac{\lambda}{D} = \frac{q}{kT} \quad (10)$$

where  $q$  is the magnitude of the charge of the ion,  $k$  is Boltzmann's constant, and  $T$  is the absolute temperature. In order to design new high-sensitivity buffers, one should therefore focus on singly charged ions with low diffusion coefficients.

Finally, we would like to point out that the buffers described here are only a very small selection of all possible buffers. While these buffers are optimized for high sensitivity they may not be optimized for protein solubility. We have used HEPES buffers in the structure determination of two proteins and a protein-complex in our laboratory without encountering any solubility problems. In other cases, different buffers or mixtures of

buffers and neutral salts might have to be tested, using a systematic method such as the button test<sup>29</sup>.

## **Conclusions**

The results described here demonstrate that the exact type of buffer used for NMR experiments, especially in cryogenic probes, can have a dramatic effect on the achieved sensitivity. Specifically, careful choice of buffers can result in sensitivities of well over 50% more than that obtained with the most commonly used buffers. In addition, we have described a simple method that is based on conductivity measurements that allows researchers to identify new high-sensitivity buffers. Although the sensitivity obtained with proteins dissolved in reverse micelles in organic fluids is still superior to that obtained with the best buffers, the simplicity of the buffer method and its robustness make it very attractive in particular for applications that do not allow for lengthy sample preparation procedures, such as high throughput screening applications.



## **Acknowledgements**

We thank Zach Serber and Anson Nomura for discussion and critical comments.

Financial support was provided by NIH (PO1 DK58390), the UCSF Innovations in Basic Sciences Award and the Sandler Family Supporting Foundation. A.E.K. and H.D.O. were supported by an NIH Training Grant (GM08284).

## FIGURE CAPTIONS

**Figure 1.** Comparison of the sensitivity obtained with a 2 mM para-aminobenzoic-acid sample dissolved in 200 mM HEPES buffer (titrated with NaOH), 200 mM Tris buffer (titrated with HCl), 200 mM sodium phosphate buffer, 200 mM NaCl or 200 mM pentasodium tripolyphosphate buffer. The first three buffers are identical with the ones used for the measurements in Table 2 and the last two buffers with the ones used in Table 1. Sensitivities relative to pentasodium tripolyphosphate are given in parentheses. The two phosphate-based buffers showed increased noise around the water resonance that is not observed with the other buffers. Therefore, the noise level was determined between 9 and 10 ppm.

**Figure 2.** Dependence of the  $R_s/R_c$  value on the conductivity of the sample. Pentasodium tripolyphosphate solutions ranging from 8 to 200 mM were used to measure the calibration curve shown in the inserted graph. Virtually identical results were obtained with NaCl samples. Based on this calibration curve the  $R_s/R_c$  values for all buffers used in the experiments reported in Tables 1 and 2 were calculated from their DC conductivities. Open circles represent the three HEPES buffers. In addition, the theoretical line with a slope of 1 is also shown.

**Figure 3.** One-dimensional spectra of a 1 mM lysozyme sample measured in 50 mM sodium phosphate, 50 mM HEPES/NaOH or 50 mM MOPS/Bis-Tris propane buffer, all pH 7, and in 50 mM MES/Bis-Tris, pH 6.0. Only the most high-field shifted region of the spectra are shown.

## References

- (1) Ernst, R. R.; Anderson, W. A. *Rev. Sci. Instr.* **1966**, *37*, 93.
- (2) Cavanagh, J.; Palmer, A. G.; Wright, P. E.; Rance, M. *J. Magn. Reson.* **1991**, *91*, 429.
- (3) Kay, L. E.; Keifer, P.; Saarinen, T. *J. Am. Chem. Soc.* **1992**, *114*, 10663-10665.
- (4) Muhandiram, D. R.; Kay, L. E. *J. Magn. Reson. B* **1994**, *103*, 203-216.
- (5) Styles, P.; Soffe, N. F.; Scott, C. A.; Cragg, D. A.; White, D. J.; White, P. C. *J. J. Magn. Reson.* **1984**, *60*, 397-404.
- (6) Styles, P.; Soffe, N. F. *J. Magn. Reson.* **1989**, *84*, 376-378.
- (7) Anderson, W. A.; Brey, W. W.; Brooke, A. I.; Cole, B.; Delin, K. A.; Fuks, L. F.; Hill, H. D. W.; Kotsubo, V. Y.; Nast, R.; Withers, R. S.; Wong, W. H. *Bull. Magn. Reson.* **1995**, *17*, 98-.
- (8) Hill, H. D. W. *IEEE Trans. Appl. Superconductivity* **1997**, *7*, 3750-3755.
- (9) Triebe, R.; Nast, R.; Marek, D.; Withers, R.; Baselgia, L.; Häberli, M.; Gerfin, T.; Calderon, P. In *40<sup>th</sup> Experimental Nuclear Magnetic Resonance Conference*: Orlando, USA, 1999, p 198.
- (10) Withers, R. S.; Cole, B. F.; Johansson, M. E.; Liang, G.; Zaharchuk, G. *SPIE Proceedings* **1994**, *2156*, 27-35.
- (11) Withers, R. S.; Liang, G.; Cole, B. F.; Johansson, M. E. *IEEE Transactions on applied superconductivity* **1993**, *3*, 2450-2453.

- (12) Hajduk, P. J.; Gerfin, T.; Bohlen, J. M.; Häberli, M.; Marek, D.; Fesik, S. W. *J. Med. Chem.* **1999**, *42*, 2315-2317.
- (13) Serber, Z.; Richter, C.; Moskau, D.; Böhlen, J.-M.; Gerfin, T.; Marek, D.; Häberli, M.; Baselgia, L.; Laukien, F.; Stern, A. S.; Hoch, J. C.; Dötsch, V. *J. Am. Chem. Soc.* **2000**, *122*, 3554-3555.
- (14) Serber, Z.; Richter, C.; Dötsch, V. *ChemBioChem* **2001**, *2*, 247-251.
- (15) Flynn, P. F.; Mattiello, F. L.; Hill, H. D. W.; Wand, A. J. *J. Am. Chem. Soc.* **2000**, *122*, 4823-4824.
- (16) Hubbard, J.; Johnson, P.; Ong, B.; Laddes, J.; King, G.; MacLachlan, L. K. In *42nd ENC: Orlando, USA, 2001*.
- (17) Ehrhardt, M. R.; Flynn, P. F.; Wand, A. J. *J. Biomol. NMR* **1999**, *14*, 75-78.
- (18) Babu, C. R.; Flynn, P. F.; Wand, A. J. *J. Am. Chem. Soc.* **2001**, *123*, 2691-2692.
- (19) Wand, A. J.; Ehrhardt, M. R.; Flynn, P. F. *Proc. Natl. Acad. Sci. USA* **1998**, *95*, 15299-15302.
- (20) Sambrook; Fritsch; Maniatis *Molecular Cloning, a laboratory manual*; 2nd ed.; Cold Spring Harbor Laboratory Press, 1989.
- (21) Hoult, D. I.; Richards, D. E. *J. Magn. Reson.* **1976**, *24*, 71-85.
- (22) Hoult, D. I.; Lauterbur, P. C. *J. Magn. Reson.* **1979**, *34*, 425-433.
- (23) Gadian, D. R.; Robinson, F. N. H. *J. Magn. Reson.* **1979**, *34*, 449-455.
- (24) Hoult, D. In *Encyclopedia of NMR*; Vol. 7, p 4261.
- (25) Note that while the use of a saddle coil instead of a cylindrical coil changes the form of this equation somewhat, it does not alter the strict linear dependence of the sample resistance, induced by the coil, on the conductivity of the sample.

- (26) Barry, P. H.; Lynch, J. W. *J. Membrane Biol.* **1991**, *121*, 101-117.
- (27) Ng, B.; Barry, P. H. *J. Neuroscience Methods* **1995**, *56*, 37-41.
- (28) Chang, R. *Physical Chemistry*; 3rd ed.; University Science Books: Sausalito, 2000.
- (29) Bagby, S.; Tong, K. I.; Ikura, M. *Meth. Enzymol.* **2001**, *339*, 20-41.

**Table 1.**  $R_s/R_c$  values, expected sensitivity factor L and DC conductivity of several different salts, all at 200 mM concentration.

Buffer	$R_s/R_c$	Sensitivity Factor L	Conductivity (mS/cm)
Pentasodium Tripolyphosphate	2.71 ± 0.04	0.22	31.3
Potassium Chloride	1.93 ± 0.04	0.26	23.3
Disodium Phosphate (Na <sub>2</sub> HPO <sub>4</sub> )	1.89 ± 0.04	0.26	22.0
Sodium Pyrophosphate	1.70 ± 0.04	0.27	20.2
Sodium Chloride	1.64 ± 0.04	0.28	18.1
PIPES	1.33 ± 0.04	0.30	14.8
β-glycerophosphate	1.31 ± 0.04	0.30	14.9
Potassium Phosphate (KH <sub>2</sub> PO <sub>4</sub> )	1.25 ± 0.04	0.31	14.1
TRIS HCl	1.24 ± 0.04	0.31	14.1
BIS-TRIS HCl	1.12 ± 0.03	0.33	13.62
Sodium Acetate	1.11 ± 0.03	0.33	12.2
Sodium Phosphate (NaH <sub>2</sub> PO <sub>4</sub> )	0.95 ± 0.03	0.35	11.0
Sodium TAPS	0.90 ± 0.03	0.36	9.55
Sodium MES	0.88 ± 0.03	0.36	10.18
Sodium MOPS	0.88 ± 0.03	0.36	9.86
Sodium TES	0.84 ± 0.03	0.37	9.41
Sodium HEPES	0.84 ± 0.03	0.37	9.25
Tetrabutylammonium Dihydrogen Phosphate	0.69 ± 0.03	0.40	9.00
HEPES	0.22 ± 0.02	0.62	0.06
TAPS	0.14 ± 0.02	0.70	0.29
CAPS	0.14 ± 0.02	0.70	0.7
TES	0.12 ± 0.02	0.73	0.25
MOPS	0.10 ± 0.02	0.76	0.04
CHES	0.08 ± 0.02	0.79	0.06
MES	0.08 ± 0.02	0.80	0.15
Bicine	0.05 ± 0.02	0.86	0.031
BIS-TRIS Propane	0.05 ± 0.02	0.86	0.022
TRIS Base	0.03 ± 0.02	0.91	0.1
BIS-TRIS	0.02 ± 0.02	0.93	0.0236
Deionized Distilled H <sub>2</sub> O	0.01 ± 0.02	0.98	0.0023

**Table 2.**  $R_s/R_c$  values, expected sensitivity factor L and DC conductivity for several buffers, adjusted to specific pH values with different acids or bases.

Buffer	Titrated With	pH	$R_s/R_c$	Sensitivity Factor L	Conductivity (mS/cm)
BIS-TRIS Propane	HCl	6.8	$1.76 \pm 0.04$	0.27	19.34
	PIPES		$0.84 \pm 0.03$	0.37	8.75
TRIS Base	HCl	8.0	$0.88 \pm 0.03$	0.36	9.60
	TES		$0.60 \pm 0.03$	0.43	5.71
Sodium Phosphate		7.0	$1.63 \pm 0.04$	0.28	17.34
MOPS	BIS-TRIS propane	7.0	$0.22 \pm 0.02$	0.61	2.40
Bicine	NaOH	8.0	$0.26 \pm 0.02$	0.58	2.61
	TRIS base		$0.29 \pm 0.02$	0.56	2.50
HEPES	BIS-TRIS Propane	7.0	$0.31 \pm 0.02$	0.55	1.30
	NaOH		$0.41 \pm 0.02$	0.50	2.44

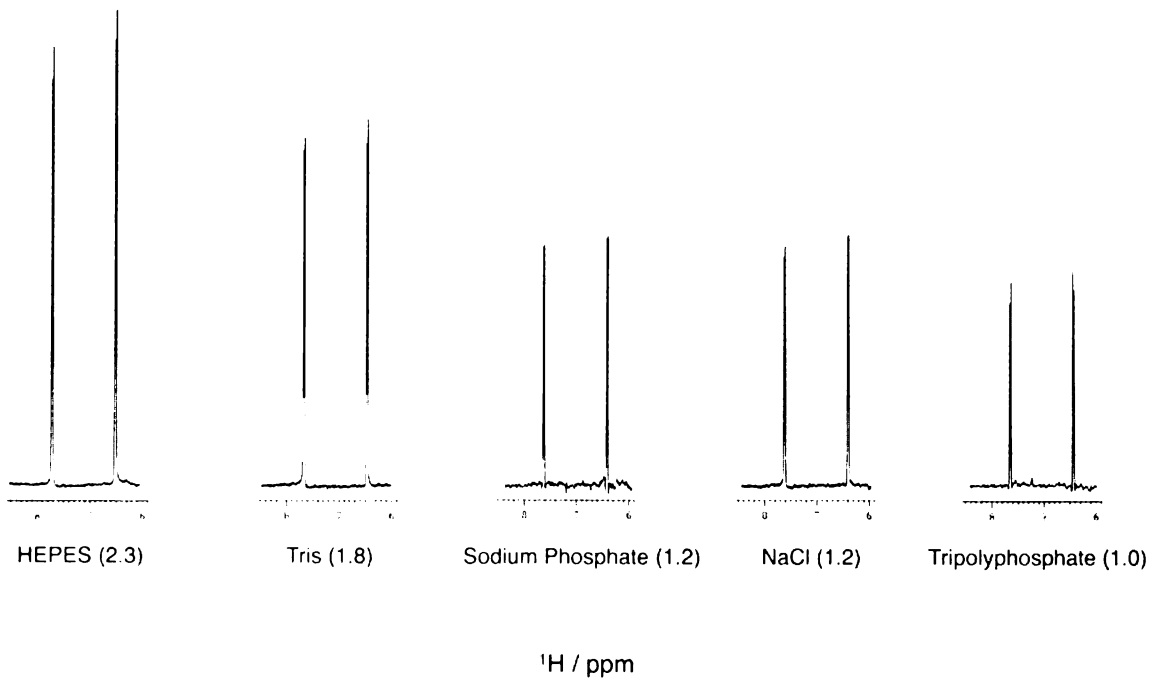


Figure 1



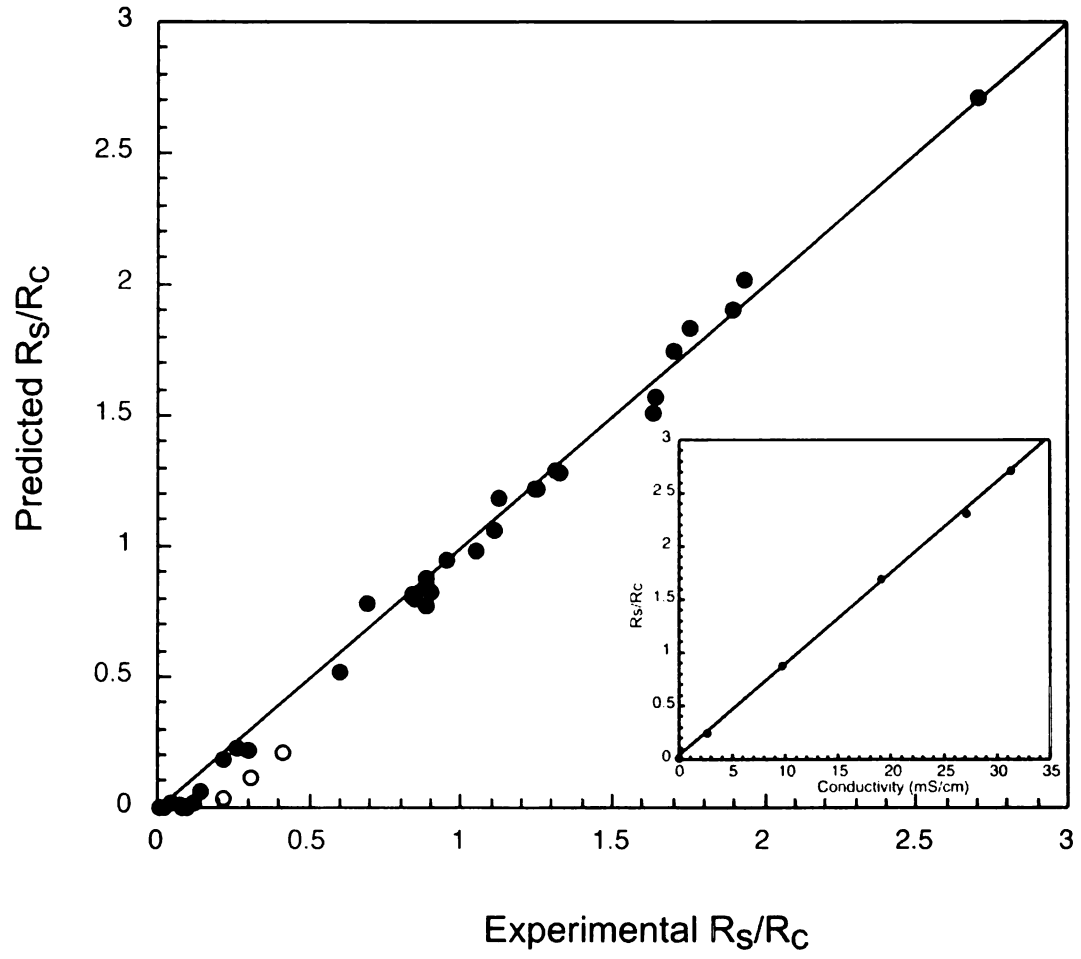


Figure 2

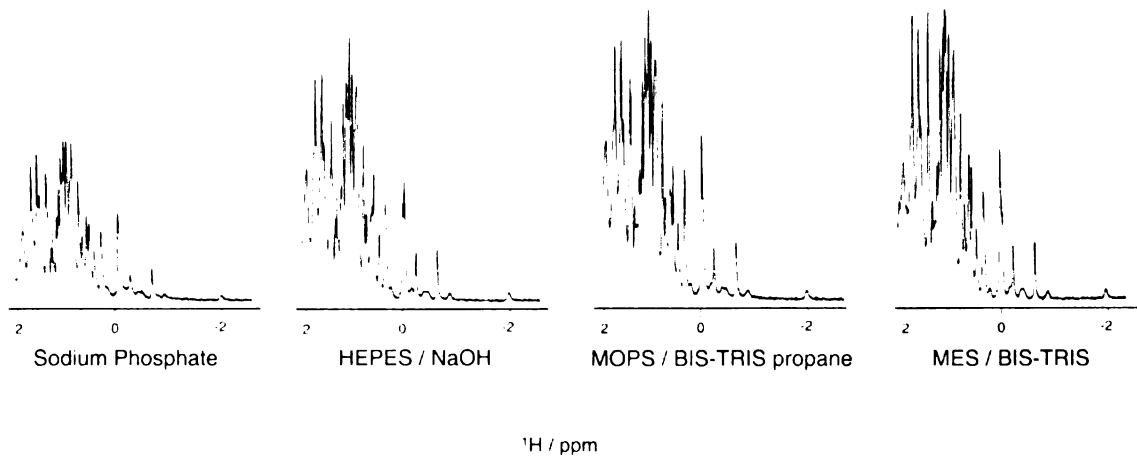


Figure 3

## **Chapter 4**

### **Future Directions**

After working on so many different projects in two different labs, there are a number of things I would love to see done in the future. There are three areas of research I feel need more attention: the role of the WH2 in the cytoskeleton, elucidation of the molecular mechanism of activation of the Arp2/3 complex, and the mode of regulation of WAVE/Scar proteins. Below I will describe some experiments that will hopefully further our understanding of each.

### *WH2 domains*

Our work on the WH2 domain from Scar suggests that the WH2 domain itself serves to allow for barbed end elongation and provides a high local concentration of ATP-actin monomers. It appears that the C-terminal extension of WH2 domains dictate the specificity and function of the protein of interest. However, the spir WH2 cluster retains activity even when the WH2 domains are joined together by Gly-Ser linkers. Therefore, it is possible that the orientation and affinity of the sequences give rise to actin nucleation and understanding this process will be a central goal of the lab. To further increase our knowledge of the WH2 domain, it is necessary to identify new WH2 domain containing proteins. Using a simple motif search, I was able to identify three new human WH2 domain proteins: Espin (see **Appendix A**), JMY, and NP\_071934. Junction-mediating and regulatory protein (JMY) is a CBP/p300 co-factor that augments the p53 response. It contains a C-terminal VCA peptide that is 71% identical to that of Scar1 VCA and has a nearby poly-proline region. All amino acids that are important for Arp2/3 activation are present. Testing the nucleation activity and its role in apoptosis may lead to some exciting findings. In addition, we found an unidentified protein, NP\_071934, in the NCBI database that appears to be a formin with the FH1 domain replaced by a WH2

domain. This is quite intriguing, since the WH2 domain could directly bind and feed monomers to the FH2 domain and bypass its connection to profilin. Again, testing its nucleation ability will undoubtedly further our understanding of both WH2 domains and formin function. Sequence homology alone cannot be used to discover all WH2 domains, however, since many proteins such as thymosin  $\beta$ 4 have highly divergent sequences yet are structurally homologous to WASp WH2 domains. To tackle this problem I suggest a combined approach incorporating known actin binding WH2 motifs into a Hidden Markov model and filtering the hits from this HMM with scores for helical and disorder prediction. Since all WH2 domains undergo a disorder-to-order transition upon binding actin, this should help find new candidates.

#### *Arp2/3 activation*

Our studies have shown that the actin monomer plays an active role in activating the Arp2/3 complex. However, our understanding of the structure of the activated state and where the monomer adds on is lacking. A myriad of experiments can be envisioned to address these questions but I will only mention a few here. Crystal structures of the Arp2/3 complex bound to an NPF, F-actin and an actin monomer would help to elucidate the mechanism of activation. However, this is complicated by several technical considerations. First, we currently do not have a technique for ensuring a homogeneous population of filaments. The Arp2/3 complex binds to at least three monomers within a filament such that isolation of crosslinked actin trimers may be possible, if not for the pointed end binding activity of the complex. Second, the complex appears to be in a dynamic conformational equilibrium even when bound to an NPF. This could be circumvented by introducing a single crosslink between the NPF peptide and the

complex, effectively removing the off rate. Third, the daughter monomer appears to be dynamic, binding to both the C domain and the activated state of the complex, which then results in Arp2 ATP hydrolysis. Interestingly, in my crosslinking studies I do observe a crosslink between Arp2/3 and monomeric actin, which could be used for this purpose. Lastly, another strategy would be to introduce cysteine residues into yeast Arp2/3 that could form disulfides only in the activated state. Another possible approach would be to do cryo-electron microscopy or rotary shadowing on samples containing the necessary components for activation.

A final proof of the role of the actin monomer could be accomplished by undertaking simple experiments using reagents and methods already described in **Chapter 2**, namely, comparing the nucleation activity of a CA domain crosslinked to monomeric actin via the C domain and VCA domain chemically crosslinked to monomeric actin via the WH2 domain. The CA construct should be easy to make since the crosslinking can only occur via C and the VCA construct would require one further purification step to ensure that the crosslinking is via the WH2 and not the C domain. e.g. by separation on a WH2 column. Since we show that C domain binds to actin and Arp2/3 in a mutually exclusive way, for the crosslinked CA species, the C domain would be unable to dissociate from the actin to interact with the Arp2/3, whereas for the VCA species, the C domain would be able to. If the “dynamic equilibrium” hypothesis is correct, then, the crosslinked CA species should be unable to activate the Arp2/3 complex, whereas the crosslinked VCA species will be able to.

*Regulation of WAVE/Scar proteins*

We have shown that human Scar1 contains a stretch of ~100 residues that can activate the Arp2/3 complex independent of the VCA region. It is unknown if this activity is conserved among species and this would need to be tested.

The molecular details of WAVE/Scar inhibition are unclear. As noted previously (**Chapter 1**), the binding site for the repression complex is found in the SHD, which we have shown to be a coiled-coil dimer (**Appendix B**). Since the WASp proteins are inhibited by binding of the GBD to the C domain, it would make sense that WAVE/Scar proteins are inhibited in a similar manner with the repression complex binding directly to the C domain as well. One simple experiment would be to see if the assembled complex could bind to the C domain. Another mode of regulation could be through regulating the oligomerization state of the SHD and this could be tested using the best technique in the world, analytical ultracentrifugation.

## Appendix A

### **Targeted espins reveal a novel, WH2 domain-dependent mechanism for making actin bundles in cells**

The data presented here is part of a larger work that is currently in review at the *Journal of Cell Science*. Our collaborator, James Bartles at Northwestern University, first contacted us after seeing my poster on the work from **Chapter 2** at the ASCB conference. He was excited about the presence of a WH2 domain in a family of cytoskeleton proteins known as Espins. These proteins cause the formation of very large parallel actin bundles in specialized cell types such as microvilli and stereocilia. A mutation in the F-actin bundling site causes deafness in mice and is known as the jerker mutation. The juxtaposition of a F-actin bundling domain and a WH2 domain appears to have novel activities *in vitro* and reinforces the notion that the WH2 domain is modular and can be attached to other actin binding domains to create new functionalities.



## **Abstract**

The espin actin-bundling proteins, which are the target of deafness mutations, are present in the parallel actin bundles of stereocilia and microvilli and appear to increase their steady-state length. Here, we report a new activity of the espins, one that depends on their enigmatic WH2 domain: the ability to assemble a large actin bundle when targeted to a specific subcellular location. This activity was observed for espins targeted to the centrosome by the dyneindynactin motor complex or to the nucleolus as a result of the jerker deafness mutation. This activity, which appears specific to espins, requires two espin F-actin-binding sites and the actin monomer-binding activity of the espin WH2 domain, but can be mimicked by adding a WH2 domain to an unrelated actin-bundling protein, villin. Espins do not activate the Arp2/3 complex in vitro, and bundle assembly is not indicative of in-vitro nucleation activity. Our results suggest a novel mechanism for building actin bundles at specific sites in cells.

## **Results**

### *Further characterization of the WH2 domain requirement*

Although espins do not contain an obvious WASP-like C peptide, they do resemble WASP family proteins in linear domain organization: basic region (required for binding phosphatidylinositol 4,5-bisphosphate), proline-rich peptide, WH2 domain, and COOH-terminal peptide containing clusters of acidic amino acids. Therefore, we tested whether espins could act as nucleation-promoting factors for Arp2/3 complex-mediated actin polymerization. Espin 3A failed to activate the Arp2/3 complex in vitro, even at relatively high concentrations (400 nM in Fig 1B). At this same concentration, the Scar1

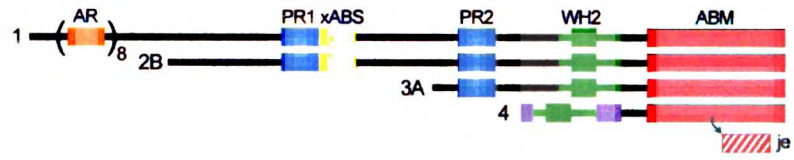
VCA peptide (V, alternative abbreviation for the WH2 domain) caused pronounced activation (Fig. 1B), even though it is a relatively weak nucleation-promoting factor that is 16 and 68-fold less active than the VCA peptides of WASP and NWASP, respectively. To address the possibility of autoinhibition, we also tested an espin COOH-terminal construct that began just 12 aa upstream of the 17-aa core of the WH2 domain and, hence, was missing an NH2-terminal peptide. This espin “WA” fragment also failed to activate the Arp2/3 complex (Fig. 1B). A slight shortening of the polymerization lag time was noted with espin 2B at concentrations greater than 250 nM (400 nM shown in Fig. 1B), but this effect was also observed in the absence of the Arp2/3 complex (see below). In fact, the polymerization curves obtained with the different espins constructs were similar in the presence and absence of Arp2/3 complex (data not shown). Thus, espins did not appear to activate the Arp2/3 complex directly.

The slight lag-shortening effect observed at higher concentrations of espin 2B, which could be indicative of weak nucleation activity, prompted additional experiments examining the domain dependence of espin’s effects on actin polymerization in the absence of the Arp2/3 complex. Espin 3A inhibited actin polymerization by extending the lag time and decelerating polymerization relative to actin alone (Fig. 1C). As expected at this 1:10 molar ratio of espin to actin, deletion of the 17-aa core of the WH2 domain from espin 3A had little effect (Fig. 1C), suggesting that the deceleration stemmed largely from a reduced availability of filament ends, presumably due to bundling. Some deceleration was also evident with espin 2B, but it appeared to be counteracted by the shortening of lag time (Fig. 1C). The lag-shortening effect required all three of espin 2B’s actin-binding regions. Deletion of the 23-aa additional F-actinbinding site from espin 2B

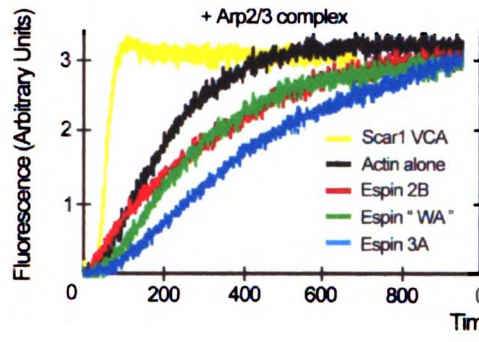
**brought** about a large increment in lag time, causing the early part of the polymerization **curve** to approach that for espin 3A (Fig. 1C), which does not contain this binding site (Fig. 1A). By comparison, deletion of the 17-aa core of the WH2 domain caused the early **part** of the curve to be more similar to that for actin alone, with deceleration being **observed** at later times (Fig. 1C). Deletion of the actin-bundling module caused the curve to be highly similar to that of actin alone throughout the entire time course (data not shown), reinforcing the conclusion that the deceleration resulted from filament bundling. Note that this construct, which contains both the 23-aa additional F-actin-binding site and the WH2 domain and is also free from the deceleration effect, failed to shorten the lag time.

**Figure 1.** Espin isoform, domains and activities. A, Representatives of the four major espin isoform size classes. AR, ankyrin-like repeat; PR, proline-rich peptide; xABS, 23-aa additional F-actin-binding site; ABM, actin-bundling module; je, jerker peptide (red and white diagonal stripe; sequence shown in F), the frameshifted peptide that replaces the COOH-terminal part of the espin actin-bundling module at the site of the jerker deafness mutation (black arrow, illustrated for espin 4); purple, peptides unique to espin 4. B and C, Pyrene-actin polymerization assay for the designated construct (0.4  $\mu$ M) in the presence (B) or absence (C) of 10 nM Arp2/3 complex showing little or no nucleation-promoting or nucleation activity of espins *in vitro*. Espin “WA”, espin COOH-terminal peptide that begins 12 aa upstream of the 17-aa core of the WH2 domain.

A



B



C

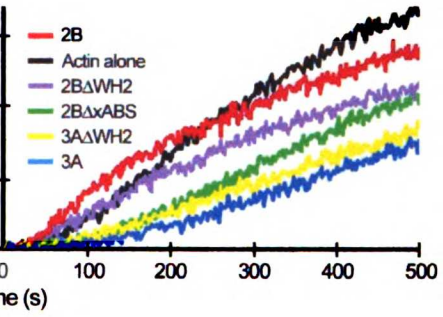


Figure 1

## **Appendix B**

### **Biochemical Studies of Human Scar1**

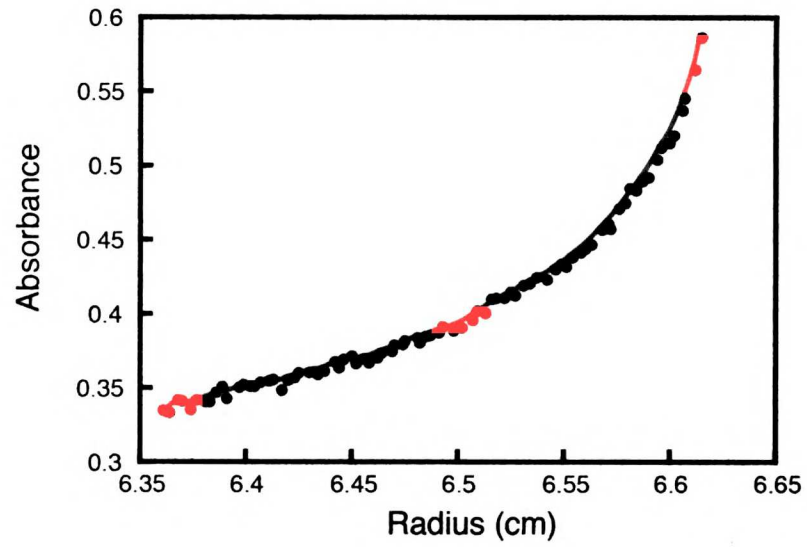
The Scar Homology domain (SHD) has no homology to any other known proteins, yet has a conserved leucine-zipper like motif. Using the program “COILS”, this region was predicted to adopt a coiled-coil structure, much like a number of proteins that regulate the cytoskeleton. We expressed this 65-residue fragment and showed by analytical equilibrium ultracentrifugation that it exists as a tight dimer, with  $K_d$  of approximately 300 nM (Fig. 1A).

Using pyrene fluorescence assays, we have shown that residues 196-277 activate the Arp2/3 complex (Fig. 1B). This region of Scar is located in the same relative position as the GBD from WASp. This peptide, which we refer to as the “Secondary Activation Domain”, does not contain any regions with homology to the VCA region but does inhibit the activity of VCA *in trans*.

**Fig. 1.** Biophysical characterization of human Scar1. *A*, Sedimentation equilibrium analysis of human Scar1 (residues 45-95) using a model XL/I analytical ultracentrifuge (Beckman Instruments). Global fitting of data sets from three different concentrations and velocities reveals that the SHD is a dimer. *B*, Time course of pyrene-actin polymerization. Mg-ATP-actin monomers (4  $\mu$ M 5% pyrene-labelled) and 10 nM Arp2/3 complex were polymerized in 10 mM HEPES pH 7.0, 50 mM KCl, 1 mM EGTA and 1 mM MgCl<sub>2</sub> at 22°C, either alone or with 0.5  $\mu$ M Scar1 VCA [residues 489-559] or 1  $\mu$ M Scar1 SAD [residues 196-277].



A



B

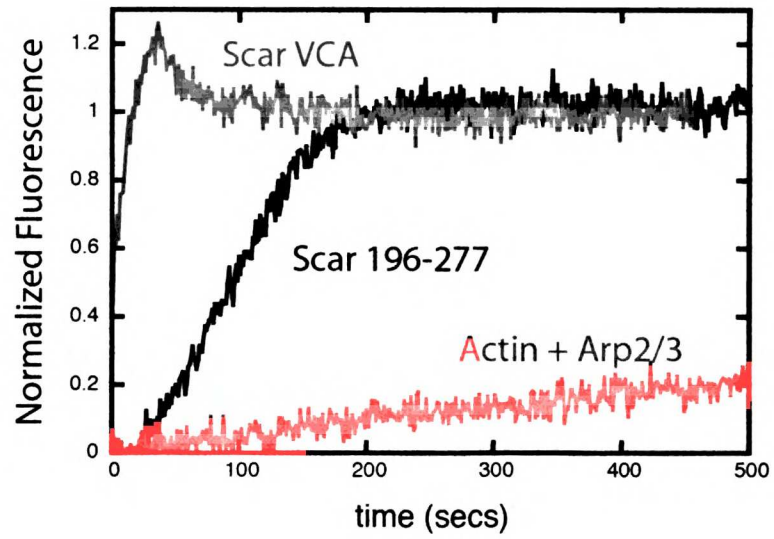


Figure 1

## **Appendix C**

### **Permissions**

**JBC Online**[www.universal-imaging.com](http://www.universal-imaging.com)

QUICK SEARCH: [advanced]

Author: Keyword(s):

Go

Year:

Vol:

Page:

[HOME](#) [HELP](#) [FEEDBACK](#) [SUBSCRIPTIONS](#) [ARCHIVE](#) [SEARCH](#)Institution: [University of California, San Francisco](#) [Sign In as Member/Non-Member](#)

## Copyright Permission Policy

### **ASBMB Journals**

*Journal of Biological Chemistry**Molecular and Cellular Proteomics**Journal of Lipid Research**Biochemistry and Molecular Biology Education**ASBMB Today*

### **ASBMB does not charge for and grants use without requiring your copyright permission request for:**

- Original authors wanting to reproduce portions of their own work; or to republish their material in not-for-profit formats or venues.
- Students wanting to reproduce or republish their work for educational purposes.
- Students using other authors' material for their theses.
- Reproduction or republication of abstracts only.
- Photocopying up to 5 copies for personal use.
- Non-profit educational institutions making multiple photocopies of articles for classroom use; all such reproduction must utilize institutionally owned equipment for this purpose.

***Use of copyrighted material requires proper citation.***

### **For all other uses, contact [Copyright Clearance Center](#).**

[HOME](#) [HELP](#) [FEEDBACK](#) [SUBSCRIPTIONS](#) [ARCHIVE](#) [SEARCH](#)[All ASBMB Journals](#)[Molecular and Cellular Proteomics](#)[Journal of Lipid Research](#) [Biochemistry and Molecular Biology Education](#)

**Copyright © 2005 by the American Society for Biochemistry and Molecular Biology.**

## ACS PUBLICATIONS DIVISION GUIDELINES

### FOR THESES AND DISSERTATIONS

#### ATTENTION: STUDENTS, STUDENT ADVISORS, AND TEACHERS

**Permission is automatically granted to include your paper(s) or portions of your paper(s) in your thesis; please pay special attention to the implications paragraph below. The Copyright Subcommittee of the Joint Board/Council Committees on Publications approved the following:**

Copyright permission for published and submitted material from theses and dissertations

ACS extends blanket permission to students to include in their theses and dissertations their own articles, or portions thereof, that have been published in ACS journals or submitted to ACS journals for publication, provided that the ACS copyright credit line is noted on the appropriate page(s).

Publishing implications of electronic publication of theses and dissertation material

Students and their mentors should be aware that posting of theses and dissertation material on the Web prior to submission of material from that thesis or dissertation to an ACS journal may affect publication in that journal. Whether Web posting is considered prior publication may be evaluated on a case-by-case basis by the journal's editor. If an ACS journal editor considers Web posting to be "prior publication", the paper will not be accepted for publication in that journal. If you intend to submit your unpublished paper to ACS for publication, check with the appropriate editor prior to posting your manuscript electronically.

If your paper has not yet been published by ACS, we have no objection to your including the text or portions of the text in your thesis/dissertation in **print and microfilm formats**; please note, however, that electronic distribution or Web posting of the unpublished paper as part of your thesis in electronic formats might jeopardize publication of your paper by ACS. Please print the following credit line on the first page of your article: "Reproduced (or 'Reproduced in part') with permission from [JOURNAL NAME], in press (or 'submitted for publication'). Unpublished work copyright [CURRENT YEAR] American Chemical Society." Include appropriate information.

If your paper has already been published by ACS and you want to include the text or portions of the text in your thesis/dissertation in **print or microfilm formats**, please print the ACS copyright credit line on the first page of your article: "Reproduced (or 'Reproduced in part') with permission from [FULL REFERENCE CITATION.] Copyright [YEAR] American Chemical Society." Include appropriate information.

**Note:** If you plan to submit your thesis to UMI or to another dissertation distributor, you should not include the unpublished ACS paper in your thesis if the thesis will be disseminated electronically, until ACS has published your paper. After publication of the paper by ACS, you may release the entire thesis (**not the individual ACS article by itself**) for electronic

dissemination; ACS's copyright credit line should be printed on the first page of the ACS paper.

**SUMMARY:** The inclusion of your ACS unpublished or published manuscript is permitted in your thesis in print and microfilm formats. If ACS has published your paper you may include the manuscript in your thesis on an intranet that is not publicly available. Your ACS article cannot be posted electronically on a publicly available medium, such as but not limited to, electronic archives, Internet, intranet, library server, etc. The only material from your paper that can be posted on a public electronic medium is the article abstract, figures, and tables and you may link to the article's DOI.

Questions? Please contact the ACS Publications Division Copyright Office at [copyright@acs.org](mailto:copyright@acs.org) or at 202-872-4368.

Alexander E. Kelly  
Graduate Student  
UCSF

1161 Stanyan Street #2  
San Francisco, CA 94117  
415-577-2235  
aek@mullinslab.ucsf.edu

September 2, 2005

ProQuest Information and Learning  
300 North Zeeb Road  
Ann Arbor, Michigan 48103-1500  
(800)-521-0600

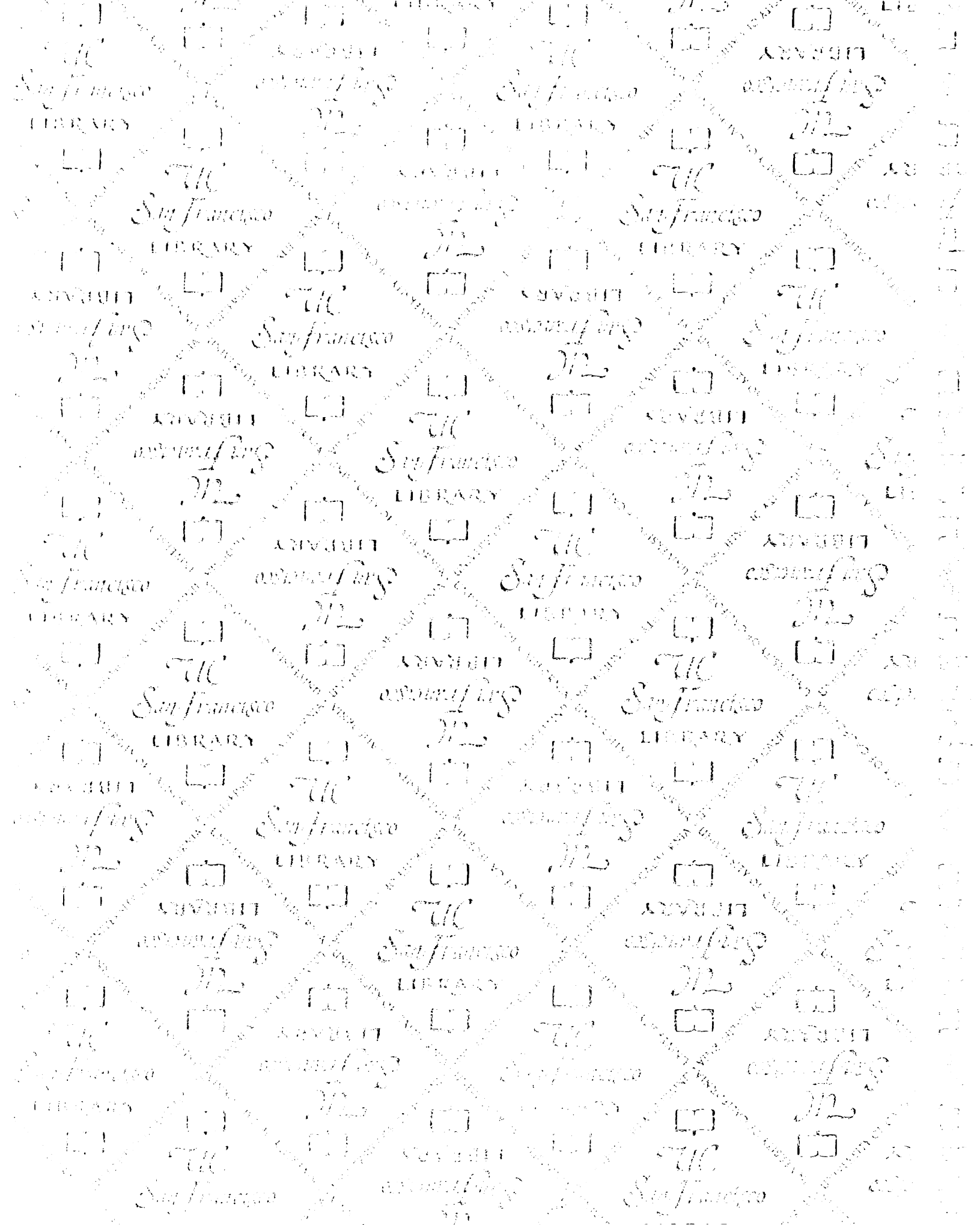
To Whom it May Concern:

I am writing to request that all sales of my manuscript entitled "Biochemical and Structural Insights into the Activation Mechanism of the Arp2/3 Complex" be restricted to the author only for copyright reasons.

Please contact me at the address above until 9/8/05. After that, all correspondence should be addressed to: 238 E. 81<sup>st</sup> Street, Apt. 9B, New York, NY 10028.

Best regards,

Alexander E. Kelly



Not to be taken  
from the room.

# For reference

8070974



3 1378 00807 0974



